Copy
RM E56I04

NACA RM E56I04

NACA

RESEARCH MEMORANDUM

THEORETICAL ANALYSIS OF TOTAL-PRESSURE LOSS AND AIRFLOW DISTRIBUTION FOR TUBULAR TURBOJET COMBUSTORS WITH CONSTANT ANNULUS AND LINER CROSS-SECTIONAL AREAS

By Charles C. Graves and Jack S. Grobman

Lewis Flight Propulsion Laboratory
Cleveland, Ohio

NATIONAL ADVISORY COMMITTEE
FOR AERONAUTICS
WASHINGTON

January 4, 1957

TABLE OF CONTENTS

NATIONAL ADVISORY COMMITTEE FOR AERONAUTICS

RESEARCH MEMORANDUM

THEORETICAL ANALYSIS OF TOTAL-PRESSURE LOSS AND AIRFLOW DISTRIBUTION FOR TUBULAR TURBOJET COMBUSTORS WITH CONSTANT ANNULUS AND LINER CROSS-SECTIONAL AREAS

By Charles C. Graves and Jack S. Grobman

SUMMARY

Compressible- and incompressible-flow calculations were made of the combustor total-pressure-loss coefficient and liner airflow distribution for tubular turbojet combustors having constant annulus and liner cross-sectional areas along the combustor axis. Information on static- and total-pressure distribution and liner air-jet entrance angles along the length of the combustor was obtained as an intermediate step in the calculations. The calculations include the effects of heat release, annulus wall friction, and variation in discharge coefficients of the liner wall openings along the combustor.

The combustor total-pressure-loss coefficient and liner airflow distribution are presented graphically in terms of the following dimensionless parameters: (1) combustor reference Mach number, (2) ratio of combustor-exit to -inlet total temperature, (3) fraction of total airflow passing through the liner dome, (4) $A_{h,T}/A_r$, and (5) A_L/A_r, where $A_{h,T}$ is the total liner open hole area and A_L and A_r are the liner and combustor total cross-sectional areas, respectively.

INTRODUCTION

In the design of combustors for turbojet and ram-jet engines, it is desirable to be able to predict the combustor total-pressure loss and liner airflow distribution from the combustor geometry and operating conditions. Low values of combustor total-pressure loss are desired since such losses reduce engine thrust and cycle efficiency (ref. 1). Airflow distribution and liner air-jet entrance angles are of direct interest to the combustor designer since they influence combustion efficiency and stability and combustor-outlet temperature profile (ref. 2). A combustion research program being conducted at the Lewis laboratory is concerned with these aerodynamic aspects of combustor design.

The loss in total pressure across a combustor may be attributed primarily to losses resulting from (1) mixing of high-velocity liner air jets with the liner gas stream, (2) heat release in the liner, and (3) annulus wall friction. The effects of these factors on combustor total-pressure loss are considered in the calculations of the present report. The liner airflow distribution and liner air-jet entrance angles are obtained in the course of the combustor total-pressure-loss calculations.

Previous analytical investigations of combustor total-pressure loss and liner airflow distribution have involved stepwise calculations in which the combustor is divided into an arbitrary number of transverse sections. In a trial-and-error method presented in reference 3, the liner airflow distribution and combustor total-pressure loss are calculated for an assigned liner open hole area distribution. In a more rapid method presented in reference 4, the liner open hole area distribution is calculated for an assigned liner airflow distribution and combustor total-pressure loss. Both methods include the effects of heat release on the calculated values and could account for variation along the combustor of the discharge coefficient of the liner wall openings.

For particular combustor configurations, stepwise calculation methods such as presented in references 3 and 4 have been used to calculate the combustor flow conditions. However, there is a need for generalized curves that can be used to obtain preliminary estimates of combustor total-pressure loss, liner airflow distribution, and liner air-jet entrance angles. Such curves are not intended as a substitute for the stepwise calculation methods, but would serve as a supplement. The curves would also be useful in indicating the relative effects of combustor geometry and operating conditions on combustor total-pressure loss and airflow distribution. The present report is concerned with the development of such generalized curves for tubular combustors having (1) constant annulus and liner cross-sectional areas along the combustor axis and (2) flush circular holes in the liner wall. The results should apply approximately to can annular combustors and to annular combustors having equal velocities in the inner and outer annuli at all stations along the combustor.

From compressible- and incompressible-flow calculations, the combustor total-pressure-loss coefficient and fractional liner airflow distribution are obtained in terms of the following dimensionless parameters: (1) combustor reference Mach number, (2) ratio of combustor-exit to -inlet total temperature, (3) fraction of total airflow passing through the liner dome, (4) $A_{h,T}/A_r$, and (5) A_L/A_r, where $A_{h,T}$ is the liner total open hole area and A_L and A_r are the liner and combustor total cross-sectional areas, respectively. The calculations include the effects of heat release, annulus wall friction, and variation in the discharge coefficient of the liner wall openings along the combustor.

ANALYSIS

The present report considers the effect on combustor total-pressure loss of (1) mixing of high-velocity liner air jets with the liner gas stream, (2) heat release, and (3) annulus wall friction. The total-pressure loss resulting from these factors is calculated for tubular combustors having constant annulus and liner cross-sectional areas along the combustor axis and flush circular liner wall openings.

Values of the combustor total-pressure-loss coefficient for cold flow are presented for the cases of incompressible and compressible flow. Compressible-flow calculations were made for reference Mach numbers up to 0.15. All values of the combustor total-pressure-loss coefficient for flow with heat release were obtained from the incompressible-flow calculations. The liner airflow distribution and liner air-jet entrance angles are obtained in the course of the calculations of the total-pressure-loss coefficient. A list of the symbols used in the calculations is presented in appendix A.

A sketch of the tubular, parallel-wall combustor considered is presented in figure 1(a). In this figure, station 1 is the combustor inlet, station 2 is just upstream of the first air admission opening in the liner wall excluding openings in the liner dome, and station 3 is just downstream of the last air admission opening in the liner wall. The cross-sectional area at station 1 is the combustor reference cross-sectional area A_r, and inlet flow conditions are referenced at this station. If the air distribution along the combustor is directly proportional to liner open hole area, the liner airflow distribution for a representative turbojet combustor might correspond to the segmented curve of figure 1(b). The fraction of the total airflow passing through the liner at a given station w_L/w_T is plotted against the dimensionless parameter x/l, where l is the axial distance between stations 2 and 3 and x is the axial distance downstream of station 2. The segmented distribution curve corresponding to a finite number of liner wall openings may be replaced approximately by the continuous distribution curve corresponding to an infinite number of liner wall openings or, rather, to continuous slots between stations 2 and 3.

The orifice discharge equation for a given liner wall opening, such as is illustrated in figure 1(c), is given by

$$\Delta w_L = C\rho_{st,j}V_j\Delta A_h \tag{1}$$

For a differential portion of the air passing through the opening, equation (1) becomes

$$dw_L = C\rho_{st,j}V_j dA_h \tag{2}$$

In the use of equation (2), it is assumed that the flow in the jet from the annulus to the vena contracta is isentropic and that the static pressure in the vena contracta equals that within the liner at the station considered. The effect of cross-sectional area blockage of the liner gas stream by the air jet on the local static pressure at the vena contracta is neglected. The term $\rho_{st,j}V_j$ in equation (2) may then be determined from the annulus total pressure and temperature and the liner static pressure at the station considered. In the calculation of flow conditions in the parallel wall combustor, the airflow distribution in the liner was assumed to be of a continuous form such as illustrated by the smooth curve of figure 1(b), thus allowing the integration of equation (2).

Incompressible-Flow Calculations

Combustor total-pressure-loss coefficient. - As shown in appendix B, for the case of incompressible flow, equation (2) may be rearranged and integrated between stations 2 and 3 to obtain the dimensionless equation

$$\int_{w_{L,2}/w_T}^{1} \frac{d\frac{w_L}{w_T}}{C\sqrt{\frac{P_A - p_L}{q_r}}} = \frac{A_{h,T}}{A_r} \tag{3}$$

In equation (3) the annulus total pressure P_A may be calculated from the combustor-inlet total pressure and the friction pressure drop along the annulus, while the liner static pressure p_L may be calculated from the momentum equation for the liner gas stream. For the case where the annulus and liner cross-sectional areas are constant along the combustor, the term $(P_A - p_L)/q_r$ of equation (3) is related to the combustor total-pressure-loss coefficient $\Delta P/q_r$ by

$$\frac{P_A - p_L}{q_r} = \frac{P_1 - P_{L,3}}{q_r} - \frac{P_1 - P_A}{q_r} - \left(\frac{A_r}{A_L}\right)^2\left[\frac{T_{L,3}}{T_1} - 2\frac{T_L}{T_1}\left(\frac{w_L}{w_T}\right)^2\right] + \frac{A_r}{A_L}\frac{A_r}{A_A}\left(1 - \frac{w_L}{w_T}\right)^2 \tag{4}$$

where $(P_1 - P_{L,3})/q_r$ is the combustor total-pressure-loss coefficient $\Delta P/q_r$. The principal assumptions required in the derivation of equation (4) are

(1) The actual flow can be approximated with sufficient accuracy by one-dimensional equations.

(2) The liner air jets mix instantaneously with the liner gas stream.

(3) The effect of fuel flow on molecular weight and weight flow of the liner gas stream can be neglected.

(4) Heat transfer between the annulus and liner gas streams is negligible.

(5) Mixing losses in the annulus are negligible.

(6) Liner wall friction is negligible.

(7) Density is independent of pressure changes along the combustor and is affected only by the temperature changes along the combustor associated with heat release.

The relation between $\Delta P/q_r$ and $A_{h,T}/A_r$ is obtained by the simultaneous solutions of equations (3) and (4). A value of $A_{h,T}/A_r$ is obtained for specified values of $\Delta P/q_r$ and A_L/A_r, and values of $(P_1 - P_A)/q_r$ and T_L/T_1 along the combustor. In equation (4), T_L and $T_{L,3}$ are the average temperatures of the liner gas stream at a given station and at the combustor exit, respectively. The evaluation of T_L with combustion would require knowledge of the fuel-air ratio and average combustion efficiency along the combustor. In typical combustors, the major portion of the inlet air is bypassed around the liner dome where all of the fuel is injected. Accordingly, the average fuel-air ratio of the liner gas stream may vary from values well in excess of stoichiometric at the upstream end of the combustor to lean fuel-air ratios at the combustor exit. For the case where all the fuel is injected at the liner dome, the average fuel-air ratio F_L of the liner gas stream at various stations along the combustor is given by

$$F_L = \frac{F_{L,3}}{\frac{w_L}{w_T}} \tag{5}$$

where $F_{L,3}$ is the over-all fuel-air ratio of the combustor.

In the present calculations, the combustion efficiency was assumed to be 100 percent in the downstream portion of the combustor where the average fuel-air ratio of the liner gas stream is stoichiometric or leaner. In the upstream portion of the combustor where the overrich

fuel-air ratios exist, the average temperature of the liner gas stream was assumed to be that corresponding to a stoichiometric fuel-air ratio and 100-percent combustion efficiency. The accuracy of the calculated hot-flow total-pressure-loss coefficient is limited by the accuracy in the determination of gas stream temperature T_L along the combustor.

Figure 2 presents values of T_L/T_1 for 100-percent combustion efficiency and a range of fuel-air ratios. The curve was calculated by the method of references 5 and 6 for T_1 equal to 728° R and for normal octane at an initial temperature of 540° R. From figure 2 and equation (5), the temperature ratio T_L/T_1 of equation (4) may be calculated for various values of w_L/w_T and $F_{L,3}$. Values of $F_{L,3}$ may be obtained from figure 2 and assigned values of the combustor over-all temperature ratio $T_{L,3}/T_1$.

The annulus total-pressure-loss term $(P_1 - P_A)/q_r$ of equation (4) can be calculated from the relation

$$\frac{P_1 - P_A}{q_r} = \frac{4f_A \frac{l}{D}}{\left(\frac{A_A}{A_r}\right)^2\left[1 - \left(1 - \frac{A_A}{A_r}\right)^{1/2}\right]} \int_0^{x/l} \left(1 - \frac{w_L}{w_T}\right)^2 d\left(\frac{x}{l}\right) \qquad (6)$$

where the friction factor f_A is assumed to be constant. The use of equation (6) requires a preliminary estimation of liner airflow distribution along the combustor. In the present calculations, and for the case of zero flow through the liner dome, the liner airflow distribution used in equation (6) was

$$\frac{w_L}{w_T} = \left(\frac{x}{l}\right)^2 \qquad (7)$$

Values of f_A and l/D of 0.005 and 4, respectively, were used in equation (6).

Airflow distribution and air-jet entrance angles. - The liner airflow distribution is obtained as shown in appendix B from the relation

$$\frac{\int_{w_{L,2}/w_T}^{w_L/w_T} \frac{d\left(\frac{w_L}{w_T}\right)}{C\sqrt{\frac{P_A - p_L}{q_r}}}}{\int_{w_{L,2}/w_T}^{1} \frac{d\left(\frac{w_L}{w_T}\right)}{C\sqrt{\frac{P_A - p_L}{q_r}}}} = \frac{A_h}{A_{h,T}} \tag{8}$$

From equation (8), values for the fractional liner open hole area $A_h/A_{h,T}$ may be calculated for various values of w_L/w_T.

For thin-walled air-admission openings in the liner, the entrance angle θ of the liner air jets (fig. 1) is calculated from the relation

$$\theta = \cos^{-1}\frac{V_A}{V_j} \tag{9}$$

where

$$\frac{V_A}{V_j} = \frac{\left(1 - \frac{w_L}{w_T}\right)}{\frac{A_A}{A_r}\sqrt{\frac{P_A - p_L}{q_r}}} \tag{10}$$

Compressible-Flow Calculations

The compressible-flow calculations of the combustor total-pressure-loss coefficient, airflow distribution, and liner air-jet entrance angles are similar to the incompressible-flow calculations. The assumptions made in the use of equation (2) as well as assumptions (1) to (6) made in the derivation of equation (4) are also made in the compressible-flow calculations. As a result of the complexity of the compressible-flow relations, however, the relation between liner static pressure and annulus total pressure is not obtained directly as in equation (4) for

the case of incompressible flow. Details of the compressible-flow calculations are presented in appendix C. The compressible-flow calculations presented herein were made only for the case of cold flow. However, the equations and procedure used for the case of flow with combustion are presented in appendix C.

Combustor total-pressure-loss coefficient. - As shown in appendix C, equation (2) may be rearranged and integrated along the combustor between stations 2 and 3 to yield the following dimensionless equation:

$$\int_{w_{L,2}/w_T}^{1} \frac{M_1^* \, d\left(\frac{w_L}{w_T}\right)}{C\left(\frac{\rho_{st}V}{\rho_t a_t}\right)_j \frac{P_A}{P_1}} = \frac{A_{h,T}}{A_r} \tag{11}$$

M_1^* in equation (11) is related to the combustor reference Mach number M_r. The term $(\rho_{st}V/\rho_t a_t)_j$ is obtained from the momentum equation for the liner. As shown in appendix C, values of $(\rho_{st}V/\rho_t a_t)_j$ for cold flow may be calculated in terms of w_L/w_T for specified values of $\Delta P/q_r$, A_L/A_r, and M_r. As in the incompressible-flow calculations, the annulus total pressure P_A is obtained from friction pressure-drop relations and a preliminary estimate of the liner airflow distribution. For the compressible-flow calculations, the liner airflow distribution used to calculate friction pressure drop was also assumed to follow equation (7), and the values of f_A and l/D were also assumed to equal 0.005 and 4, respectively. Then from equation (11), values of $A_{h,T}/A_r$ for cold flow may be obtained for specified values of $\Delta P/q_r$, A_L/A_r, and M_r.

Airflow distribution and air-jet entrance angles. - The liner airflow distribution for the compressible-flow case is obtained as shown in appendix C from

$$\frac{\int_{w_{L,2}/w_T}^{w_L/w_T} \frac{M_1^* \, d\left(\frac{w_L}{w_T}\right)}{C\left(\frac{\rho_{st}V}{\rho_t a_t}\right)_j \frac{P_A}{P_1}}}{\int_{w_{L,2}/w_T}^{1} \frac{M_1^* \, d\left(\frac{w_L}{w_T}\right)}{C\left(\frac{\rho_{st}V}{\rho_t a_t}\right)_j \frac{P_A}{P_1}}} = \frac{A_h}{A_{h,T}} \tag{12}$$

From equation (12), values of $A_h/A_{h,T}$ may be calculated for various values of w_L/w_T.

The entrance angle θ of the liner air jets (see fig. 1(c)) is obtained as shown in appendix C from the relation

$$\theta = \cos^{-1} \frac{M_A}{M_j} \tag{13}$$

Discharge Coefficient of Liner Wall Openings

Values of the liner wall opening discharge coefficient C required in the calculations of the combustor total-pressure-loss coefficient and airflow distribution may be obtained from correlations such as those presented in reference 7. The present calculations were based on the correlation from reference 7 for a 3/4-inch-diameter hole in a 0.040-inch wall. The correlation curves for this opening are presented in figure 3. In figure 3(a), the discharge coefficient C_p corrected to a static-pressure ratio p_A/p_j of unity is plotted against the correlating parameter $\frac{P_A - p_j}{P_A - p_A}$. In figure 3(b), the ratio C/C_p is plotted against the static-pressure ratio p_A/p_j. The discharge coefficient C is obtained from the relation

$$C = C_p \left(\frac{C}{C_p}\right) \tag{14}$$

For incompressible-flow calculations, the correlation parameter $\frac{P_A - p_j}{P_A - p_A}$ of figure 3(a) may be taken equal to $\left(\frac{V_j}{V_A}\right)^2$ and the pressure-ratio correction C/C_p of figure 3(b) can be neglected; thus, the discharge coefficient C is obtained directly from figure 3(a) and the given value of $(V_j/V_A)^2$.

In theory, one would expect that the discharge coefficient C is related to the product of the discharge coefficient for flow normal to the hole C_n and the ratio of the normal component of velocity to the resultant jet velocity V_n/V_j. The term V_n/V_j is related to the air-jet entrance angle θ from the complementary function of equation (9) by

$$\frac{V_n}{V_j} = \sqrt{1 - \frac{V_A^2}{V_j^2}} = \sin \theta \tag{15}$$

The relation between the experimental value of C taken from the data of figure 3(a) and $\sin \theta$ is shown in figure 4. The dashed curve represents the theoretical equation

$$C = C_n \sin \theta \tag{16}$$

where C_n was obtained from the experimental curve at $\sin \theta = 1.0$. The experimental curve exhibited linearity only for values of $\sin \theta$ greater than 0.45. For values of $\sin \theta$ greater than 0.45, the experimental-discharge-coefficient data of figure 3(a) can be represented by the following empirical equation:

$$C = 0.827 \sin \theta - 0.232 \tag{17}$$

The data of figure 3, however, were used directly for calculations involving discharge coefficients in this report because of their wider range of application.

The correlation of figure 3 gives only the effect of annulus flow on the discharge coefficient. Data of references 8 and 9 indicate that there can also be a large effect of liner gas stream velocity on the discharge coefficient. However, provided the component of the jet velocity normal to the liner wall is larger than the local liner gas stream velocity, the effect of liner gas stream velocity on the discharge coefficient would appear to be small (refs. 8 and 9). Since such a condition existed for most of the calculations of the present report, the effect of liner gas stream velocity on the discharge coefficient was neglected.

RESULTS AND DISCUSSION

Results presented herein pertain only to parallel-wall combustors with flush liner hole openings. The results are considered representative of typical flush liner wall openings even though they are based on only one particular air admission hole geometry, since the data of reference 7 showed that the effects of hole diameter and wall thickness on discharge coefficient were small compared to the effects of annulus flow shown in figure 3. The data may not be applicable to combustor liners having a substantial portion of the air admitted through louvers or through holes having intake scoops to direct the air through them.

The calculation of combustor total-pressure loss and airflow distribution requires a knowledge of static and total pressures in the annulus and in the liner along the axis of the combustor from station 2 to station 3 (fig. 1). Figure 5(a) shows the variation of calculated static and total pressures along the combustor expressed as a ratio of pressure at a given station to the inlet total pressure at station 1.

This pressure ratio is plotted against the fractional distance along the combustor axis from station 2 to 3. The data for figure 5 were computed for a reference velocity V_r of 100 feet per second, an inlet total pressure P_1 of 30 inches of mercury absolute, and zero flow through the liner dome ($w_{L,2}/w_T = 0$), using incompressible-flow equations including annulus wall friction. The calculations were made for a combustor with a ratio of liner cross-sectional area to reference area A_L/A_r of 0.6, a ratio of total liner open hole area to reference area $A_{h,T}/A_r$ of 1.09, and a total-temperature ratio across the combustor $T_{L,3}/T_1$ of 1 (cold flow) and 3. The curves shown are for the case of uniformly distributed liner wall openings along the length of the combustor.

It may be seen in figure 5(a) that the total pressure of the liner gas stream increases with an increase in x/l in the upstream portion of the combustor, reaches a maximum, and then decreases in the downstream portion of the combustor. The variation in the total pressure of the liner gas stream for cold-flow conditions is a result of the difference in velocity of the annulus and liner gas streams. In the upstream portion of the combustor, annulus air at high axial velocity mixes with the low-velocity liner airstream and, hence, increases the total pressure of the liner airstream. In the downstream portion of the combustor, the mixing of the low-velocity annulus air with the high-velocity liner airstream results in a decrease in total pressure of the liner airstream. The maximum total pressure of the liner airstream for cold flow occurs at the station where the axial velocities of the two streams are equal. The curve for the static pressure of the liner airstream exhibits a similar trend, although differing in location of the maximum pressure and the magnitude of the pressure variation. The curves shown in figure 5(a) are intended only to illustrate typical trends in pressure along a combustor; actual values of pressure will vary with combustor geometry and operating conditions.

The static-pressure drop across the liner wall openings is shown in figure 5(b) to reach a minimum in the upstream portion of the combustor and then to increase steadily along the axis of the combustor. The pressure-drop terms required for the determination of the flow parameter $\frac{P_A - p_j}{P_A - p_A}$ (fig. 3(a)) are also presented in figure 5(b). The calculated flow parameter is plotted against fractional liner distance in figure 5(c). A comparison of the curves of figures 3(a) and 5(c) shows that in a parallel-wall combustor the discharge coefficients of the liner hole openings are a minimum at the upstream end of the combustor and a maximum at the exhaust end. Discharge coefficients range from about 0.1 for the upstream liner holes, to about 0.6 for the holes at the extreme end of the liner. A variation in discharge coefficients along the liner such as

is illustrated by these data would be expected in all parallel-wall combustors with flush liner hole openings; the actual values of discharge coefficients for any given combustor will vary, however, as the pressure distribution along the liner is altered. Since the discharge coefficient and static-pressure drop are indicative of the relative airflow through openings of a given size, it is evident that the openings in the upstream region of the liner pass less flow per unit area than those in the downstream region of the liner.

Combustor Total-Pressure-Loss Coefficient

Effect of liner cross-sectional area and liner total open hole area. - Figure 6 shows the effect of (1) the ratio of liner total open hole area to combustor reference area and (2) the ratio of the liner cross-sectional area to combustor reference area on the combustor total-pressure-loss coefficient $\Delta P/q_r$. The data were calculated from incompressible-cold-flow relations described in appendix B with zero flow through the liner dome, and with and without considering the effects of annulus wall friction. For any given value of A_L/A_r, the pressure-loss coefficient $\Delta P/q_r$ asymptotically approaches a minimum value as $A_{h,T}/A_r$ is increased over a value of about 1.5. For any given value of A_L/A_r, the pressure-loss coefficient, $\Delta P/q_r$, increases very rapidly as $A_{h,T}/A_r$ is decreased to values below about 1.0.

The consideration of annulus wall friction in the pressure-loss calculations tends to increase $\Delta P/q_r$ for given values of $A_{h,T}/A_r$ and A_L/A_r. The effect of annulus wall friction increased as the annulus area decreased, that is, as A_L/A_r increased. The importance of annulus wall friction on the calculations will, of course, vary with the combustor l/D and airflow distribution. The dashed curves of figure 6 were calculated for an l/D of 4, which is higher than that found in practice, and for an airflow distribution given by equation (7), which corresponds approximately to some fractional open hole area distributions found in practice. Values of $\Delta P/q_r$ for an l/D less than 4 and for the airflow distribution given by equation (7) may be estimated from linear interpolation between the solid curves (negligible wall friction) and the dashed curves of figure 6.

Figure 7 presents the variation of the minimum combustor total-pressure-loss coefficient $\Delta P/q_r$ with the ratio of liner cross-sectional area to reference area A_L/A_r. The data for figure 7 were calculated from incompressible-cold-flow relations assuming annulus wall friction

negligible with zero flow through the liner dome $\left(\frac{w_{L,2}}{w_T} = 0\right)$. The minimum combustor total-pressure-loss coefficient is obtained by arbitrarily setting liner static pressure equal to annulus static pressure at station 2 and is calculated from equation (B24) of appendix B. The value obtained for the minimum total-pressure-loss coefficient for any given value of A_L/A_r is independent of the discharge coefficients of the liner wall openings and corresponds to relatively large values of liner total open hole area $\left(\frac{A_{h,T}}{A_r} > 2.0\right)$. Figure 7 shows that a minimum cold flow $\Delta P/q_r$ is obtained by using a liner that blocks 50 percent of the total cross-sectional area of the combustor. Either increasing or decreasing the percent blocked area from a mean of 50 percent tends to increase $\Delta P/q_r$. The data of figures 6 and 7 show that for a parallel-wall combustor an $A_{h,T}/A_r$ greater than 1.0 and an A_L/A_r between 0.4 and 0.6 are desirable in order to obtain a low cold-flow total-pressure loss.

Effect of airflow through liner dome. - The effects of the fraction of total airflow passing through the liner dome $w_{L,2}/w_T$ on the calculated combustor total-pressure-loss coefficient are illustrated in figure 8. The values were calculated from the incompressible-flow relations neglecting the effect of annulus wall friction. As would be expected, an increase in $w_{L,2}/w_T$ decreases the total-pressure-loss coefficient throughout the range of values of $A_{h,T}/A_r$ covered in the figure because the effective open hole area of the liner has been increased by opening holes in the liner dome. The value of $A_{h,T}/A_r$ does not include the open hole area in the liner dome. The open hole area in the liner dome required to pass the specified $w_{L,2}/w_T$ may be calculated from the orifice discharge equation in conjunction with the total pressure upstream of the liner dome, values of the discharge coefficient of the liner dome openings, and the static pressure in the liner at station 2 $p_{L,2}$. Discharge coefficients for swirler-type liner dome openings are presented in reference 10. Values of $p_{L,2}$ may be obtained from equation (B18) of appendix B for w_L/w_T equal to $w_{L,2}/w_T$.

Effect of combustor reference Mach number. - The effects of combustor reference Mach number M_r at station 1 (see fig. 1) on the calculated combustor total-pressure-loss coefficient are illustrated in figures 9, 10, and 11. The curves for M_r equal to 0.05, 0.10, and 0.15 were calculated from the compressible-flow relations of appendix C. The incompressible-flow data of figure 6 are also included in these

figures for comparison with the compressible-flow data. The data were computed for an A_L/A_r of 0.5, 0.6, and 0.7 with cold flow and with zero flow through the liner dome. The data of figures 9 and 10 were computed neglecting annulus wall friction. A comparison of data calculated with and without the effects of annulus wall friction is shown in figure 11.

Figure 9 indicates that increasing M_r up to 0.10 results in a relatively small increase in $\Delta P/q_r$; therefore, at values of M_r below 0.1, the results of the incompressible-flow relations agree quite well with the results of the compressible-flow relations. The incompressible-flow relations are considered sufficiently accurate for design purposes for combustors operating below an M_r of 0.1. However, for M_r above approximately 0.10, there is an increase in $\Delta P/q_r$ with increase in M_r, particulary at values of A_L/A_r over about 0.6. The effect of reference Mach number on $\Delta P/q_r$ is shown more clearly in figure 10 in which the data of figure 9 are cross-plotted for a value of $A_{h,T}/A_r = 1.0$. Figure 11 indicates the calculated increase in $\Delta P/q_r$ with M_r when annulus wall friction effects are included.

Effect of heat release. - The variation in $\Delta P/q_r$ with $A_{h,T}/A_r$ for various values of temperature ratio across the combustor $T_{L,3}/T_1$ and various values of A_L/A_r is presented in figure 12. The data for these curves were obtained from incompressible-flow relations including annulus wall friction for a $w_{L,2}/w_T$ of 0 and 0.1. The curves for a $w_{L,2}/w_T$ of 0.1 were obtained from the calculations for a $w_{L,2}/w_T$ of zero by the method presented in appendix B. Use of this method for the case where annulus wall friction effects are included in the calculations necessitated the preliminary estimation of the airflow distribution by the curves of figure 13 in the calculations of annulus total pressure. The curve for a $w_{L,2}/w_T$ of zero corresponds to that of equation (7). Approximate values of the combustor total-pressure-loss coefficient for values of $w_{L,2}/w_T$ between 0 and 0.1 may be obtained from linear interpolation between the solid and dashed curves of figure 12.

The combustor total-pressure-loss coefficient increases as combustor exhaust temperature is increased. The relative effect of airflow through the liner dome and annulus wall friction on $\Delta P/q_r$ is the same for hot flow as it was for cold flow. The data of figure 12 are cross-plotted in figure 14 to show the effect of the temperature ratio $T_{L,3}/T_1$ on $\Delta P/q_r$. Curves of $\Delta P/q_r$ against $T_{L,3}/T_1$ are shown for A_L/A_r values

of 0.5, 0.6, and 0.7 and $A_{h,T}/A_r$ values of 0.6 and 1.6. For a given value of $A_{h,T}/A_r$ the total-pressure-loss coefficient increases with temperature ratio at a more rapid rate as A_L/A_r decreases. As a result, at higher values of temperature ratio, larger A_L/A_r values are required to minimize $\Delta P/q_r$. A value of A_L/A_r of 0.5 provided minimum $\Delta P/q_r$ under cold-flow conditions; a value of 0.6 provides the lowest total-pressure loss at temperature ratios above about 2.0. This effect is shown more clearly in figure 15 where $\Delta P/q_r$ is plotted against A_L/A_r for various temperature ratios across the combustor. These data were obtained from incompressible-flow relations including annulus wall friction with zero liner dome flow for values of $A_{h,T}/A_r$ of 0.6 and 1.6. For combustors with $A_{h,T}/A_r$ equal to 0.6 or 1.6 the value of A_L/A_r for a minimum $\Delta P/q_r$ shifts from 0.5 to 0.6 as combustor exhaust temperature is increased.

Airflow Distribution

The airflow distribution curves obtained from incompressible- and compressible-flow calculations are presented in figures 16 to 23. Except for the effects of variation in annulus wall friction with airflow distribution, the relations between w_L/w_T and $A_h/A_{h,T}$ presented in figures 16 to 23 are independent of the distribution of air entry holes along the liner. Accordingly, the variation of w_L/w_T along the combustor for a particular liner configuration may be estimated from the given values of $A_h/A_{h,T}$ along the combustor and the appropriate figure from figures 16 to 23. If, for example, there is a linear increase in liner open hole area along the combustor ($A_h/A_{h,T} = x/l$), the curves of figures 16 to 23 represent the variation in liner airflow with distance along the combustor. It is emphasized that the relations presented are representative only for parallel-wall combustors having flush liner air openings (see fig. 1).

Effect of liner total open hole area. - The fraction of total air passing through the liner at any given station along the combustor w_L/w_T is plotted against the fraction of liner total open hole area $A_h/A_{h,T}$ in figure 16 for values of A_L/A_r of 0.5, 0.6, and 0.7. Curves are shown for various values of $A_{h,T}/A_r$, and the data were obtained from compressible-flow relations for reference Mach numbers of 0.05, 0.10, and 0.15. Data obtained from the incompressible-flow relations are also presented. Cold-flow conditions with zero liner dome flow

($w_{L,2}/w_T = 0$) and with negligible annulus wall friction were assumed. The 45° dashed line on the airflow distribution curves represents the airflow distribution that would be obtained if each hole in the liner admitted a quantity of air directly proportional to its area. Increasing the liner total open hole area $A_{h,T}$ decreases the fraction of total air entering the upstream region of the combustor liner. This decrease in upstream liner airflow becomes appreciable at large values of $A_{h,T}/A_r$. This reduction in w_L/w_T is a result of higher reductions in pressure drop and discharge coefficient for the holes at the upstream stations than for those at the downstream stations. The reduction becomes more critical as A_L/A_r is increased from 0.5 to 0.7. This effect is partially due to increased velocities in the upstream region of the annulus, which reduce the discharge coefficient of upstream holes in the liner (ref. 7).

Effect of combustor reference Mach number. - The effect of reference Mach number on combustor airflow distribution is shown in figure 16 for cold flow. Increasing reference Mach number decreases the fraction of the total airflow entering the liner through the upstream liner hole openings. The increased velocity in the upstream end of the annulus reduced the static-pressure drop and the discharge coefficient of upstream holes in the liner. The effect of Mach number becomes more pronounced as A_L/A_r is increased because of increased upstream velocities in the annulus. For the data presented in figure 16 annulus wall friction was neglected. Figure 17 shows the airflow distribution calculated from the compressible-flow relations with annulus wall friction included. The results are similar to those shown in figure 16 with the exception that annulus wall friction tends to increase the fraction of air entering the liner through the upstream holes in the liner. Friction reduced the total pressure in the downstream end of the annulus, resulting in a lower pressure drop across the holes in this region, and hence, reduced airflow. The effect of reference Mach number on airflow distribution is shown more clearly in figure 18 where the data of figures 17(c) to (e) are replotted for $A_{h,T}/A_r$ equal to 0.6 and 1.6. Larger reductions in the fraction of total air entering the liner through the holes in the upstream region of the combustor occur at higher values of $A_{h,T}/A_r$ and at higher values of M_r.

The airflow distributions obtained from incompressible-flow relations with and without annulus wall friction are compared in figure 19 for $A_{h,T}/A_r$ equal to 0.6 and 1.6 and A_L/A_r equal to 0.5, 0.6, and 0.7. Including annulus wall friction in the computations tends to increase the fraction of total air entering the upstream region of the liner. The effect is more pronounced at higher values of A_L/A_r and at higher values of $A_{h,T}/A_r$. The change in airflow distribution is a

direct result of the added pressure loss in the annulus; increased A_L/A_r increases the velocity in the annulus, which in turn increases pressure loss due to friction.

Effect of heat release. - The effect of heat release on airflow distribution is shown in figure 20 for A_L/A_r equal to 0.5, 0.6, and 0.7. These data were obtained from the incompressible-flow relations with annulus wall friction included and zero liner dome flow. Curves are shown for values of $T_{L,3}/T_1$ of 1, 2, 3, and 4. Increases in combustor temperature ratio tend to decrease the fraction of total air entering the upstream region of the liner. Heat release affects the liner pressures and velocities along the combustor, which in turn affect the static-pressure drop and the discharge coefficient of the liner wall openings. The data for $A_{h,T}/A_r$ equal to 0.6 and 1.6 are cross-plotted in figure 21 to show more clearly the effect of temperature ratio on airflow distribution. The decrease in upstream liner airflow with increasing combustor temperature ratio is more pronounced for larger values of $A_{h,T}/A_r$ and smaller values of A_L/A_r.

Effect of liner cross-sectional area. - The effect of the ratio of liner cross-sectional area to reference area on airflow distribution is shown in figure 22 for flow with and without heat release. The data were obtained from incompressible-flow relations for values of $A_{h,T}/A_r$ of 0.6 and 1.6 with annulus wall friction and zero liner dome flow. The fraction of total air entering the upstream region of the combustor increases as the combustor liner area is reduced for cold flow (fig. 22(a)). The effect is similar to that of reference Mach number; that is, as velocity in the annulus is reduced by a reduction in reference Mach number or an increase in annulus area, the static-pressure drop and the orifice coefficients of the upstream liner holes increase. Calculations showed, however, that an A_L/A_r of 0.4 would have about the same cold-flow airflow distribution as an A_L/A_r of 0.6 despite the effect of reduced upstream annulus velocity. This reversal is attributed to high velocities in the downstream end of the liner, which increase the static-pressure drop across the holes in the downstream region in the liner and thus increase the fraction of total air entering this region.

The effect of combustor liner area on airflow distribution with a temperature ratio of 4 across the combustor is shown in figure 22(b). In this case the fraction of total air entering the upstream region of the combustor increases as A_L/A_r is increased from 0.5 to 0.7. The increased sensitivity of the airflow distribution to changes in $T_{L,3}/T_1$ for the smaller values of A_L/A_r causes a reversal in the effect of

annulus area on airflow distribution. For cold flow ($T_{L,3}/T_1 = 1$) an increase in A_L/A_r from 0.5 to 0.7 reduces the flow to the upstream end of the combustor. However, the opposite trend is found for $T_{L,3}/T_1$ equal to 4.

Effect of airflow through liner dome. - The effect of flow through the liner dome on the airflow distribution is illustrated in figure 23 for the case of incompressible cold flow and negligible annulus wall friction. An increase in the flow through the liner dome for a given value of $A_{h,T}/A_r$ increases the flow through the upstream end of the combustor. Adding air through openings in the liner dome also tends to distribute the air in more direct proportion to the open area.

Liner Air-Jet Entrance Angle

The variation of liner air-jet entrance angle θ with x/l for various values of $A_{h,T}/A_r$ and A_L/A_r is shown in figure 24. The calculations are for cold flow and include the effects of annulus wall friction. The curves shown are for the case of liner wall openings uniformly distributed along the length of the combustor. The value of θ is a minimum at low values of x/l at the upstream end of the combustor where the static-pressure drop across the holes is lower and the annulus velocity higher than corresponding values for the downstream liner openings. The air jet is not perpendicular to the plane of the hole until the last liner hole station is approached. Increasing $A_{h,T}/A_r$ from 0.6 to 1.6 and increasing A_L/A_r from 0.5 to 0.7 decreases the relative value of θ, the reduction being more pronounced in the upstream portion of the combustor. It is to be noted that the data of figure 24 do not include the effect of liner air-jet deflection by the liner gas stream; this deflection can be appreciable in the downstream region of the combustor liner.

SIGNIFICANCE OF RESULTS TO TURBOJET COMBUSTOR DESIGN

The thrust and cycle efficiency of a turbojet engine may be increased by reducing the total-pressure loss associated with the combustion chamber. Curves are presented in this report that show the effect of a number of combustor geometric and flow variables on the total-pressure-loss coefficient for a parallel-wall combustor. It is shown that the hot-flow pressure loss can be minimized by designing the combustor with a ratio of liner to total cross-sectional area of 0.6 and a total liner open hole area greater than the total cross-sectional area. The percent total-pressure loss of a combustor with a constant total-pressure-loss coefficient increases with the square of reference Mach

number $\left(\frac{\Delta P}{P} = \frac{\Delta P}{q_r}\frac{\gamma_a}{2}\left(\frac{p}{P}\right)_r M_r^2\right)$. The total-pressure loss becomes even more severe when the total-pressure-loss coefficient $\Delta P/q_r$ also increases with reference Mach number. The severity of the increase in total-pressure loss can be minimized, however, by adequately designing the liner cross-sectional area and total open hole area as suggested previously. Increasing the combustor frontal area is another means of reducing reference velocity and the pressure losses related to high velocity.

It is shown that the percent of total air entering the upstream region of the liner where combustion of the fuel occurs is reduced as combustor exhaust temperature is increased. The application of turbine cooling techniques to turbojet engines will permit higher combustor exhaust gas temperatures for increased thrust output. These conditions will require the use of a larger percentage of the total airflow in the combustion process. If the combustion process is to occur in the same upstream region for high-temperature operation as for low-temperature operation then a larger percentage of air must be admitted into the upstream region. Future combustors may also be required to operate at higher reference Mach numbers because of the increased mass flow per unit frontal area that can be handled by the newer compressor designs. It was found that increasing reference Mach number also decreases the fraction of total air entering the upstream region of the liner.

Desirable decreases in pressure loss of the combustor may be obtained by increasing the liner total open hole area. This also entails reductions in the upstream liner airflow. Thus, providing for adequate air into the upstream primary combustion zone of combustors without inducing excessive pressure losses will be a big problem in future combustor development. Increasing the fraction of total open hole area in the upstream region of the liner may or may not alleviate the problem since the discharge coefficient of upstream liner holes can vary over a wide range as annulus flow conditions are varied. Providing adequate air admission for the severe operating conditions by increasing upstream total open hole area could result in excessive air admission for the less severe operating conditions. The use of scoops or shrouds in the primary or upstream end of the combustor may provide at least a partial solution to this problem.

This report illustrates the effects of geometric configurations and operating conditions on the distribution of air to the combustion chamber without considering the effects of these factors on combustor performance and stability. The effect of mass-flow distribution on the performance of a homogeneous ram-jet combustor, based on theoretical calculations, is presented in reference 11. Also available are experimental design data for turbojet combustors which show the effects on performance of a number of geometric variables, including the open hole area distribution (ref. 12).

APPLICATION OF ANALYTICAL TECHNIQUE

The combustor total-pressure-loss coefficient and the airflow distribution of a given parallel-wall tubular combustor design can be estimated from the curves provided in the report by determining the dimensionless parameters M_r, $T_{L,3}/T_1$, $w_{L,2}/w_T$, $A_{h,T}/A_r$, A_L/A_r, and l/D. The curves based on compressible-flow relations are preferred over the incompressible-flow relations for all cases for determining the combustor total-pressure loss and the airflow distribution. However, the results comparing compressible- and incompressible-flow relations show that at reference Mach numbers below about 0.1 similar results should be obtained from both curves. Appreciable error can be introduced using incompressible-flow relations at higher reference Mach numbers, especially for combustors with small annulus air passages which have relatively high annulus velocities. Generalized curves are presented which both include and neglect the effect of annulus wall friction for a tubular combustor with an l/D of 4. For many combustor designs, this effect will be small. If the curves presented herein show appreciable effects of annulus wall friction, the choice between the curves will depend on the l/D of the design combustor. For example, the combustor aerodynamics of a design with an l/D of 2 could be determined by interpolating halfway between the curves calculated with and without annulus wall friction.

The curves presented herein can be applied to an annular combustor only if the velocities in the inner and outer annuli at any station are the same and if the walls are parallel.

CONCLUSIONS

The effects of a number of geometric and operating variables of turbojet combustors on combustor total-pressure loss and airflow distribution were determined analytically from compressible- and incompressible-flow relations. The following conclusions were reached for combustors having a given maximum (reference) cross-sectional area, constant annulus and liner cross-sectional areas along the axis, and flush liner wall openings:

(1) Combustor total-pressure loss increases rapidly as liner cross-sectional area is increased above 70 percent of reference area. For a given liner total open hole area, the minimum total-pressure loss is obtained when the liner cross-sectional area is 60 percent of the reference area for combustor temperature ratios from 3 to 4.

(2) Combustor total-pressure loss increases rapidly as the liner total open hole area is decreased below 100 percent of the reference area.

Increasing the liner total open hole area above about 200 percent has little effect on reducing the combustor total-pressure-loss coefficient.

(3) The combustor total-pressure-loss coefficient increases with increasing reference velocities and annulus velocities and with increasing combustor exhaust temperature.

(4) The distribution of air entering the combustor liner is approximately proportional to the open-hole-area distribution only for low values of total open hole area, which entail high pressure losses. Airflow distribution for larger total open hole area required for low pressure losses deviated appreciably from the open-hole-area distribution. For a given liner open-hole-area distribution, the fraction of total air entering the upstream region of the combustor under burning conditions decreased with an increase in liner total open hole area, reference Mach number, and combustor temperature ratio. The discharge coefficients of upstream holes are markedly lower than 0.6; the discharge coefficients of downstream holes approach 0.6.

(5) The liner air-jet entrance angle in the upstream region of the liner is markedly reduced with increases in total open hole area. The jet entrance angle for holes in the downstream region of the liner approaches 90°.

Lewis Flight Propulsion Laboratory
National Advisory Committee for Aeronautics
Cleveland, Ohio, September 17, 1956

APPENDIX A

SYMBOLS

The symbols used in the analysis are as follows:

A	cross-sectional area of any given flow passage, sq ft
A_A	cross-sectional area of annulus formed by outer diameter of liner d and inner diameter of combustor housing D, sq ft
A_h	liner open hole area from station 2 to station at x, sq ft
ΔA_h	liner open hole area from station at x to station at $x + \Delta x$, sq ft
$A_{h,T}$	total open hole area in liner wall (excluding liner dome openings), sq ft
A_L	cross-sectional area of liner, sq ft
A_r	total combustor cross-sectional area; reference area, sq ft
a_t	speed of sound at local total temperature
C	orifice discharge coefficient, ratio of measured to theoretical flow through hole
C_p	orifice discharge coefficient, corrected for pressure-ratio effect
D	inner diameter of combustor housing, ft
d	outer diameter of liner, ft
F	fuel-air ratio by weight
f	Fanning friction factor
g	gravitational constant, 32.2 ft/sec^2
l	length of combustor from station 2, just upstream of first row of holes in liner, to station 3, downstream of last row of holes at end of combustor
M	Mach number based on local average velocity and local static temperature

$M_{t,A}$ Mach number based on local average velocity and local total temperature in annulus of combustor, V/a_t

M^* $\frac{w}{\rho_t a_t A}, \frac{\rho_{st} V}{\rho_t a_t}$

M_1^* $\frac{w_T}{(\rho_t a_t)_1 A_r}, \left(\frac{\rho_{st} V}{\rho_t a_t}\right)_1$

P local total pressure, lb/sq ft

$\Delta P/q_r$ combustor total-pressure-loss coefficient

p local static pressure, lb/sq ft

q dynamic pressure, lb/sq ft

q_r reference dynamic pressure; $\frac{w_T^2}{2g\rho_{st,1}A_r^2}; \frac{\gamma_a}{2} p_1 M_r^2; \frac{\text{lb}}{\text{sq ft}}$

r_H hydraulic radius, ft

T local total temperature, $^\circ R$

t local static temperature, $^\circ R$

V local average velocity, ft/sec

w weight-flow rate of air passing through any given flow passage, lb/sec

w_A weight-flow rate of air passing through annulus at given station, lb/sec

w_L weight-flow rate of air passing through liner at given station, lb/sec

$w_{L,2}/w_T$ fraction of total air passing through liner dome openings

Δw_L weight-flow rate of air passing through liner from station at x to station at $x + \Delta x$, lb/sec

w_T total weight-flow rate of air passing through combustor, lb/sec

x distance along combustor measured from station 2 just upstream of first holes in liner, ft

β,β' functions

γ_a specific-heat ratio of air

γ_g specific-heat ratio of combustion gases

θ entrance angle of air issuing from liner wall openings, deg

ρ_{st} density based on static pressure and static temperature, lb/cu ft

ρ_t density based on total pressure and total temperature, lb/cu ft

φ function

ψ,ψ' functions

Subscripts:

A annulus

j jet issuing from liner wall opening

L liner

n flow normal to hole

r reference

1 combustor inlet

2 station just upstream of first liner wall opening

3 combustor-exit station downstream of last liner wall opening

APPENDIX B

INCOMPRESSIBLE-FLOW CALCULATIONS FOR TUBULAR TURBOJET COMBUSTOR WITH CONSTANT ANNULUS AND LINER CROSS-SECTIONAL AREAS

The orifice discharge equation for a given liner wall opening such as illustrated in figure 1(c) is given by

$$\Delta w_L = C\rho_{st,j}V_j\Delta A_h \tag{1}$$

For a differential portion of the air passing through the opening, equation (1) becomes

$$dw_L = C\rho_{st,j}V_j dA_h \tag{2}$$

It is assumed that the static and total pressures in the vena contracta of the jet are equal to the liner static and annulus total pressures, respectively, at the station considered; then the term $\rho_{st,j}V_j$ in equations (1) and (2) can be determined from Bernoulli's equation for incompressible flow

$$P_A = p_L + \frac{\rho_{st,j}V_j^2}{2g} = p_L + q_j \tag{B1}$$

If the density ρ_{st} is assumed to be independent of pressure changes along the combustor but to vary only with temperature changes resulting from combustion, equation (2) can be put in the following dimensionless form by the substitution of equation (B1) and the introduction of the reference dynamic-pressure term q_r:

$$d\left(\frac{w_L}{w_T}\right) = C\sqrt{\frac{P_A - p_L}{q_r}}\, d\left(\frac{A_h}{A_r}\right) \tag{B2}$$

Equation (B2) may be rearranged and integrated from station 2 (fig. 1) to a given station along the combustor to yield

$$\int_{w_{L,2}/w_T}^{w_L/w_T} \frac{d\left(\frac{w_L}{w_T}\right)}{C\sqrt{\frac{P_A - p_L}{q_r}}} = \int_0^{A_h/A_r} d\left(\frac{A_h}{A_r}\right) = \frac{A_h}{A_r} \tag{B3}$$

The combustor total open hole area $A_{h,T}$ for various combustor total-pressure losses is obtained from

$$\int_{w_{L,2}/w_T}^{1} \frac{d\left(\frac{w_L}{w_T}\right)}{C\sqrt{\frac{P_A - p_L}{q_r}}} = \int_0^{A_{h,T}/A_r} d\left(\frac{A_h}{A_r}\right) = \frac{A_{h,T}}{A_r} \tag{3}$$

while the fractional liner open hole areas $A_h/A_{h,T}$ for various fractional liner airflows w_L/w_T are obtained from

$$\frac{\int_{w_{L,2}/w_T}^{w_L/w_T} \frac{d\left(\frac{w_L}{w_T}\right)}{C\sqrt{\frac{P_A - p_L}{q_r}}}}{\int_{w_{L,2}/w_T}^{1} \frac{d\left(\frac{w_L}{w_T}\right)}{C\sqrt{\frac{P_A - p_L}{q_r}}}} = \frac{A_h}{A_{h,T}} \tag{8}$$

The term $(P_A - p_L)/q_r$ in equations (B3), (3), and (8) is obtained from the solution of the momentum equation. For a differential cross-sectional volume of the parallel-wall combustor of figure 1(a) it is assumed that (1) the flow is one dimensional, (2) the wall friction in the liner is negligible, and (3) the force exerted on the edge of the liner wall openings by the airstream is negligible. Then the differential momentum equation for both the annulus and liner is (see e.g., ref. 13)

$$A_A dp_A + \frac{w_A}{g} dV_A + \frac{V_A}{g} dw_A + \frac{f_A q_A A_A l}{r_{H,A}} d\left(\frac{x}{l}\right) + A_L dp_L + \frac{w_L}{g} dV_L + \frac{V_L}{g} dw_L = 0 \tag{B4}$$

For the annulus alone, the differential momentum equation is

$$A_A dp_A + \frac{w_A}{g} dV_A + \frac{f_A q_A A_A l}{r_{H,A}} d\left(\frac{x}{l}\right) = 0 \tag{B5}$$

If it is assumed that the air crosses the plane of the liner wall opening with an axial component of velocity equal to V_A, subtracting equation (B5) from (B4) gives the differential momentum equation for the liner as

$$A_L dp_L + \frac{w_L}{g} dV_L + \frac{V_L}{g} dw_L - \frac{V_A}{g} dw_L = 0 \tag{B6}$$

since

$$dw_A = -dw_L \tag{B7}$$

For this case of constant A_L, equation (B6) may be expressed as

$$d(p_L + 2q_L) - \frac{w_T}{gA_L} V_A d\left(\frac{w_L}{w_T}\right) = 0 \tag{B8}$$

Equation (B8) may be integrated from the end of the combustor (station 3) to a given station to give

$$p_L + 2q_L - (p_{L,3} + 2q_{L,3}) - \frac{w_T}{gA_L} \int_1^{w_L/w_T} V_A d\left(\frac{w_L}{w_T}\right) = 0 \tag{B9}$$

Again, assuming density to be a function of temperature only

$$\rho_{st,A} = \rho_{st,1} \tag{B10}$$

and

$$\rho_{st,L} = \rho_{st,1} \frac{T_1}{T_L} \tag{B11}$$

The relation between annulus and liner weight flows at any station is given by

$$\frac{w_L}{w_T} = 1 - \frac{w_A}{w_T} \tag{B12}$$

where the effect of fuel flow rate on w_L is neglected. Then from the

continuity equation and equations (B10) and (B12)

$$V_A = \frac{w_A}{\rho_{st,A} A_A} = \frac{w_T}{\rho_{st,1} A_r} \frac{A_r}{A_A} \left(1 - \frac{w_L}{w_T}\right) \tag{B13}$$

and, for constant A_A, the integral term of equation (B9) becomes

$$\frac{w_T}{g A_L} \int_1^{w_L/w_T} V_A d\left(\frac{w_L}{w_T}\right) = - \frac{w_T^2}{2g\rho_{st,1} A_r^2} \frac{A_r}{A_A} \frac{A_r}{A_L} \left(1 - \frac{w_L}{w_T}\right)^2 = -q_r \frac{A_r}{A_A} \frac{A_r}{A_L} \left(1 - \frac{w_L}{w_T}\right)^2 \tag{B14}$$

From the continuity equation and equation (B11) the dynamic pressures q_L and $q_{L,3}$ of equation (B9) can be related to the reference dynamic pressure q_r by

$$q_L = q_r \left(\frac{A_r}{A_L}\right)^2 \frac{T_L}{T_1} \left(\frac{w_L}{w_T}\right)^2 \tag{B15}$$

and

$$q_{L,3} = q_r \left(\frac{A_r}{A_L}\right)^2 \frac{T_{L,3}}{T_1} \tag{B16}$$

For incompressible flow,

$$P_{L,3} = p_{L,3} + q_{L,3} \tag{B17}$$

Then the substitution of equations (B14) to (B17) in equation (B9) gives

$$p_L = P_{L,3} + q_r \left(\frac{A_r}{A_L}\right)^2 \left[\frac{T_{L,3}}{T_1} - 2 \frac{T_L}{T_1} \left(\frac{w_L}{w_T}\right)^2\right] - q_r \frac{A_r}{A_L} \frac{A_r}{A_A} \left(1 - \frac{w_L}{w_T}\right)^2 \tag{B18}$$

Now

$$\frac{P_A - p_L}{q_r} = \frac{P_1 - p_L}{q_r} - \frac{P_1 - P_A}{q_r} \tag{B19}$$

Combining equations (B18) and (B19) yields

$$\frac{P_A - p_L}{q_r} = \frac{P_1 - P_{L,3}}{q_r} - \frac{P_1 - P_A}{q_r} - \left(\frac{A_r}{A_L}\right)^2 \left[\frac{T_{L,3}}{T_1} - 2\frac{T_L}{T_1}\left(\frac{w_L}{w_T}\right)^2\right] + \frac{A_r}{A_L}\frac{A_r}{A_A}\left(1 - \frac{w_L}{w_T}\right)^2 \tag{4}$$

where the area ratios A_A/A_r and A_L/A_r are related by

$$\frac{A_A}{A_r} = 1 - \frac{A_L}{A_r} \tag{B20}$$

The annulus total-pressure-loss coefficient $(P_1 - P_A)/q_r$ of equation (4) may be obtained by rearranging equation (B5), dividing through by the constants A_A and q_r, substituting the continuity relation, and integrating from station 2 to the station at x/l.

$$\frac{P_1 - P_A}{q_r} = -\frac{1}{q_r}\int_{p_{A,2}}^{p_A} dp_A - \frac{\rho_{st,A}}{q_r g}\int_{V_{A,2}}^{V_A} V_A dV_A = \int_0^{x/l} \frac{f_A \frac{q_A}{q_r}\, l\, d\left(\frac{x}{l}\right)}{r_{H,A}} \tag{B21}$$

The expression for the hydraulic radius of the annulus $r_{H,A}$ is

$$r_{H,A} = \frac{D - d}{4} = \frac{D}{4}\left[1 - \left(\frac{A_L}{A_r}\right)^{1/2}\right]$$

$$= \frac{D}{4}\left[1 - \left(1 - \frac{A_A}{A_r}\right)^{1/2}\right] \tag{B22}$$

The ratio of annulus dynamic pressure q_A to reference dynamic pressure q_r is given by

$$\frac{q_A}{q_r} = \left(\frac{w_A}{w_T}\right)^2 \left(\frac{A_r}{A_A}\right)^2 = \left(1 - \frac{w_L}{w_T}\right)^2 \left(\frac{A_r}{A_A}\right)^2 \tag{B23}$$

Substituting equations (B22) and (B23) into equation (B21) and assuming f_A to be constant along the combustor gives

$$\frac{P_1 - P_A}{q_r} = \frac{4f_A \frac{l}{D}}{\left(\frac{A_A}{A_r}\right)^2 \left[1 - \left(1 - \frac{A_A}{A_r}\right)^{1/2}\right]} \int_0^{x/l} \left(1 - \frac{w_L}{w_T}\right)^2 d\left(\frac{x}{l}\right) \qquad (6)$$

The use of equation (6) requires a preliminary estimation of the airflow distribution along the combustor. For the present calculations and for zero airflow through the liner dome ($w_{L,2}/w_T = 0$), the airflow distribution used in equation (6) was assumed to be

$$\frac{w_L}{w_T} = \left(\frac{x}{l}\right)^2 \qquad (7)$$

For the calculations presented herein, the correlation of reference 7 for the discharge coefficient of flush circular holes was used (see fig. 3) to obtain values of C in equations (B3), (3), and (8). For incompressible flow, the correlation parameter $(P_A - p_j)/(P_A - p_A)$ of figure 3(a) is equal to $(V_j/V_A)^2$ and the correction of figure 3(b) is neglected. The velocity ratio V_A/V_j may be obtained by relating q_j to q_A by equations (B1) and (B23) thus giving

$$\frac{V_A}{V_j} = \frac{1 - \frac{w_L}{w_T}}{\frac{A_A}{A_r}\sqrt{\frac{P_A - p_L}{q_r}}} \qquad (10)$$

The liner air-jet entrance angle θ may be obtained from equation (10) and the relation

$$\theta = \arccos \frac{V_A}{V_j} \qquad (9)$$

From equations (B3), (3), (8), (4), (B20) to (B23), (6), (7), and (10), the liner total open hole area and airflow distribution may be calculated for specified values of the combustor total-pressure-loss coefficient. However, if the specified value of the combustor total-pressure-loss coefficient in equation (4) is too low, the calculated liner static pressure p_L will be greater than the annulus static pressure p_A at some point in the combustor, and a solution for

equations (B3), (3), and (8) will not be obtained. For the parallel-wall combustor and negligible annulus wall friction, the minimum difference between the annulus and liner static pressures occurs at the upstream end of the combustor where w_L/w_T is equal to $w_{L,2}/w_T$. From equation (4) the combustor total-pressure-loss coefficient is related to difference between annulus and liner static pressures at this point by

$$\frac{P_1 - P_{L,3}}{q_r} = \left(\frac{p_A - p_L}{q_r}\right)_2 + \left(\frac{A_r}{A_L}\right)^2 \left[\frac{T_{L,3}}{T_1} - 2\frac{T_L}{T_1}\left(\frac{w_{L,2}}{w_T}\right)^2\right] - \left[\frac{A_r}{A_L}\frac{A_r}{A_A} - \left(\frac{A_r}{A_A}\right)^2\right]\left(1 - \frac{w_{L,2}}{w_T}\right)^2 \quad \text{(B24)}$$

The minimum combustor total-pressure-loss coefficient required for a solution of equations (B3), (3), and (8) is obtained from equation (B24) by setting $p_{A,2} - p_{L,2}$ equal to zero. It is noted that this minimum combustor-total-pressure loss coefficient is independent of the discharge coefficients of the liner wall openings. If annulus wall friction effects are included in the calculations, the minimum combustor total-pressure-loss coefficient will be somewhat greater than that given by equation (B24) and the minimum value of $p_A - p_L$ will occur at values of w_L/w_T greater than $w_{L,2}/w_T$.

In the present report, the solutions of equations (B3), (3), and (8) were obtained for $w_{L,2}/w_T$ equal to zero. The combustor total-pressure-loss coefficient and airflow distribution curves for values of $w_{L,2}/w_T$ other than zero were obtained by correcting the curves where $w_{L,2}/w_T$ was equal to zero by the following procedure:

(1) For given values of $A_{h,T}/A_r$, A_L/A_r, and $T_{L,3}/T_1$, $\Delta P/q_r$ is obtained from the combustor total-pressure-loss coefficient curves computed with a $w_{L,2}/w_T$ of zero. The airflow distribution curve at corresponding conditions for a $w_{L,2}/w_T$ of zero is then used to obtain a value for $A_h/A_{h,T}$ at a value of w_L/w_T equal to the chosen finite value of $w_{L,2}/w_T$.

(2) A corrected value for $A_{h,T}/A_r$ is then obtained by multiplying the value of $A_{h,T}/A_r$ corresponding to the data for $w_{L,2}/w_T$ equal to zero by the quantity $1 - A_h/A_{h,T}$, where the value of $A_h/A_{h,T}$ was obtained by step (1).

(3) Values of $A_h/A_{h,T}$ are selected from the airflow distribution curve for $w_{L,2}/w_T$ equal to zero at various values of w_L/w_T greater than the chosen finite value of $w_{L,2}/w_T$. Corrected values of $A_h/A_{h,T}$ are then obtained by subtracting the value of $A_h/A_{h,T}$ obtained in step (1) from the selected value of $A_h/A_{h,T}$ and then dividing by the quantity $1 - A_h/A_{h,T}$ obtained in step (2).

With the above procedure the major portion of the combustor total-pressure-loss coefficient and airflow distribution curves may be obtained. However, for large values of $A_{h,T}/A_r$ the use of equations (B3), (3), and (8) for the given value of $w_{L,2}/w_T$ will be required. It is noted that the use of the above procedure for the cases where annulus wall friction effects are included requires the use of airflow distributions similar to that shown in figure 13.

APPENDIX C

COMPRESSIBLE-FLOW CALCULATIONS FOR TUBULAR TURBOJET COMBUSTOR WITH CONSTANT ANNULUS AND LINER CROSS-SECTIONAL AREAS

From application of the continuity equation, the flow at any station in the combustor may be related to the total airflow through the combustor by

$$\frac{w}{w_T} = \frac{1}{M_1^*} \frac{\rho_{st}V}{\rho_t a_t} \frac{A}{A_r} \frac{P}{P_1} \left(\frac{T_1}{T}\right)^{1/2} \tag{C1}$$

where

$$M_1^* = \frac{w_T}{\rho_{t,1} a_{t,1} A_r} = \left(\frac{\rho_{st}V}{\rho_t a_t}\right)_1 \tag{C2}$$

Transposing terms in equation (C1)

$$\frac{\rho_{st}V}{\rho_t a_t} = M^* = M_1^* \frac{A_r}{A} \frac{w}{w_T} \frac{P_1}{P} \left(\frac{T}{T_1}\right)^{1/2} \tag{C3}$$

Since

$$\frac{\rho_{st}V}{\rho_t a_t} = M \frac{p}{P} \left(\frac{T}{t}\right)^{1/2} = \beta\left(\frac{p}{P}\right) \tag{C4}$$

the relation between $\rho_{st}V/\rho_t a_t$ and local Mach number, local static to total temperature and pressure ratios and other compressible-flow functions may be obtained from compressible-flow tables (e.g., ref. 14).

For any station in the liner,

$$M_L^* = M_1^* \frac{A_r}{A_L} \frac{w_L}{w_T} \frac{P_1}{P_L} \left(\frac{T_L}{T_1}\right)^{1/2} \tag{C5}$$

For the end of the liner

$$M_{L,3}^* = M_1^* \frac{A_r}{A_L} \frac{P_1}{P_{L,3}} \left(\frac{T_{L,3}}{T_1}\right)^{1/2} \tag{C6}$$

For the annulus, where the total temperature is assumed equal to the combustor-inlet total temperature

$$M_A^* = M_1^* \frac{A_r}{A_A} \frac{P_1}{P_A} \left(1 - \frac{w_L}{w_T}\right) \tag{C7}$$

The dynamic pressure q is given by

$$q = \frac{\gamma_a}{2} pM^2 = \frac{\gamma_a}{2} \frac{p}{P} M^2 P = \beta'(M^*) P \tag{C8}$$

and the combustor total-pressure-loss coefficient by

$$\frac{\Delta P}{q_r} = \frac{P_1 - P_{L,3}}{q_r} = \frac{1 - \frac{P_{L,3}}{P_1}}{\beta'(M_1^*)} \tag{C9}$$

For the compressible-flow calculations, equation (B2) is put in the dimensionless form

$$d\left(\frac{w_L}{w_T}\right) = \frac{C}{M_1^*} \left(\frac{\rho_{st} V}{\rho_t a_t}\right)_j \frac{P_j}{P_1} \left(\frac{T_1}{T_j}\right)^{1/2} d\left(\frac{A_h}{A_r}\right) \tag{C10}$$

For isentropic flow through the liner wall openings to the jet vena contracta, P_j equals P_A, and, for T_j equal to T_1, equation (C10) may be rearranged and integrated from station 2 to a given station along the combustor to obtain

$$\int_{w_{L,2}/w_T}^{w_L/w_T} \frac{M_1^* d\left(\frac{w_L}{w_T}\right)}{C\left(\frac{\rho_{st} V}{\rho_t a_t}\right)_j \frac{P_A}{P_1}} = \frac{A_h}{A_r} \tag{C11}$$

As in appendix B, the total liner open hole area is obtained from the integration from station 2 to station 3 where $w_{L,3}/w_T = 1$:

$$\int_{w_{L,2}/w_T}^{1} \frac{M_1^* d\left(\frac{w_L}{w_T}\right)}{C\left(\frac{\rho_{st}V}{\rho_t a_t}\right)_j \frac{P_A}{P_1}} = \frac{A_{h,t}}{A_r} \tag{11}$$

The airflow distribution is obtained from

$$\frac{\int_{w_{L,2}/w_T}^{w_L/w_T} \frac{M_1^* d\left(\frac{w_L}{w_T}\right)}{C\left(\frac{\rho_{st}V}{\rho_t a_t}\right)_j \frac{P_A}{P_1}}}{\int_{w_{L,2}/w_T}^{1} \frac{M_1^* d\left(\frac{w_L}{w_T}\right)}{C\left(\frac{\rho_{st}V}{\rho_t a_t}\right)_j \frac{P_A}{P_1}}} = \frac{A_h}{A_{h,t}} \tag{12}$$

If the static pressure at the jet vena contracta is assumed equal to the liner static pressure at the station considered, the term $(\rho_{st}V/\rho_t a_t)_j$ of equations (C11), (11), and (12) is obtained from the ratio of liner static to annulus total pressure p_L/P_A and equation (C4).

As in appendix B, the liner static pressure is obtained from the solution of the momentum equation. With the use of equation (C8) and the definition of $M_{t,A}$, the momentum equation (B9) can be put in the form

$$\frac{p_L}{P_L}(1 + \gamma_g M_L^2)P_L - \frac{p_{L,3}}{P_{L,3}}(1 + \gamma_g M_{L,3}^2)P_{L,3} - \gamma_a M_1^* \frac{A_r}{A_L} P_1 \int_1^{\frac{w_L}{w_T}} M_{t,A} d\left(\frac{w_L}{w_T}\right) = 0 \tag{C12}$$

From equations (C4) to (C6),

$$\frac{p_L}{P_L}\left(1 + \gamma_g M_L^2\right) = \varphi(M_L^*) \tag{C13}$$

and

$$\frac{p_{L,3}}{P_{L,3}}\left(1 + \gamma_g M_{L,3}^2\right) = \varphi(M_{L,3}^*) \tag{C14}$$

In equations (C12) to (C14), the specific-heat ratio γ_g of the liner gas stream is assumed constant along the combustor.

Combining equations (C12) to (C14) and dividing through by $M_1^* \frac{A_r}{A_L}\left(\frac{T_L}{T_1}\right)^{1/2} \frac{w_L}{w_T}$ gives

$$\frac{\varphi(M_L^*)}{M_L^*} = \frac{\left(\frac{T_{L,3}}{T_1}\right)^{1/2} \frac{\varphi(M_{L,3}^*)}{M_{L,3}^*} + \gamma_a \int_1^{\frac{w_L}{w_T}} M_{t,A}\, d\left(\frac{w_L}{w_T}\right)}{\left(\frac{T_L}{T_1}\right)^{1/2} \frac{w_L}{w_T}} \tag{C15}$$

Equation (C15) may be written

$$\psi(M_L^*) = \frac{\psi(M_{L,3}^*)\left(\frac{T_{L,3}}{T_1}\right)^{1/2} + \gamma_a \int_1^{\frac{w_L}{w_T}} M_{t,A}\, d\left(\frac{w_L}{w_T}\right)}{\left(\frac{T_L}{T_1}\right)^{1/2} \frac{w_L}{w_T}} \tag{C16}$$

where

$$\psi(M^*) = \frac{\varphi(M^*)}{M^*} \tag{C17}$$

From equation (C3), the integral in equation (C16) can be expressed as a function of M_A^*. For the present calculations, the total-pressure

ratio P_A/P_1 required in the evaluation of M_A^* was obtained by using the following relation:

$$\frac{P_A}{P_1} = 1 - \frac{\gamma_a}{2}\left(\frac{p}{P}\right)_1 M_r^2 \frac{(P_1 - P_A)}{q_r} \tag{C18}$$

and the values of $(P_1 - P_A)/q_r$ were obtained from equations (6) and (7).

For the case of negligible annulus wall friction, the integral term of equation (C16) is given by

$$\gamma_a \int_1^{\frac{w_L}{w_T}} M_{t,A}\, d\left(\frac{w_L}{w_T}\right) = \frac{-\gamma_a\left(\frac{A_A}{A_L}\right)\left[\varphi(M_A^*) - 1\right]}{M_1^*\left(\frac{A_r}{A_L}\right)} \tag{C19}$$

where

$$\varphi(M_A^*) = \frac{p_A}{P_A}(1 + \gamma_a M_A^2) \tag{C20}$$

and equation (C16) reduces to

$$\psi(M_L^*) = \frac{\psi(M_{L,3}^*)\left(\frac{T_{L,3}}{T_1}\right)^{1/2} - \gamma_a\left[1 - \left(\frac{w_L}{w_T}\right)\right]\psi'(M_A^*)}{\frac{w_L}{w_T}\left(\frac{T_L}{T_1}\right)^{1/2}} \tag{C21}$$

where

$$\psi'(M_A^*) = \frac{\varphi(M_A^*) - 1}{M_A^*} \tag{C22}$$

In table I, φ, ψ, ψ', p/P, and M^* are presented for a range of values of M and for specific-heat ratios of 1.4 and 1.3.

If values of M_1^*, A_L/A_r, $P_1/P_{L,3}$, and T_L/T_1 are specified, the right side of equation (C16) or (C21) can be calculated for various values of w_L/w_T. From these values of $\psi(M_L^*)$, values for M_L^* and the pressure ratio p_L/P_L can be obtained from table I(a). Then

$$\frac{p_L}{P_A} = \frac{p_L}{P_L}\frac{P_L}{P_1}\frac{P_1}{P_A} = \frac{p_L}{P_L}\frac{P_1}{P_A}\frac{M_1^* \frac{A_r}{A_L}\frac{w_L}{w_T}\left(\frac{T_L}{T_1}\right)^{1/2}}{M_L^*} \tag{C23}$$

where P_1/P_A is obtained from equation (C18). From this value of p_L/P_A, the term $(\rho_{st}V/\rho_t a_t)_j$ of equations (11) and (12) is obtained.

In the present report, the orifice-discharge-coefficient correlation of reference 7 was used (see fig. 3). The pressure ratio p_A/P_A of the correlation parameter of figure 3(a) is obtained from table I(a) and M_A^*, while the pressure ratio p_A/p_L of figure 3(b) is obtained from

$$\frac{p_A}{p_L} = \frac{\frac{p_A}{P_A}}{\frac{p_L}{P_A}} \tag{C24}$$

where p_L/P_A is obtained from equation (C23). With the above values of $C(\rho_{st}V/\rho_t a_t)_j$ and P_1/P_A, the integrals of equations (11) and (12) may be evaluated by trapezoidal or graphical integration.

The entrance angle θ of a liner air jet may be obtained from the relation

$$\theta = \arccos \frac{M_A}{M_j} \tag{13}$$

where M_A and M_j are obtained from table I(a) and values of M_A^* and $M_j^* = \left(\frac{\rho_{st}V}{\rho_t a_t}\right)_j$, respectively.

REFERENCES

1. Nichols, J. B.: An Energy Basis for Comparison of Performance of Combustion Chambers. Trans. A.S.M.E., vol. 75, Jan. 1953, pp. 29-33; discussion, p. 33.

2. Olson, W. T., Childs, J. Howard, and Jonash, E. R.: The Combustion-Efficiency Problem of the Turbojet at High Altitude. Trans. A.S.M.E., vol. 77, no. 5, July 1955, pp. 605-615.

3. Anon.: Quarterly Progress Report on Study of Combustors for Supersonic Ram-Jet for Period July 1-Sept. 30, 1949. Rep. No. PDN 5473, Process Div., Esso Labs., Standard Oil Dev. Co., Nov. 1, 1949. (Navy Bur. Ord. Contract NOrd-9233.)

4. Bader, Frank: A Convenient Method for Calculation of Flow Conditions within a Can-Type Burner Using Assigned Flow and Cross-Sectional Area Distributions. Rep. No. CM-642, Appl. Phys. Lab., The Johns Hopkins Univ., Sept. 28, 1950. (NOrd Contract 7386 with Bur. Ord., U.S. Navy.)

5. Turner, L. Richard, and Bogart, Donald: Constant-Pressure Combustion Charts Including Effects of Diluent Pressure. NACA Rep. 937, 1949. (Supersedes NACA TN's 1086 and 1655.)

6. Hottel, H. C., Williams, G. C., and Satterfield, C. N.: Thermodynamic Charts for Combustion Processes, pts. I and II. John Wiley & Sons, Inc., 1949.

7. Dittrich, Ralph T., and Graves, Charles C.: Discharge Coefficients for Combustor-Liner Air-Entry Holes. I - Circular Holes with Parallel Flow. NACA TN 3663, 1956.

8. Callaghan, Edmund E., and Bowden, Dean T.: Investigation of Flow Coefficient of Circular, Square, and Elliptical Orifices at High Pressure Ratios. NACA TN 1947, 1949.

9. Dewey, Paul E.: A Preliminary Investigation of Aerodynamic Characteristics of Small Inclined Air Outlets at Transonic Mach Numbers. NACA TN 3442, 1955. (Supersedes NACA RM L53C10.)

10. Knight, H. A., and Walker, R. B.: The Component Pressure Losses in Combustion Chambers. Rep. No. R.143, British N.G.T.E., Nov. 1953.

11. Rosen, Philip, and Hart, R. W.: A Constant-Area, Constant-Temperature Combustor. Jour. Aero. Sci., vol. 20, no. 8, Aug. 1953, pp. 549-554.

12. Fuels and Combustion Research Division: Adaptation of Combustion Principles to Aircraft Propulsion. Vol. II - Combustion in Air-Breathing Jet Engines. NACA RM E55G28, 1956.

13. Shapiro, Ascher H., and Hawthorne, W. R.: The Mechanics and Thermodynamics of Steady One-Dimensional Gas Flow. Jour. Appl. Mech., vol. 14, no. 4, Dec. 1947, pp. A317-A336.

14. Ames Research Staff: Equations, Tables and Charts for Compressible Flow. NACA Rep. 1135, 1953. (Supersedes NACA TN 1428.)

TABLE I. - SUBSONIC COMPRESSIBLE-FLOW PARAMETERS

(a) Specific-heat ratio γ_a, 1.4.

M	$\frac{p}{P}$	$M^* = \frac{\rho_{st}V}{\rho_t a_t}$	$\varphi = \frac{p}{P}(1 + \gamma_a M^2)$	$\psi = \frac{\varphi}{\frac{\rho_{st}V}{\rho_t a_t}}$	$\psi' = \frac{\varphi - 1}{\frac{\rho_{st}V}{\rho_t a_t}}$
0	1.00	0	1.0	∞	0
.01	.9999	.0100	1.00004	100.004	.0040
.02	.9997	.0200	1.00026	50.013	.0130
.03	.9994	.0300	1.00065	33.355	.0217
.04	.9989	.0400	1.00114	25.028	.0285
.05	.9983	.0500	1.00179	20.036	.0358
.06	.9975	.0599	1.00252	16.737	.0421
.07	.9966	.0698	1.00344	14.376	.0493
.08	.9955	.0797	1.00442	12.603	.0555
.09	.9944	.0896	1.00568	11.224	.0634
.10	.9930	.0994	1.00690	10.130	.0694
.11	.9916	.1092	1.00840	9.2344	.0769
.12	.9900	.1190	1.00996	8.4871	.0837
.13	.9883	.1287	1.01168	7.8608	.0908
.14	.9864	.1384	1.01347	7.3228	.0973
.15	.9844	.1480	1.01541	6.8609	.1041
.16	.9823	.1576	1.01751	6.4563	.1111
.17	.9800	.1671	1.01965	6.1020	.1176
.18	.9776	.1765	1.02194	5.7900	.1243
.19	.9751	.1859	1.02438	5.5104	.1311
.20	.9725	.1953	1.02696	5.2584	.1380
.21	.9697	.2045	1.02957	5.0346	.1446
.22	.9668	.2137	1.03231	4.8306	.1512
.23	.9638	.2228	1.03518	4.6462	.1579
.24	.9607	.2319	1.03817	4.4768	.1646
.25	.9575	.2408	1.04128	4.3243	.1714
.26	.9541	.2497	1.04440	4.1826	.1778
.27	.9506	.2585	1.04762	4.0527	.1842
.28	.9470	.2672	1.05094	3.9332	.1906
.29	.9433	.2758	1.05436	3.8229	.1971
.30	.9395	.2844	1.05788	3.7197	.2035
.31	.9355	.2928	1.06136	3.6249	.2096
.32	.9315	.3011	1.06504	3.5371	.2160
.33	.9274	.3093	1.06879	3.4555	.2224
.34	.9231	.3175	1.07249	3.3779	.2283

TABLE I. - Continued. SUBSONIC COMPRESSIBLE-FLOW PARAMETERS

(a) Continued. Specific-heat ratio γ_a, 1.4.

M	$\frac{p}{P}$	$M^* = \frac{\rho_{st}V}{\rho_t a_t}$	$\varphi = \frac{p}{P}(1 + \gamma_a M^2)$	$\psi = \frac{\varphi}{\frac{\rho_{st}V}{\rho_t a_t}}$	$\psi' = \frac{\varphi - 1}{\frac{\rho_{st}V}{\rho_t a_t}}$
0.35	0.9188	0.3255	1.07637	3.3068	0.2346
.36	.9143	.3334	1.08019	3.2399	.2405
.37	.9098	.3412	1.08417	3.1775	.2467
.38	.9052	.3489	1.08820	3.1189	.2528
.39	.9004	.3565	1.09213	3.0635	.2584
.40	.8956	.3640	1.09621	3.0116	.2643
.41	.8907	.3713	1.10032	2.9634	.2702
.42	.8857	.3785	1.10443	2.9179	.2759
.43	.8807	.3856	1.10868	2.8752	.2818
.44	.8755	.3926	1.11280	2.8344	.2873
.45	.8703	.3994	1.11703	2.7968	.2930
.46	.8650	.4062	1.12125	2.7603	.2985
.47	.8596	.4128	1.12544	2.7264	.3039
.48	.8541	.4193	1.12960	2.6940	.3091
.49	.8486	.4256	1.13385	2.6641	.3145
.50	.8430	.4319	1.13805	2.6350	.3196
.51	.8374	.4380	1.14233	2.6081	.3250
.52	.8317	.4440	1.14655	2.5823	.3301
.53	.8259	.4498	1.15069	2.5582	.3350
.54	.8201	.4556	1.15490	2.5349	.3400
.55	.8142	.4611	1.15901	2.5136	.3448
.56	.8082	.4666	1.16303	2.4926	.3494
.57	.8022	.4719	1.16709	2.4732	.3541
.58	.7962	.4771	1.17118	2.4548	.3588
.59	.7901	.4821	1.17515	2.4376	.3633

TABLE I. - Continued. SUBSONIC COMPRESSIBLE-FLOW PARAMETERS

(a) Concluded. Specific-heat ratio γ_a, 1.4.

M	$\frac{p}{P}$	$M^* = \frac{\rho_{st}V}{\rho_t a_t}$	$\varphi = \frac{p}{P}(1 + \gamma_a M^2)$	$\psi = \frac{\varphi}{\frac{\rho_{st}V}{\rho_t a_t}}$	$\psi' = \frac{\varphi - 1}{\frac{\rho_{st}V}{\rho_t a_t}}$
0.60	0.7840	0.4870	1.17914	2.4212	0.3678
.61	.7778	.4917	1.18299	2.4059	.3722
.62	.7716	.4964	1.18684	2.3909	.3764
.63	.7654	.5009	1.1907	2.3771	.3807
.64	.7591	.5054	1.1944	2.3633	.3846
.65	.7528	.5096	1.1981	2.3510	.3887
.66	.7465	.5137	1.2017	2.3393	.3926
.67	.7401	.5176	1.2052	2.3284	.3964
.68	.7338	.5215	1.2088	2.3179	.4004
.69	.7274	.5252	1.2122	2.3080	.4040
.70	.7209	.5288	1.2154	2.2984	.4073
.71	.7145	.5322	1.2188	2.2901	.4111
.72	.7080	.5355	1.2218	2.2816	.4142
.73	.7016	.5387	1.2250	2.2740	.4177
.74	.6951	.5418	1.2280	2.2665	.4208
.75	.6886	.5447	1.2309	2.2598	.4239
.76	.6821	.5475	1.2337	2.2533	.4268
.77	.6756	.5501	1.2364	2.2476	.4297
.78	.6690	.5527	1.2388	2.2414	.4321
.80	.6560	.5573	1.2438	2.2318	.4375

TABLE I. - Continued. SUBSONIC COMPRESSIBLE-FLOW PARAMETERS

(b) Specific-heat ratio γ_g, 1.30.

M	$\frac{p}{P}$	$M^* = \frac{\rho_{st}V}{\rho_t a_t}$	$\varphi = \frac{p}{P}(1 + \gamma_g M^2)$	$\psi = \frac{\varphi}{\frac{\rho_{st}V}{\rho_t a_t}}$
0	1.0	0	1	∞
.01	.9999	.0100	1.00003	100.003
.02	.9997	.0200	1.00022	50.011
.03	.9994	.0300	1.00057	33.352
.04	.9990	.0400	1.00108	25.027
.05	.9984	.0499	1.00164	20.073
.06	.9977	.0599	1.00237	16.734
.07	.9968	.0698	1.00315	14.372
.08	.9959	.0797	1.00419	12.600
.09	.9948	.0896	1.00528	11.220
.10	.9935	.0994	1.00642	10.125
.11	.9922	.1092	1.00781	9.2290
.12	.9907	.1190	1.00925	8.4811
.13	.9891	.1287	1.01083	7.8542
.14	.9874	.1384	1.01256	7.3162
.15	.9855	.1481	1.01433	6.8490
.16	.9835	.1577	1.01623	6.4441
.17	.9814	.1672	1.01827	6.0901
.18	.9792	.1767	1.02044	5.7750
.19	.9769	.1861	1.02275	5.4957
.20	.9744	.1955	1.02507	5.2433
.21	.9718	.2048	1.02751	5.0171
.22	.9691	.2140	1.03008	4.8135
.23	.9663	.2231	1.03275	4.6291
.24	.9634	.2322	1.03554	4.4597
.25	.9604	.2412	1.03843	4.3053
.26	.9572	.2501	1.04132	4.1636
.27	.9540	.2590	1.04441	4.0325
.28	.9506	.2677	1.04749	3.9129
.29	.9471	.2764	1.05065	3.8012
.30	.9435	.2850	1.05389	3.6979
.31	.9399	.2935	1.05732	3.6024
.32	.9361	.3018	1.06071	3.5146
.33	.9322	.3101	1.06417	3.4317
.34	.9282	.3183	1.06769	3.3544

TABLE I. - Concluded. SUBSONIC COMPRESSIBLE-FLOW PARAMETERS

(b) Concluded. Specific-heat ratio γ_g, 1.30.

M	$\frac{p}{P}$	$M^* = \frac{\rho_{st} V}{\rho_t a_t}$	$\varphi = \frac{p}{P}(1 + \gamma_g M^2)$	$\Psi = \frac{\varphi}{\frac{\rho_{st} V}{\rho_t a_t}}$
0.35	0.9241	0.3264	1.07126	3.2820
.36	.9200	.3344	1.07500	3.2147
.37	.9157	.3423	1.07867	3.1512
.38	.9113	.3500	1.08237	3.0925
.39	.9069	.3577	1.08622	3.0367
.40	.9023	.3652	1.08998	2.9846
.41	.8977	.3727	1.09387	2.9350
.42	.8930	.3800	1.09778	2.8889
.43	.8882	.3872	1.10170	2.8453
.44	.8833	.3943	1.10561	2.8040
.45	.8784	.4012	1.10964	2.7658
.46	.8734	.4081	1.11365	2.7289
.47	.8683	.4148	1.11765	2.6944
.48	.8631	.4214	1.12162	2.6617
.49	.8579	.4279	1.12568	2.6307
.50	.8525	.4341	1.12956	2.6021
.51	.8472	.4404	1.13366	2.5742
.52	.8417	.4465	1.13757	2.5477
.53	.8362	.4524	1.14156	2.5233
.54	.8307	.4583	1.14560	2.4997
.55	.8251	.4640	1.14957	2.4775
.56	.8194	.4695	1.15345	2.4568
.57	.8137	.4750	1.15738	2.4366
.58	.8079	.4803	1.16121	2.4177
.59	.8021	.4854	1.16507	2.4002
.60	.7962	.4905	1.16882	2.3829
.61	.7903	.4953	1.17259	2.3674
.62	.7843	.5001	1.17623	2.3520
.63	.7783	.5047	1.17988	2.3378

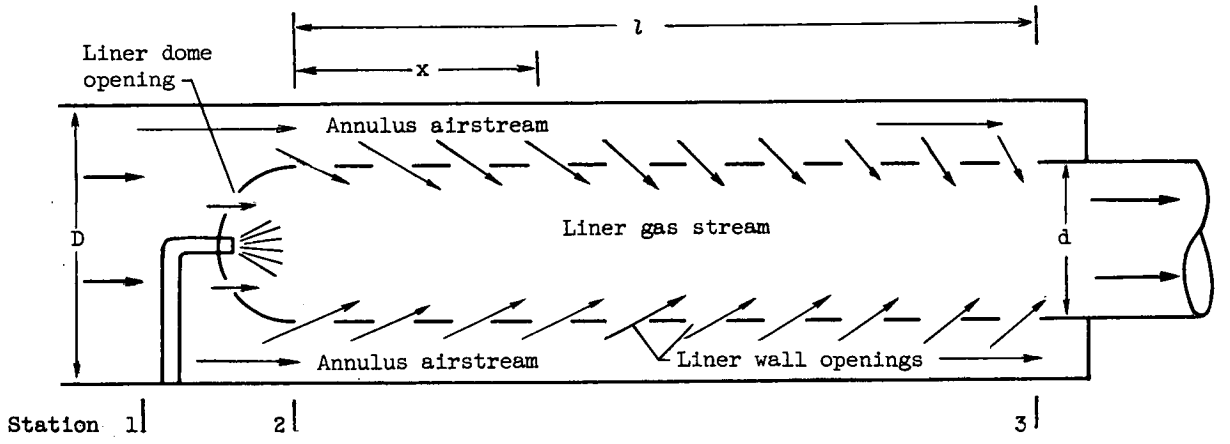

(a) Schematic sketch of parallel-wall combustor.

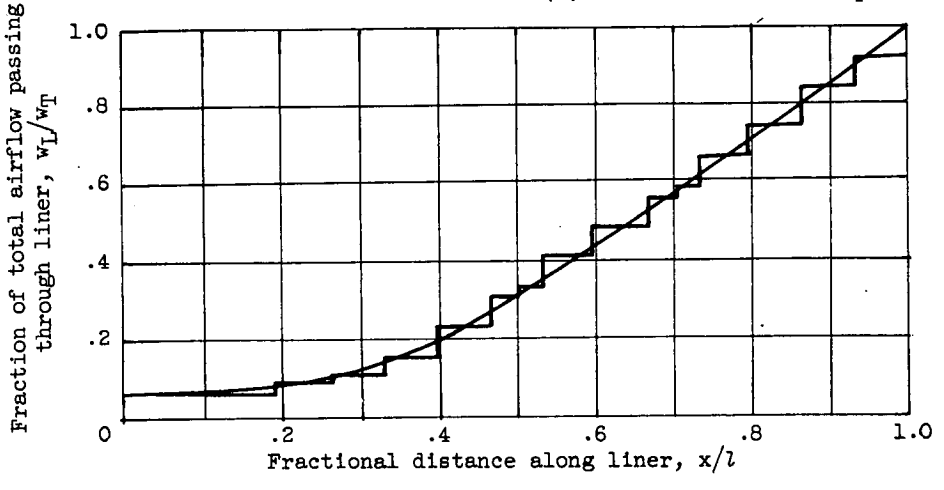

(b) Representative combustor airflow distribution.

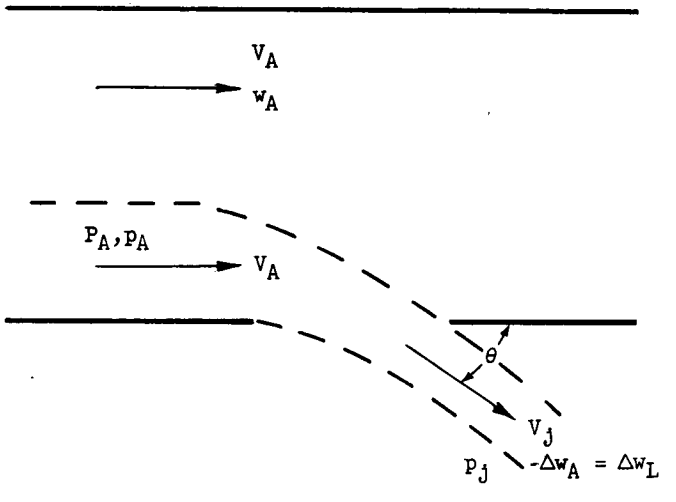

(c) Schematic sketch of flow through liner wall opening.

Figure 1. - Air admission in tubular turbojet combustor with constant annulus and liner cross-sectional areas.

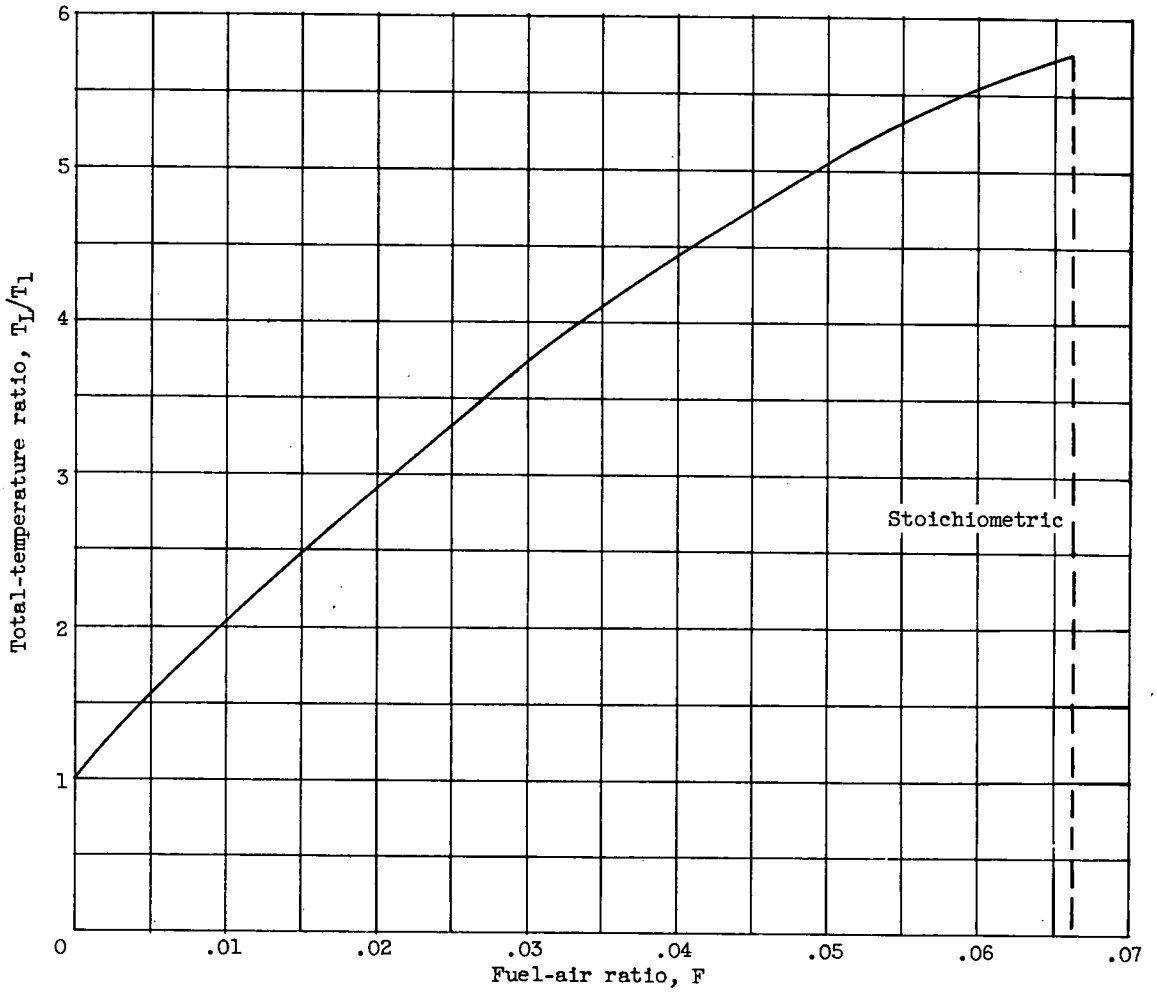

Figure 2. - Variation of exhaust- to inlet-temperature ratio with fuel-air ratio for combustion of n-octane fuel with 100-percent efficiency. Initial air temperature, 728° R; initial fuel temperature, 540° R; pressure, 1 atmosphere.

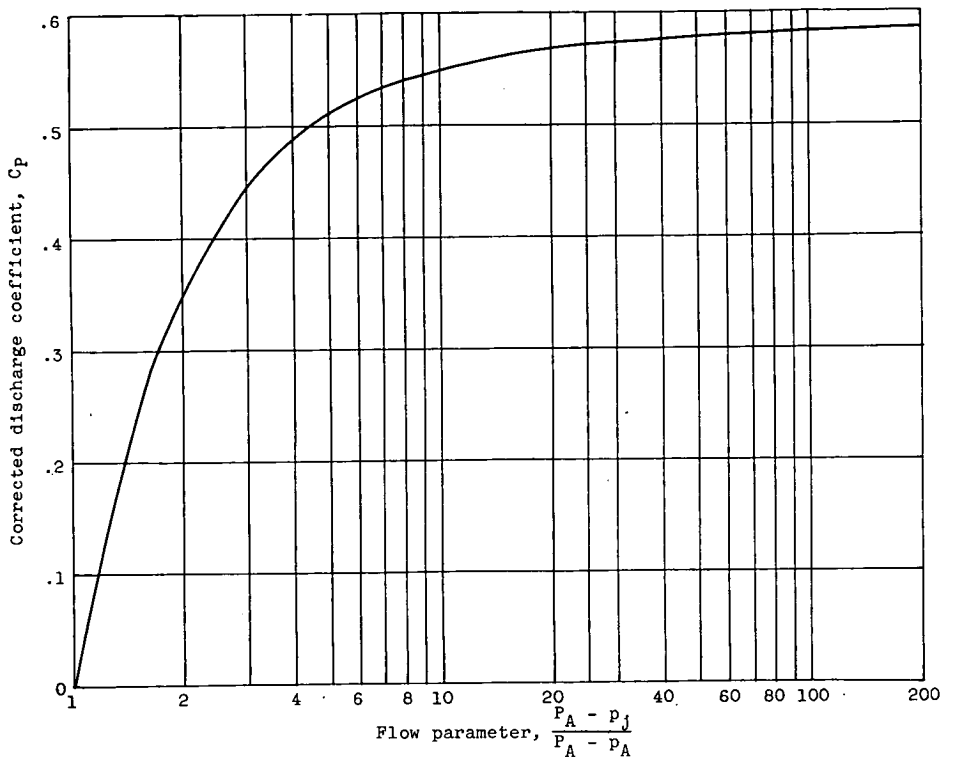

(a) Variation of corrected discharge coefficient with flow parameter.

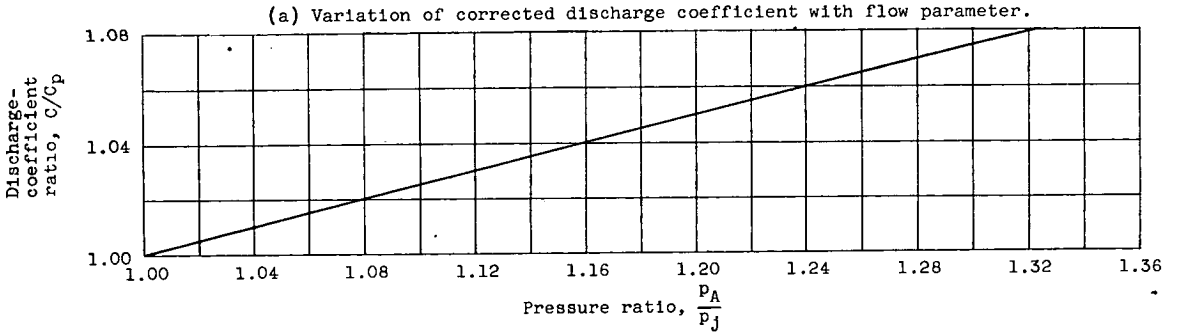

(b) Effect of pressure ratio on discharge-coefficient ratio.

Figure 3. - Discharge coefficient of 3/4-inch-diameter hole in 0.040-inch wall under external crossflow conditions (ref. 7).

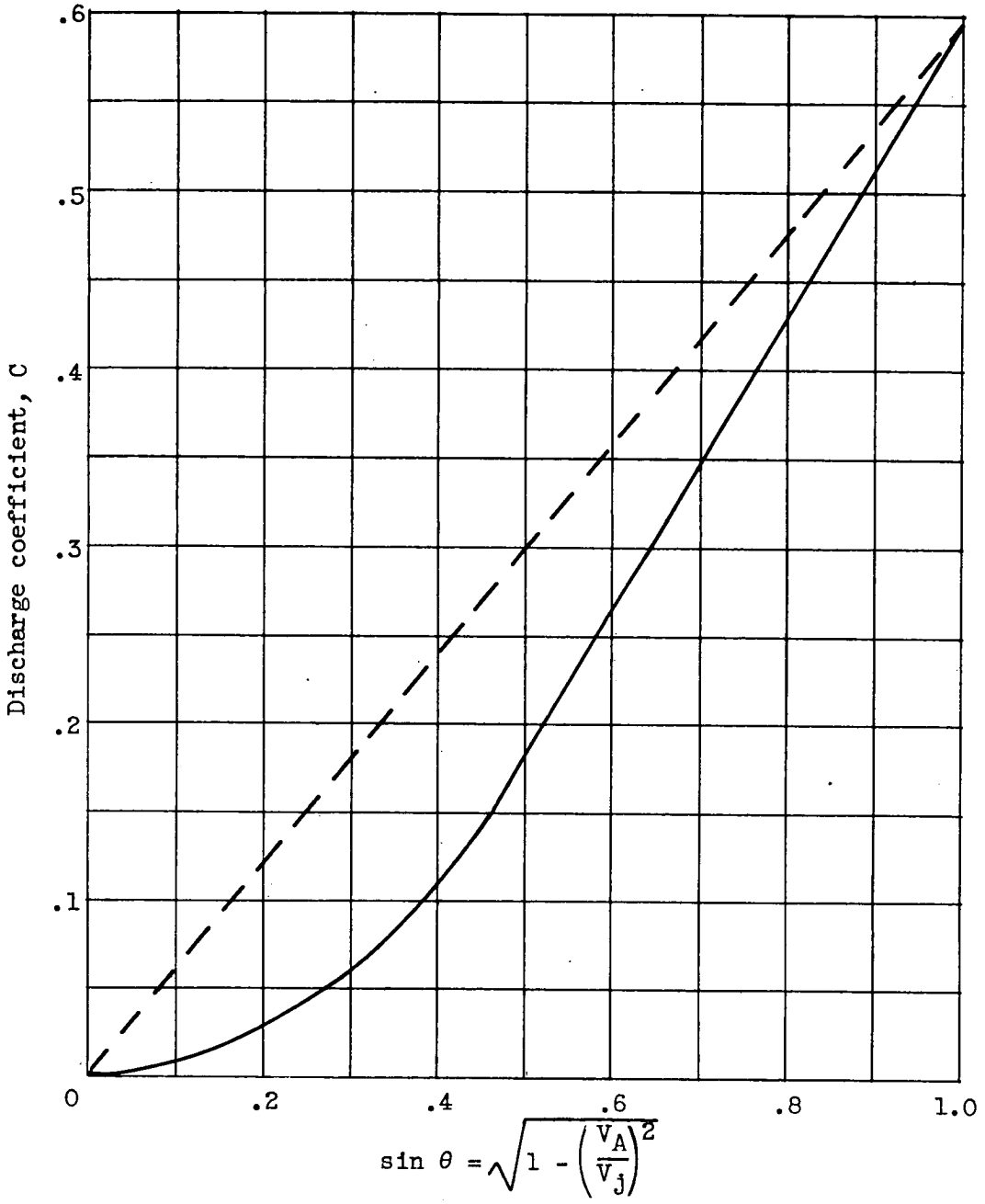

Figure 4. - Variation of discharge coefficient with sine of air-jet entrance angle θ.

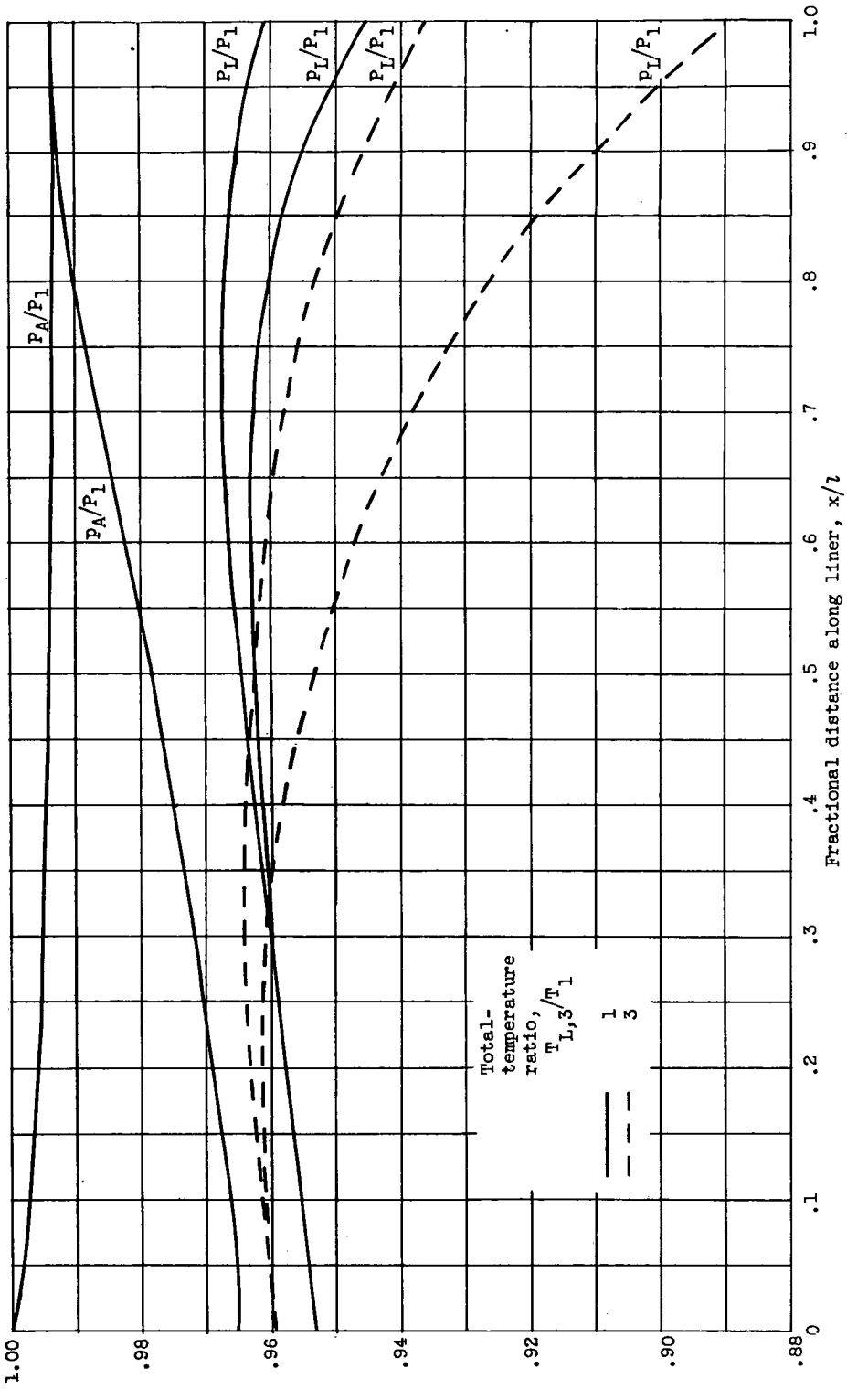

(a) Static and total pressures along length of combuster referenced to inlet total pressure.

Figure 5. - Variation in total and static pressures in annulus and liner, and pressure drop across liner along combustor. Ratio of liner cross-sectional area to reference area A_l/A_r, 0.6; ratio of total liner open hole area to reference area $A_{h,T}/A_r$, 1.09; flow through liner dome $w_{L,2}/w_T$, 0; reference velocity, 100 feet per second; inlet total pressure, 1 atmosphere.

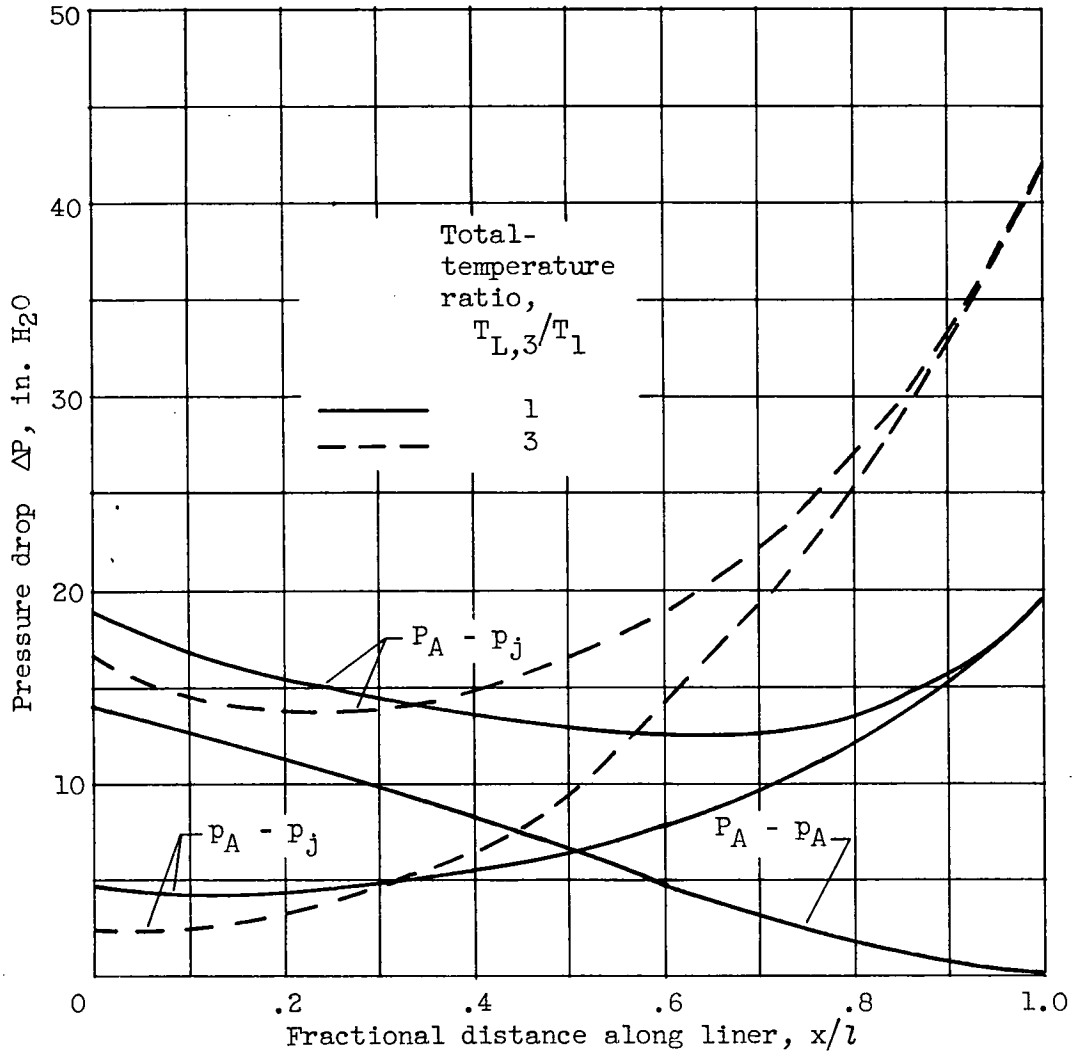

(b) Pressure drop along length of combustor.

Figure 5. - Continued. Variation in total and static pressures in annulus and liner, and pressure drop across liner along combustor. Ratio of liner cross-sectional area to reference area A_L/A_r, 0.6; ratio of total liner open hole area to reference area $A_{h,T}/A_r$, 1.09; flow through liner dome $w_{L,2}/w_T$, 0; reference velocity, 100 feet per second; inlet total pressure, 1 atmosphere.

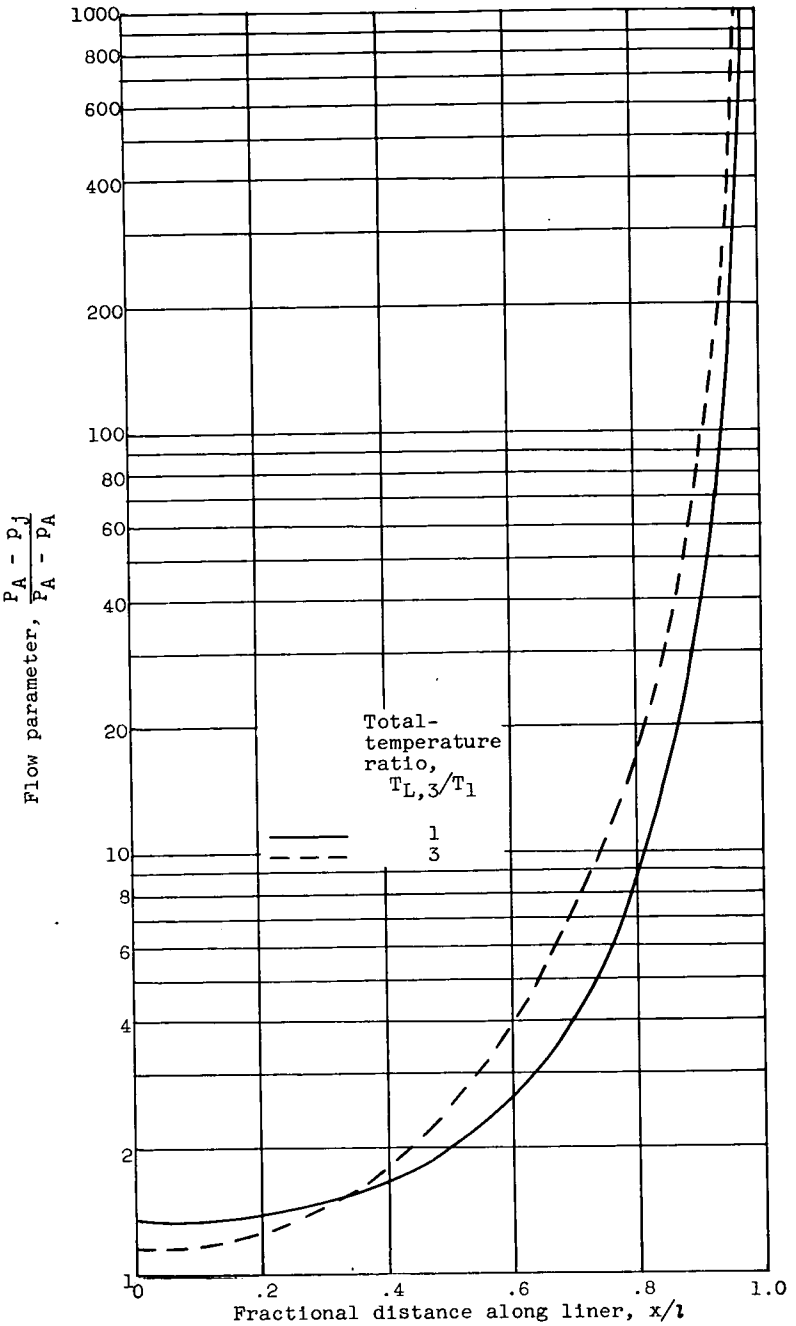

(c) Variation in flow parameter along combustor.

Figure 5. - Concluded. Variation in total and static pressures in annulus and liner, and pressure drop across liner along combustor. Ratio of liner cross-sectional area to reference area A_L/A_r, 0.6; ratio of total liner open hole area to reference area $A_{h,T}/A_r$, 1.09; flow through liner dome $w_{L,2}/w_T$, 0; reference velocity, 100 feet per second; inlet total pressure, 1 atmosphere.

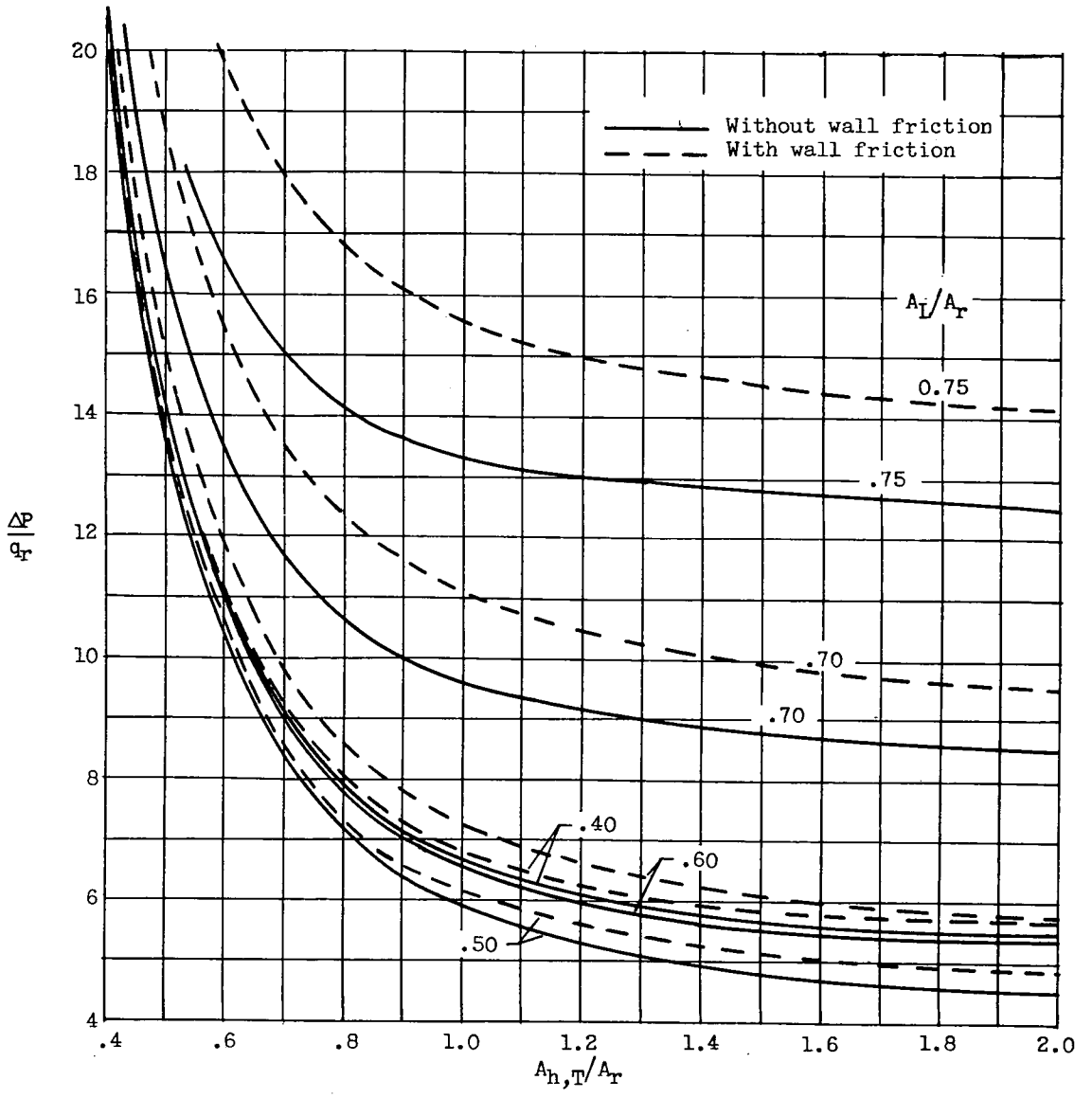

Figure 6. - Variation of total-pressure-loss coefficient $\Delta P/q_r$ with ratio of liner total open hole area to combustor reference area $A_{h,T}/A_r$ for various ratios of liner cross-sectional area to combustor reference area A_L/A_r. Data calculated from incompressible-cold-flow relations with zero flow through liner dome.

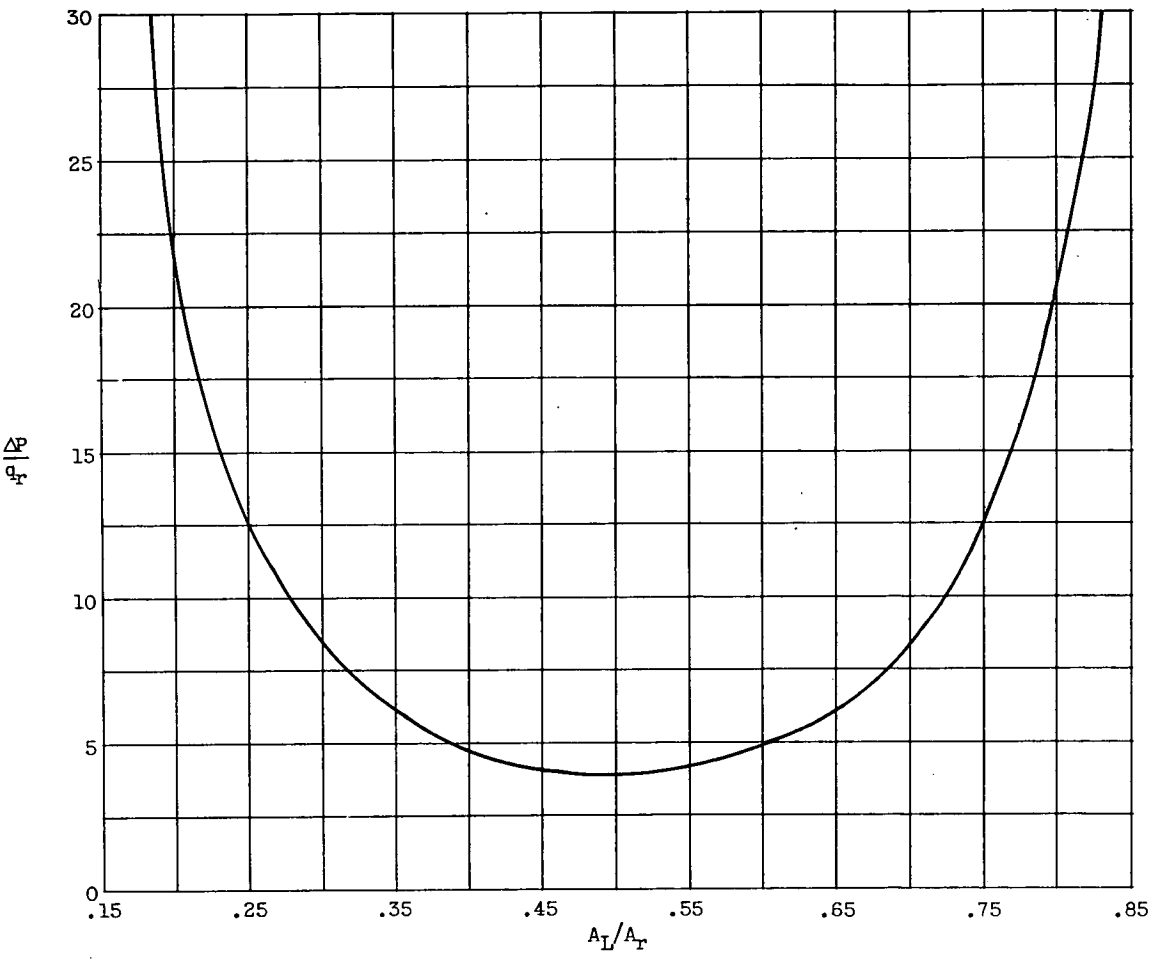

Figure 7. - Variation of minimum total-pressure-loss coefficient $\Delta P/q_r$ with ratio of liner cross-sectional area to combustor reference area A_L/A_r. Data calculated from incompressible-cold-flow relations assuming annulus wall friction negligible, zero flow through dome, and liner and annulus static pressure equal at station 2 (see fig. 1).

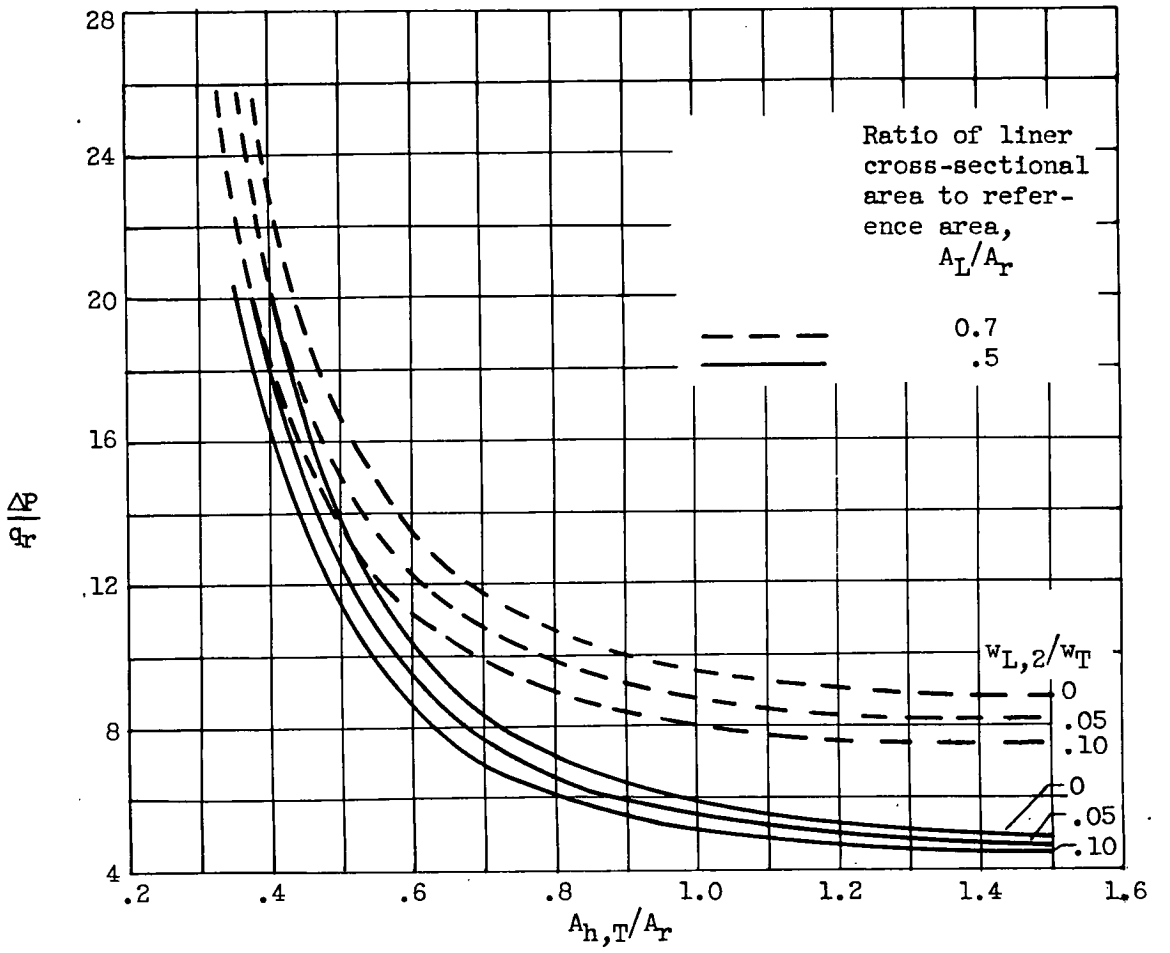

Figure 8. - Variation of total-pressure-loss coefficient $\Delta P/q_r$ with ratio of liner total open hole area to combustor reference area $A_{h,T}/A_r$ for various liner dome airflows $w_{L,2}/w_T$. Data calculated from incompressible-cold-flow relations assuming negligible annulus wall friction.

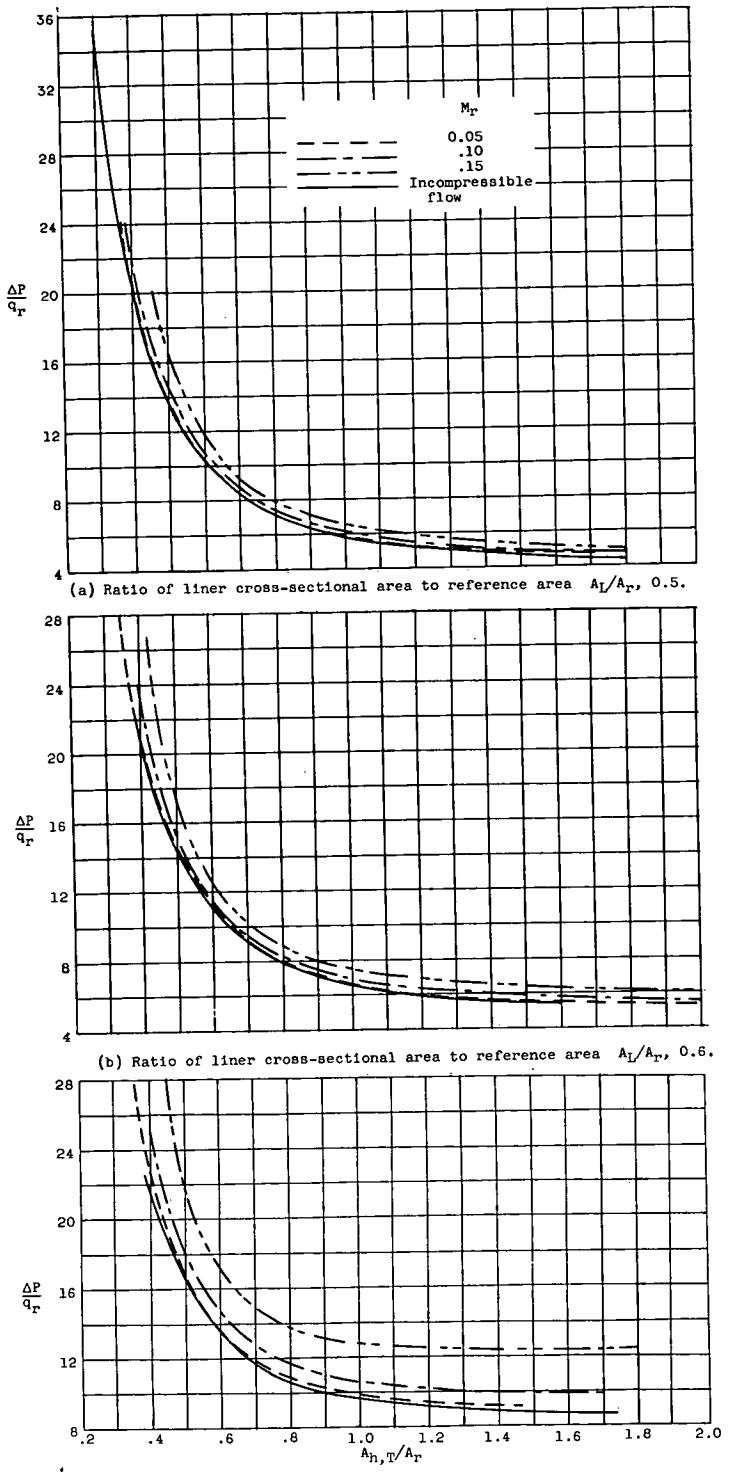

(a) Ratio of liner cross-sectional area to reference area A_L/A_r, 0.5.

(b) Ratio of liner cross-sectional area to reference area A_L/A_r, 0.6.

(c) Ratio of liner cross-sectional area to reference area A_L/A_r, 0.7.

Figure 9. - Variation of total-pressure-loss coefficient $\Delta P/q_r$ with ratio of liner total open hole area to combustor reference area $A_{h,T}/A_r$ for various combustor reference Mach numbers M_r. Data calculated for cold flow and zero liner dome flow assuming negligible annulus wall friction.

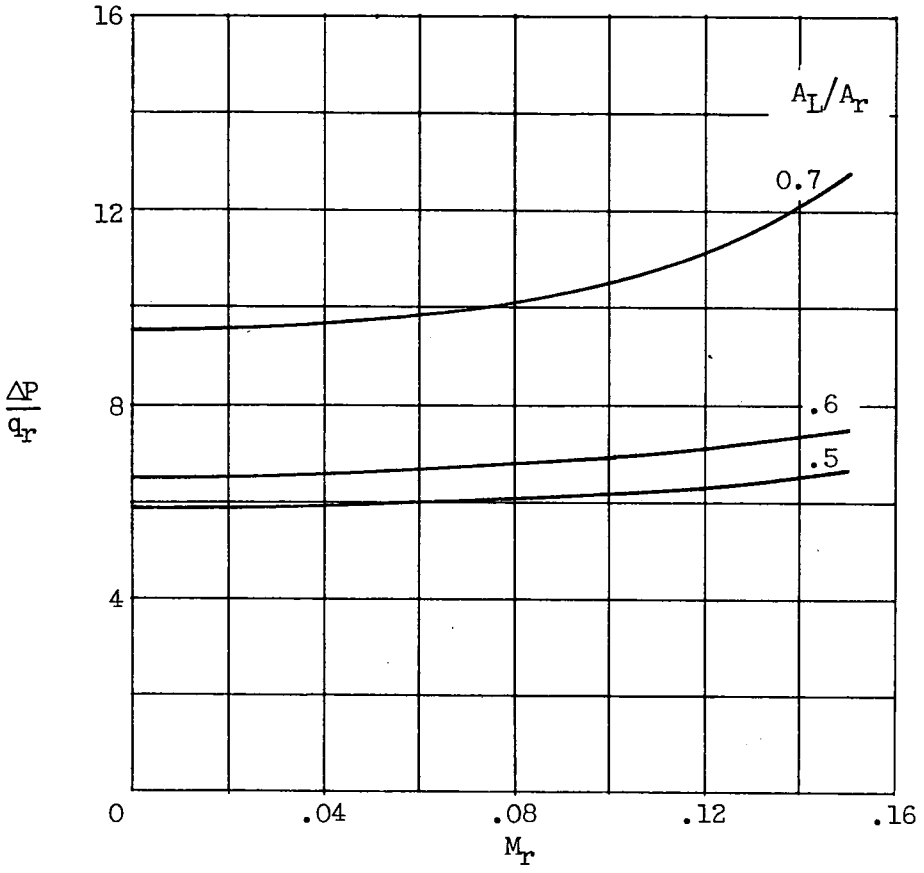

Figure 10. - Variation of total-pressure-loss coefficient $\Delta P/q_r$ with reference Mach number M_r for various ratios of liner cross-sectional area to reference area A_L/A_r. Data calculated for cold flow and zero liner dome flow assuming negligible annulus wall friction; ratio of total liner open hole area to reference area $A_{h,T}/A_r$, 1.0.

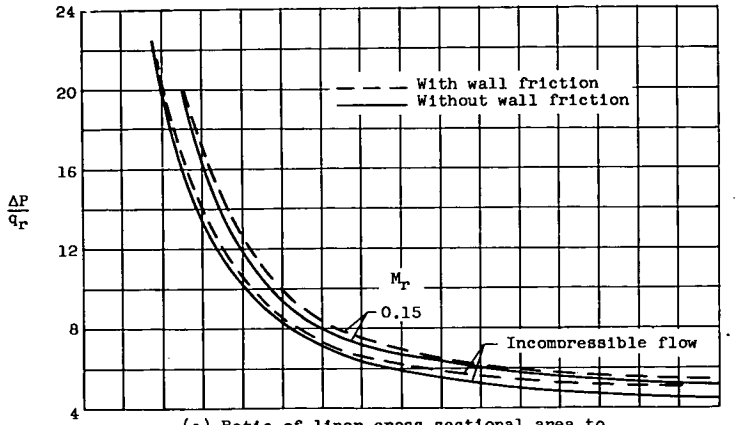

(a) Ratio of liner cross-sectional area to reference area A_L/A_r, 0.5.

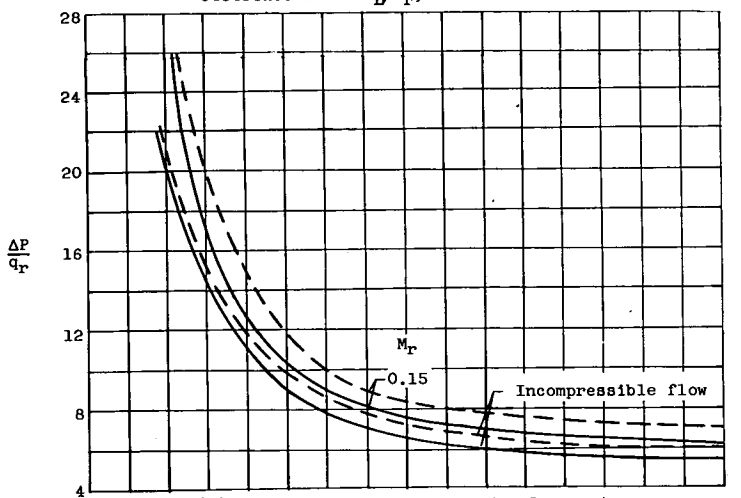

(b) Ratio of liner cross-sectional area to reference area A_L/A_r, 0.6.

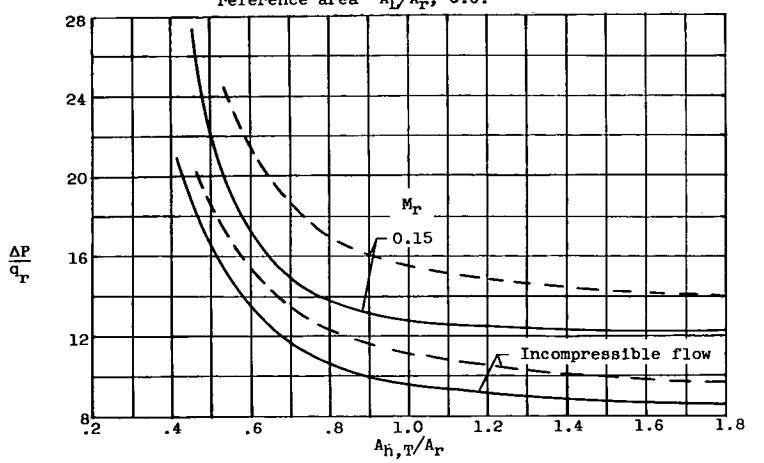

(c) Ratio of liner cross-sectional area to reference area A_L/A_r, 0.7.

Figure 11. - Variation of total-pressure-loss coefficient $\Delta P/q_r$ with ratio of liner total open hole area to combustor reference area $A_{h,T}/A_r$ calculated for combustor reference Mach number M_r of 0.15 and for incompressible flow with and without including effects of annulus wall friction.

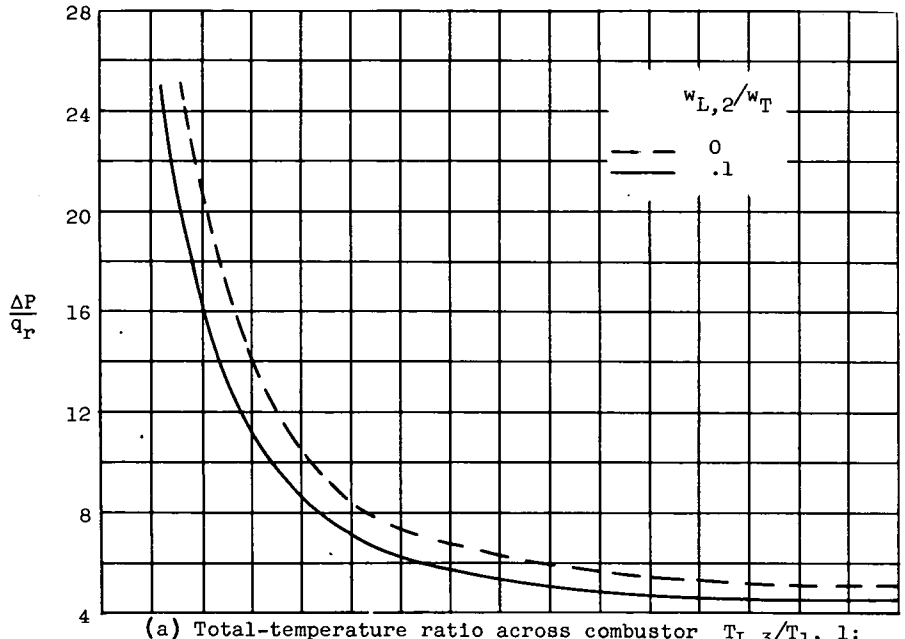

(a) Total-temperature ratio across combustor $T_{L,3}/T_1$, 1; ratio of liner cross-sectional area to reference area A_L/A_r, 0.5.

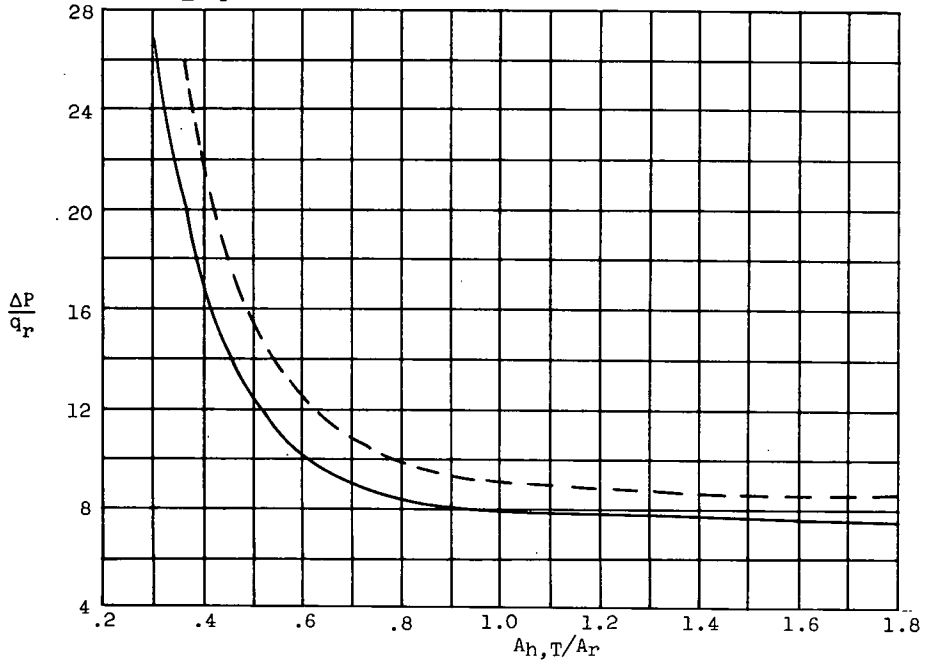

(b) Total-temperature ratio across combustor $T_{L,3}/T_1$, 2; ratio of liner cross-sectional area to reference area A_L/A_r, 0.5.

Figure 12. - Variation of total-pressure-loss coefficient $\Delta P/q_r$ with ratio of liner total open hole area to combustor reference area $A_{h,T}/A_r$ for flow ratios through liner dome $w_{L,2}/w_T$ of 0 and 0.1. Data calculated from incompressible-flow relations including annulus wall friction.

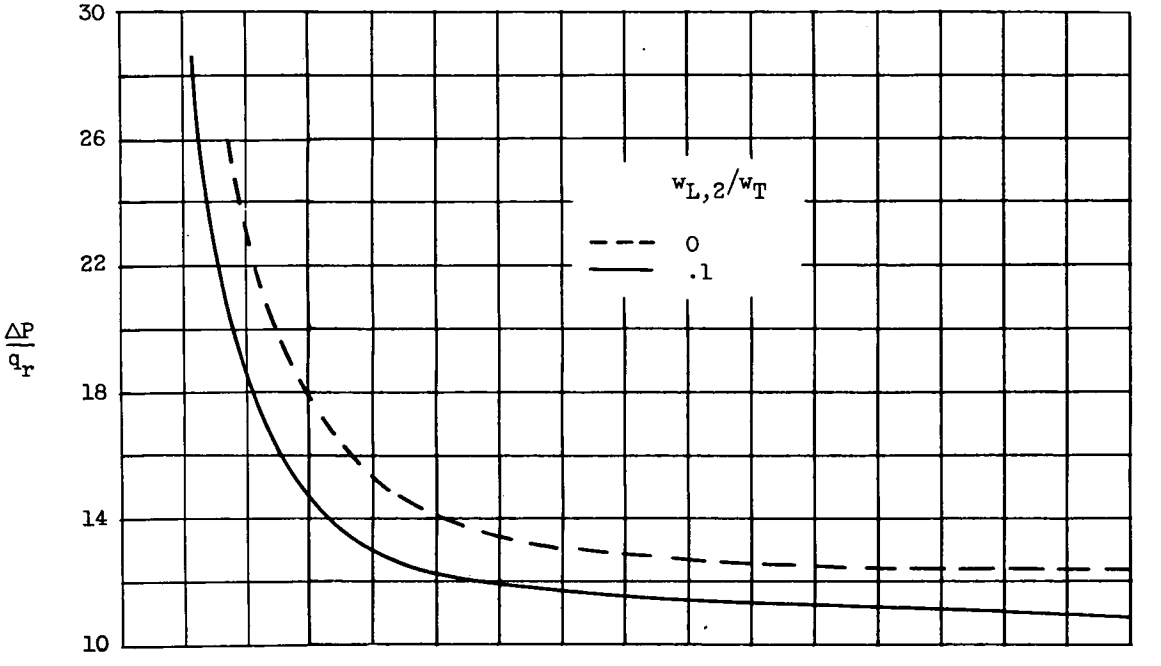

(c) Total-temperature ratio across combustor $T_{L,3}/T_1$, 3; ratio of liner cross-sectional area to reference area A_L/A_r, 0.5.

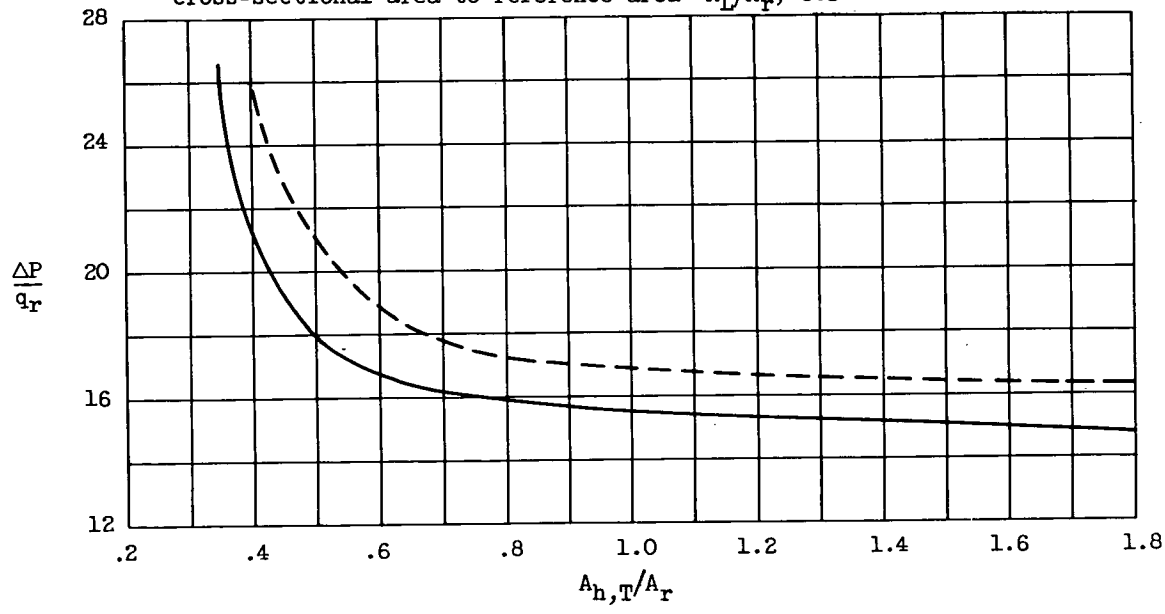

(d) Total-temperature ratio across combustor $T_{L,3}/T_1$, 4; ratio of liner cross-sectional area to reference area A_L/A_r, 0.5.

Figure 12. - Continued. Variation of total-pressure-loss coefficient $\Delta P/q$ with ratio of liner total open hole area to combustor reference area $A_{h,T}/A_r$ for flow ratios through liner dome $w_{L,2}/w_T$ of 0 and 0.1. Data calculated from incompressible-flow relations including annulus wall friction.

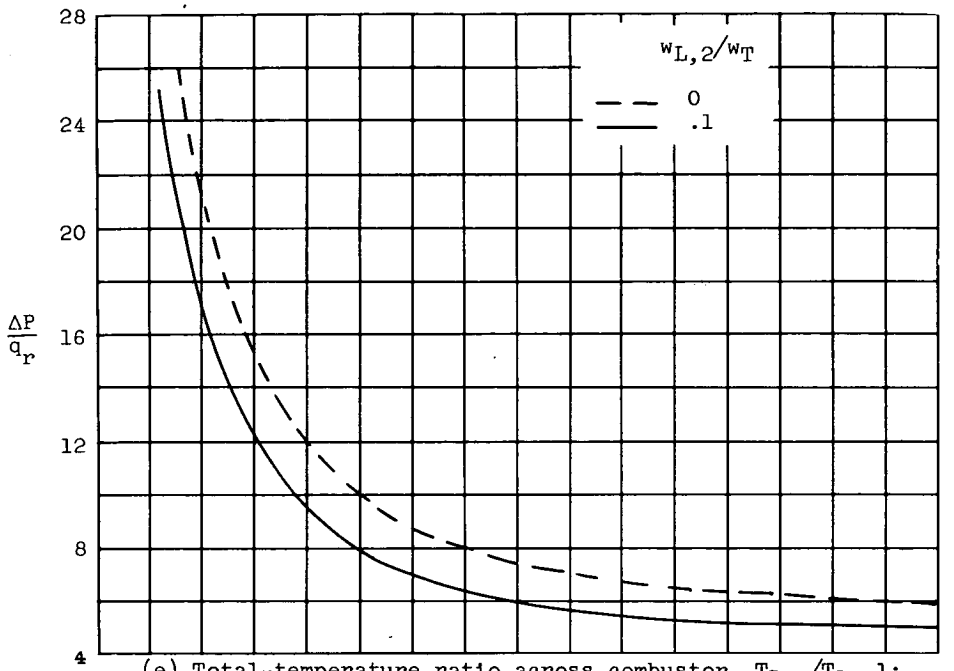

(e) Total-temperature ratio across combustor $T_{L,3}/T_1$, 1; ratio of liner cross-sectional area to reference area A_L/A_r, 0.6.

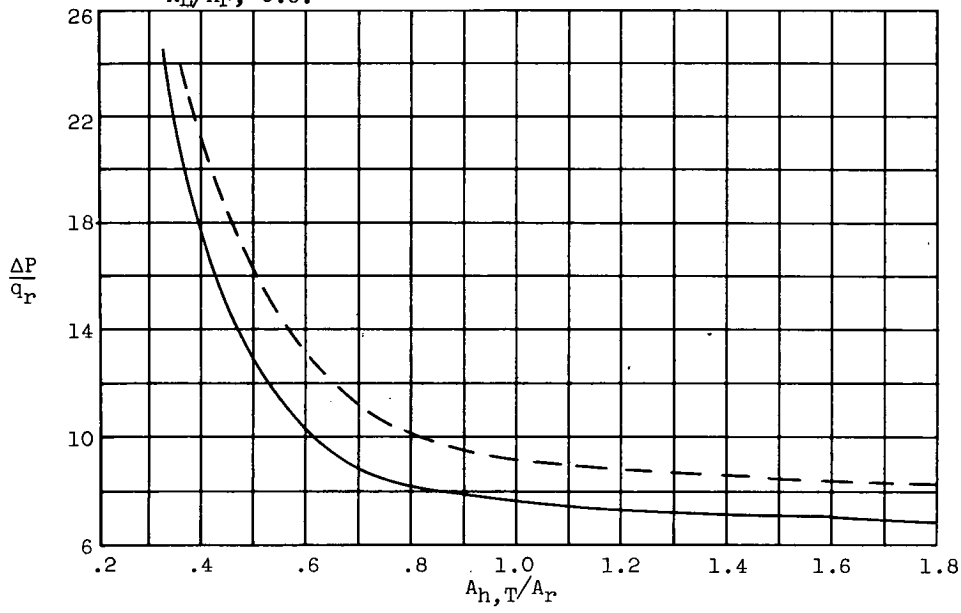

(f) Total-temperature ratio across combustor $T_{L,3}/T_1$, 2; ratio of liner cross-sectional area to reference area A_L/A_r, 0.6.

Figure 12. - Continued. Variation of total-pressure-loss coefficient $\Delta P/q_r$ with ratio of liner total open hole area to combustor reference area $A_{h,T}/A_r$ for flow ratios through liner dome $w_{L,2}/w_T$ of 0 and 0.1. Data calculated from incompressible-flow relations including annulus wall friction.

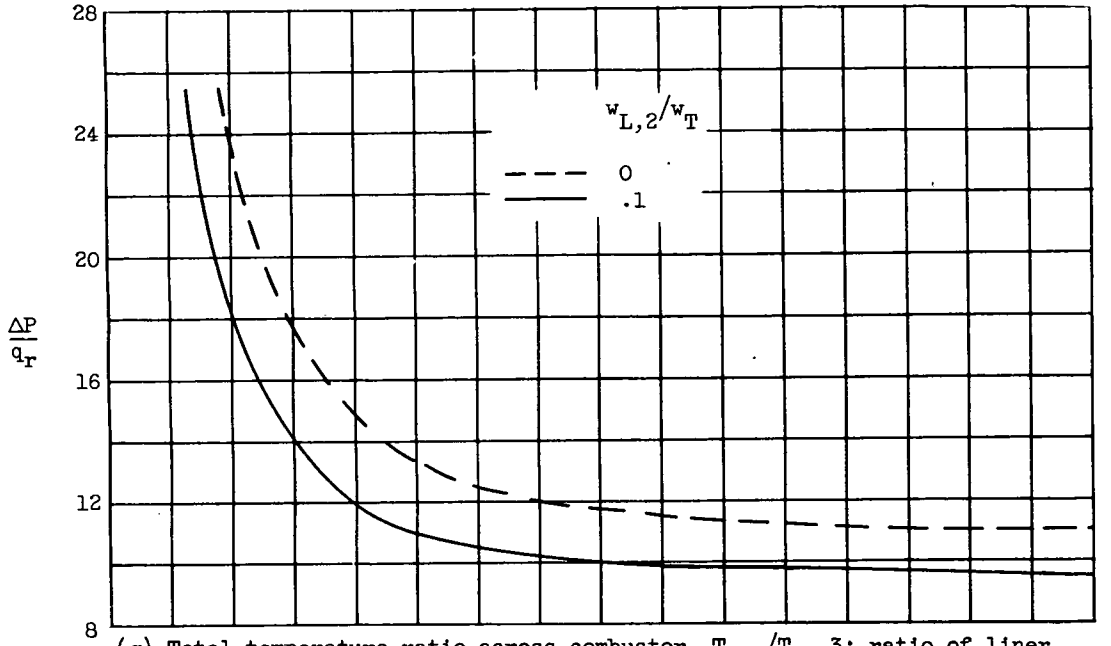

(g) Total-temperature ratio across combustor $T_{L,3}/T_1$, 3; ratio of liner cross-sectional area to reference area A_L/A_r, 0.6.

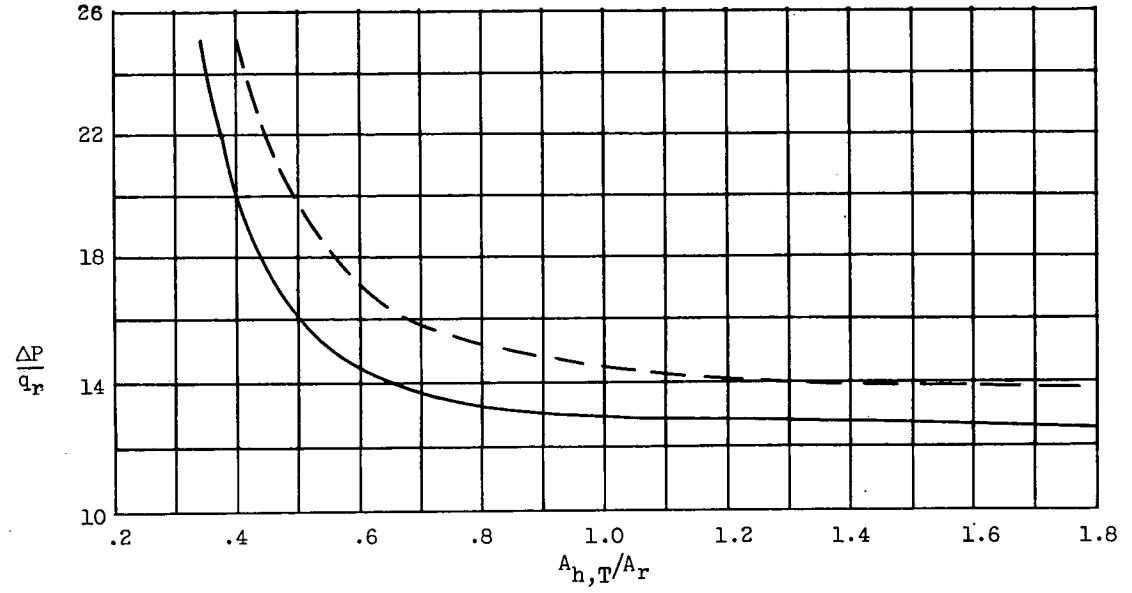

(h) Total-temperature ratio across combustor $T_{L,3}/T_1$, 4; ratio of liner cross-sectional area to reference area A_L/A_r, 0.6.

Figure 12. - Continued. Variation of total-pressure-loss coefficient $\Delta P/q_r$ with ratio of liner total open hole area to combustor reference area $A_{h,T}/A_r$ for flow ratios through liner dome $w_{L,2}/w_T$ of 0 and 0.1. Data calculated from incompressible-flow relations including annulus wall friction.

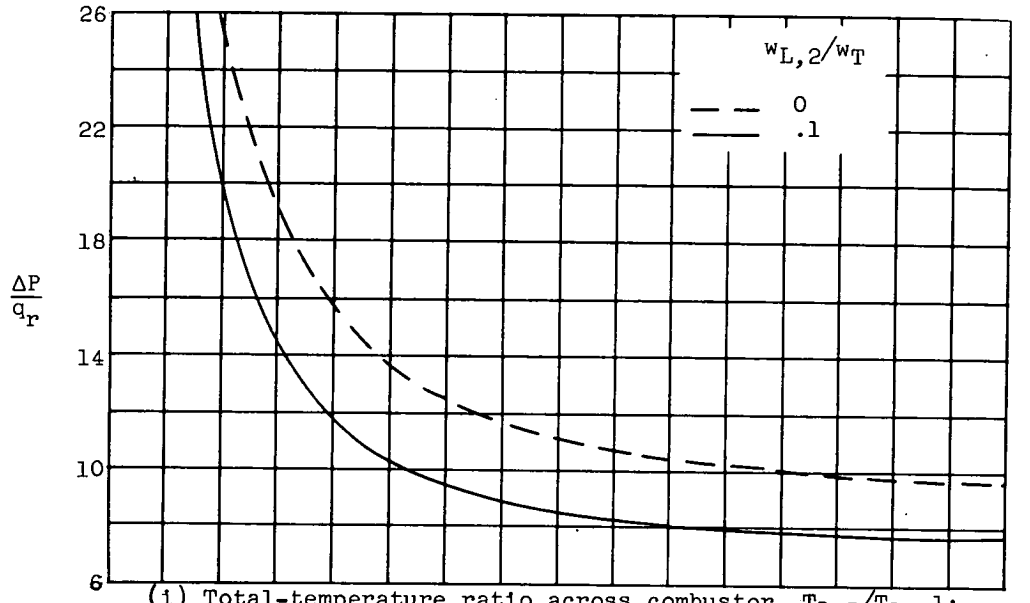

(i) Total-temperature ratio across combustor $T_{L,3}/T_1$, 1; ratio of liner cross-sectional area to reference area A_L/A_r, 0.7.

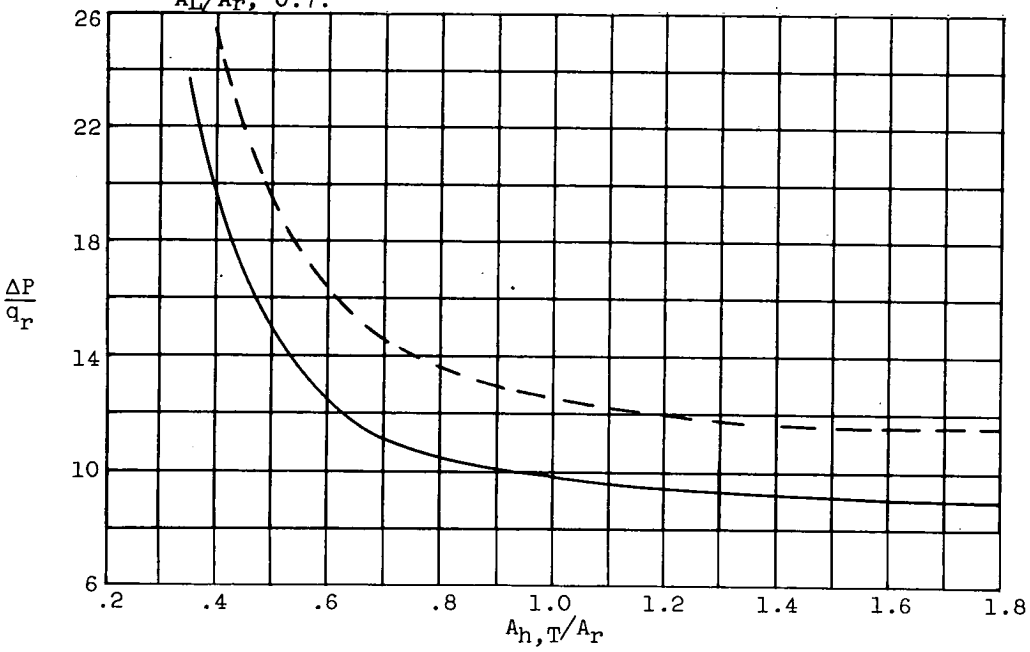

(j) Total-temperature ratio across combustor $T_{L,3}/T_1$, 2; ratio of liner cross-sectional area to reference area A_L/A_r, 0.7.

Figure 12. - Continued. Variation of total-pressure-loss coefficient $\Delta P/q_r$ with ratio of liner total open hole area to combustor reference area $A_{h,T}/A_r$ for flow ratios through liner dome $w_{L,2}/w_T$ of 0 and 0.1. Data calculated from incompressible-flow relations including annulus wall friction.

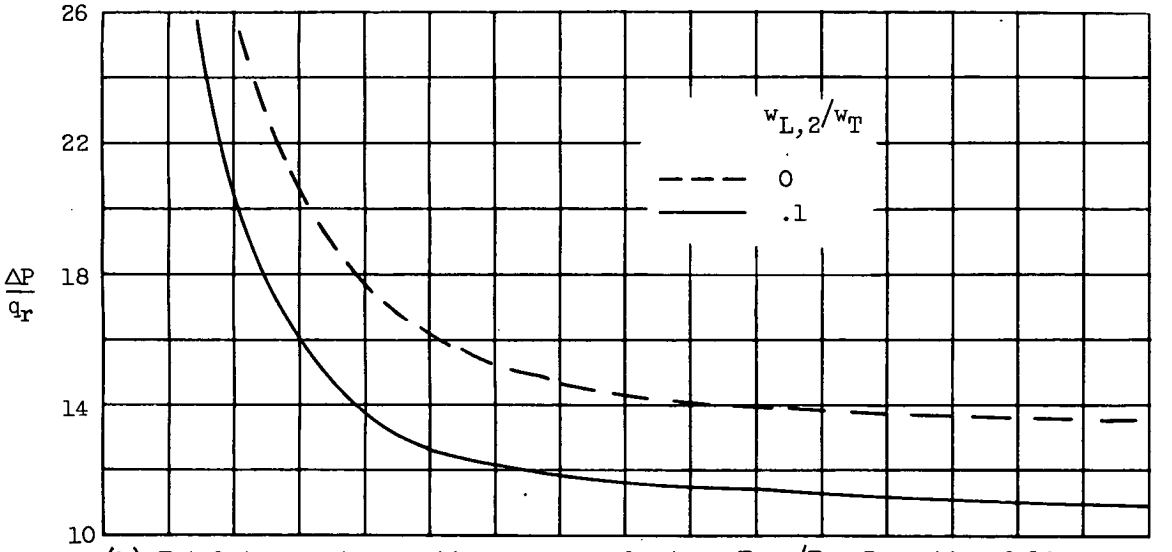

(k) Total-temperature ratio across combustor $T_{L,3}/T_1$, 3; ratio of liner cross-sectional area to reference area A_L/A_r, 0.7.

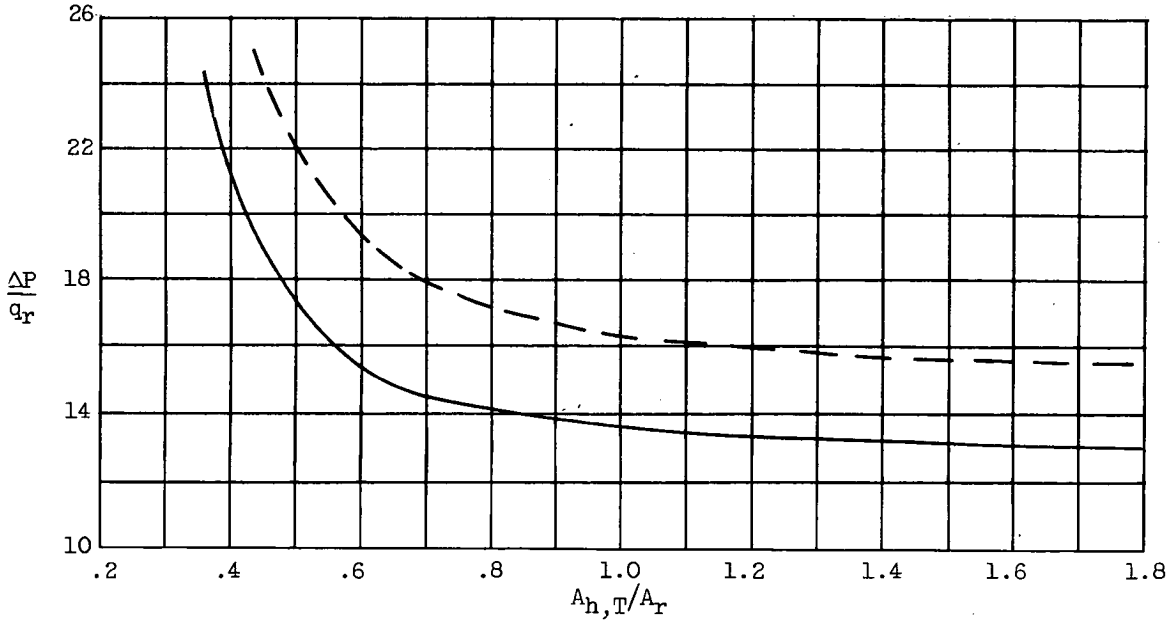

(l) Total-temperature ratio across combustor $T_{L,3}/T_1$, 4; ratio of liner cross-sectional area to reference area A_L/A_r, 0.7.

Figure 12. - Concluded. Variation of total-pressure-loss coefficient $\Delta P/q_r$ with ratio of liner total open hole area to combustor reference area $A_{h,T}/A_r$ for flow ratios through liner dome $w_{L,2}/w_T$ of 0 and 0.1. Data calculated from incompressible-flow relations including annulus wall friction.

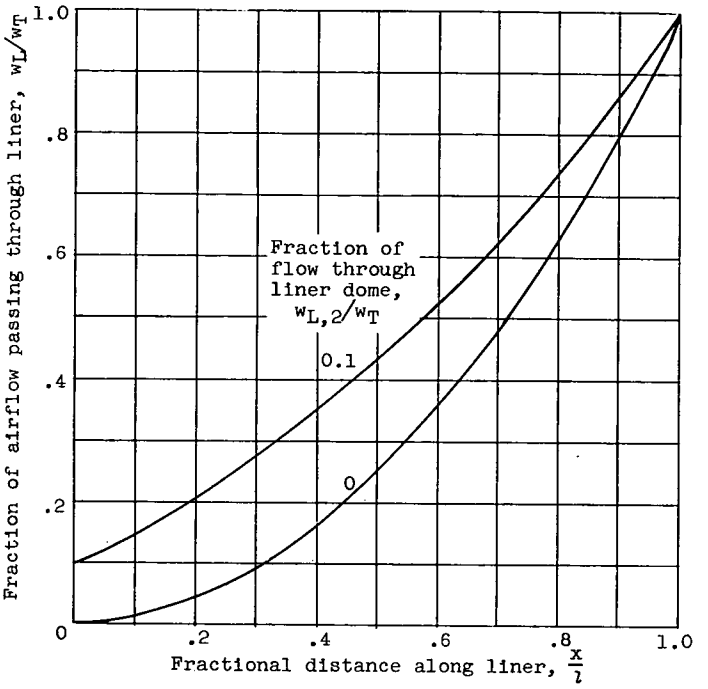

Figure 13. - Combustor airflow distributions assumed in calculations of variation in annulus total pressure along combustor.

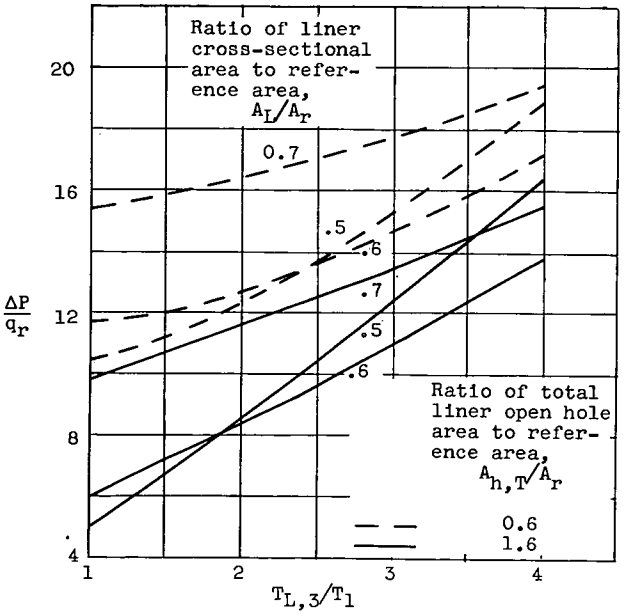

Figure 14. - Variation of total-pressure-loss coefficient $\Delta P/q_r$ with temperature ratio across combustor $T_{L,3}/T_1$. Data calculated from incompressible-flow relations including annulus wall friction with zero liner dome flow.

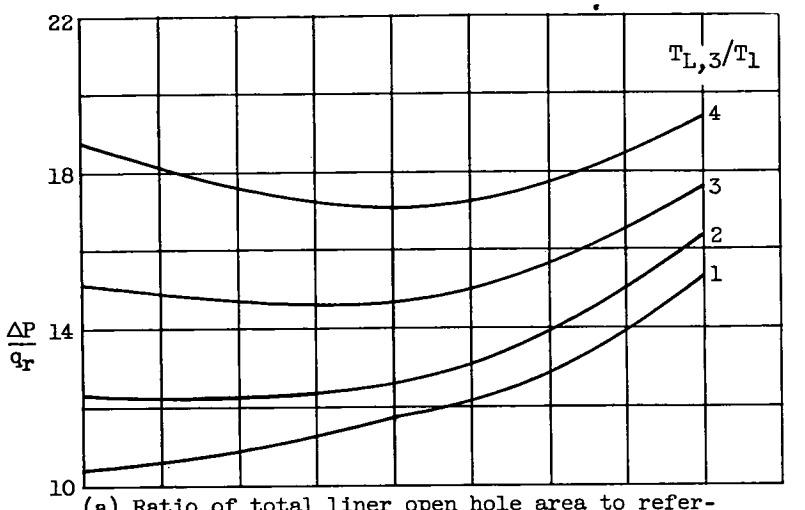

(a) Ratio of total liner open hole area to reference area $A_{h,T}/A_r$, 0.6.

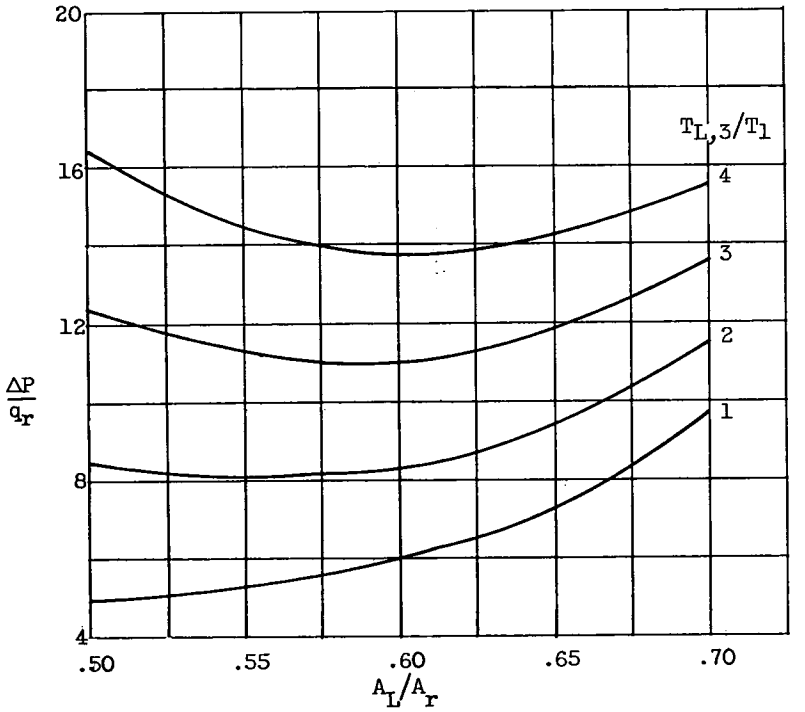

(b) Ratio of total liner open hole area to reference area $A_{h,T}/A_r$, 1.6.

Figure 15. - Variation of total-pressure-loss coefficient $\Delta P/q_r$ with ratio of liner cross-sectional area to reference area A_L/A_r for various values of temperature ratio across combustor $T_{L,3}/T_1$. Data calculated from incompressible-flow relations including annulus wall friction with zero liner dome flow.

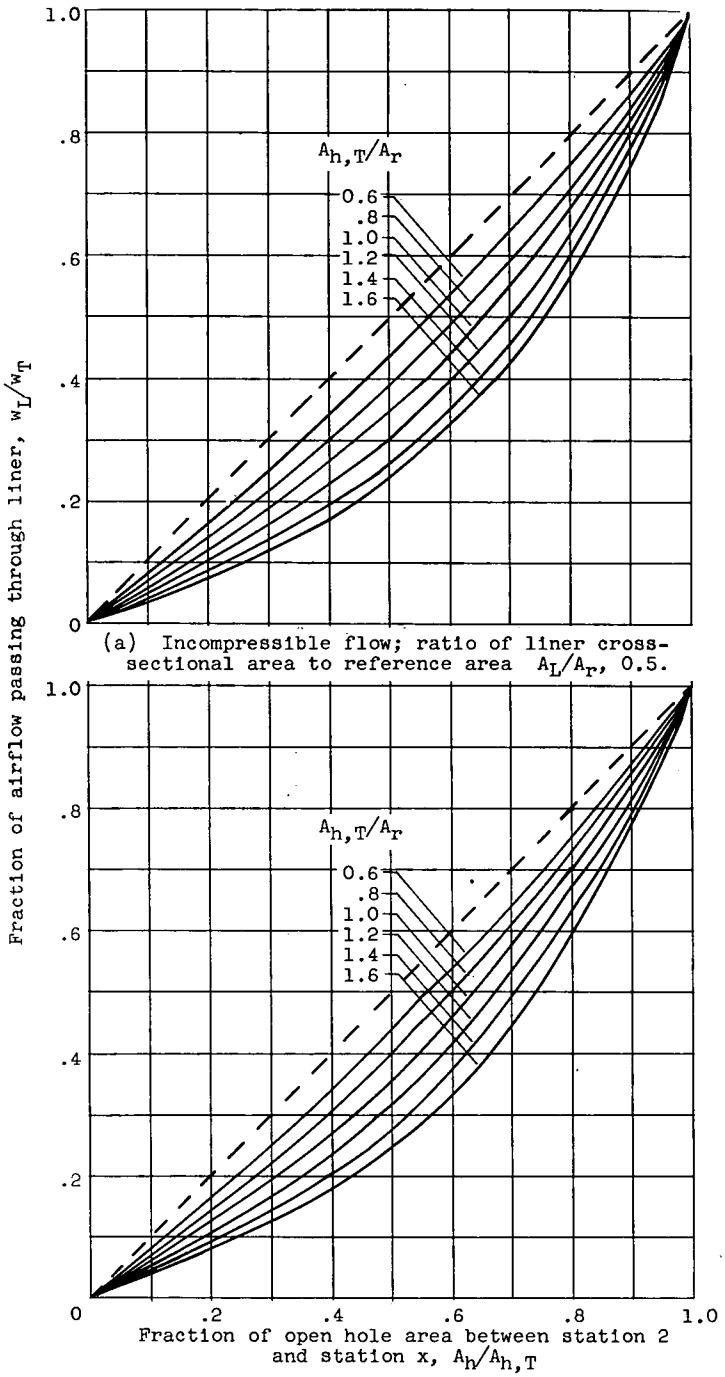

(a) Incompressible flow; ratio of liner cross-sectional area to reference area A_L/A_r, 0.5.

(b) Reference Mach number M_r, 0.05; ratio of liner cross-sectional area to reference area A_L/A_r, 0.5.

Figure 16. - Effect of ratio of liner total open hole area to combustor reference area $A_{h,T}/A_r$ on airflow distribution. Incompressible- and compressible-cold-flow relations without annulus wall friction and with zero liner dome flow.

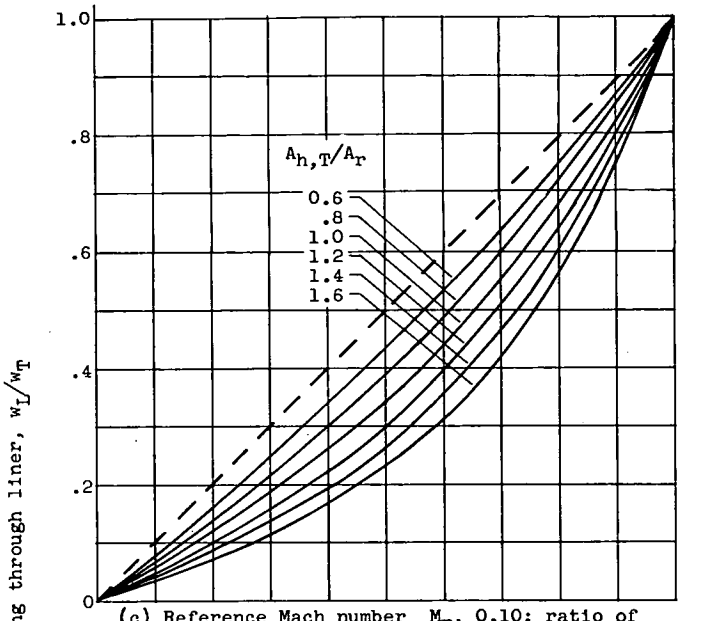

(c) Reference Mach number M_r, 0.10; ratio of liner cross-sectional area to reference area A_L/A_r, 0.5.

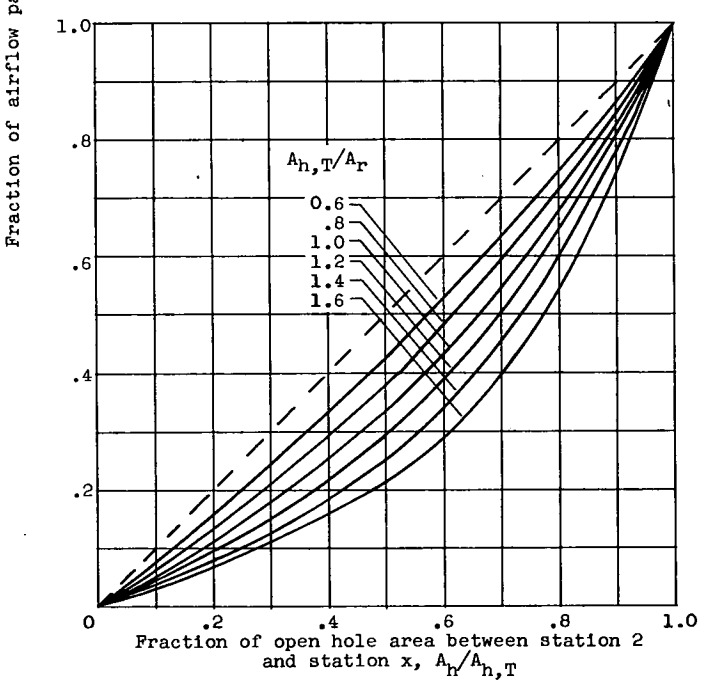

(d) Reference Mach number M_r, 0.15; ratio of liner cross-sectional area to reference area A_L/A_r, 0.5.

Figure 16. - Continued. Effect of ratio of liner total open hole area to combustor reference area $A_{h,T}/A_r$ on airflow distribution. Incompressible- and compressible-cold-flow relations without annulus wall friction and with zero liner dome flow.

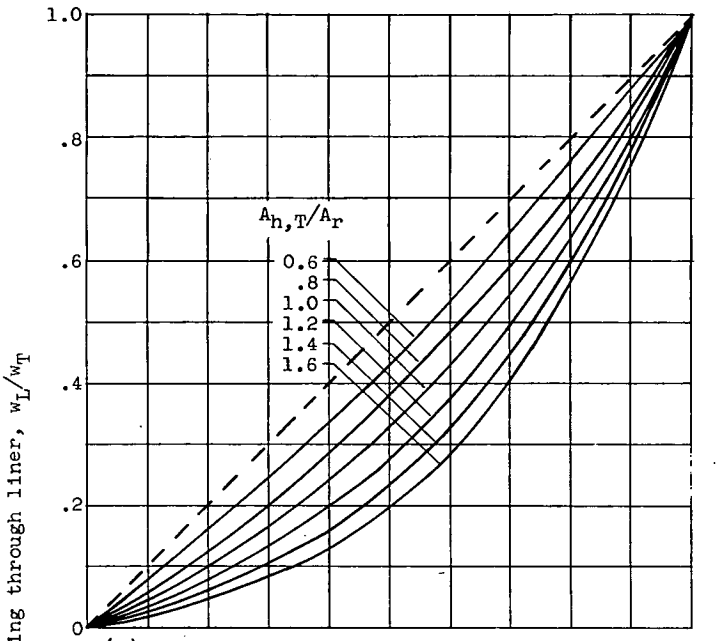

(e) Incompressible flow; ratio of liner cross-sectional area to reference area A_L/A_r, 0.6.

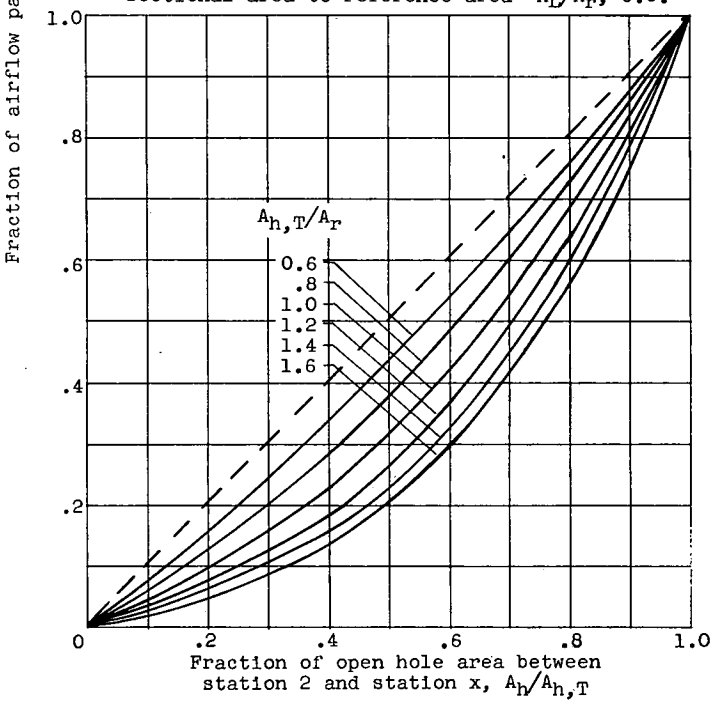

(f) Reference Mach number M_r, 0.05; ratio of liner cross-sectional area to reference area A_L/A_r, 0.6.

Figure 16. - Continued. Effect of ratio of liner total open hole area to combustor reference area $A_{h,T}/A_r$ on airflow distribution. Incompressible- and compressible-cold-flow relations without annulus wall friction and with zero liner dome flow.

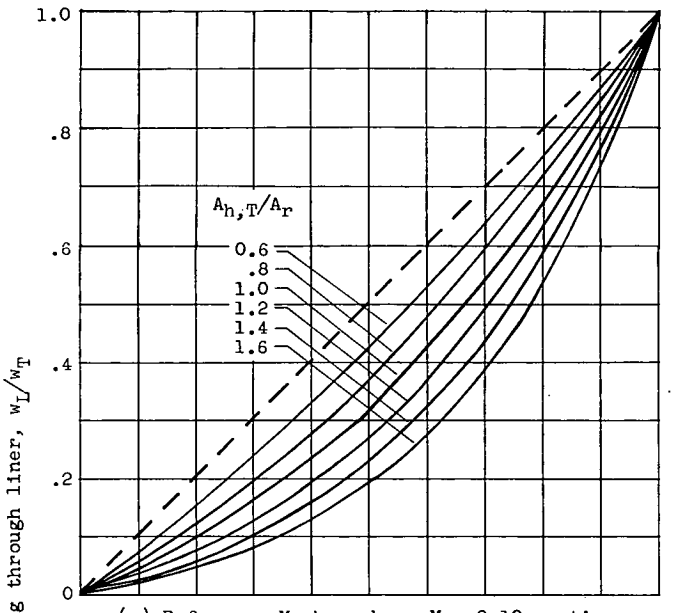

(g) Reference Mach number M_r, 0.10; ratio of liner cross-sectional area to reference area A_L/A_r, 0.6.

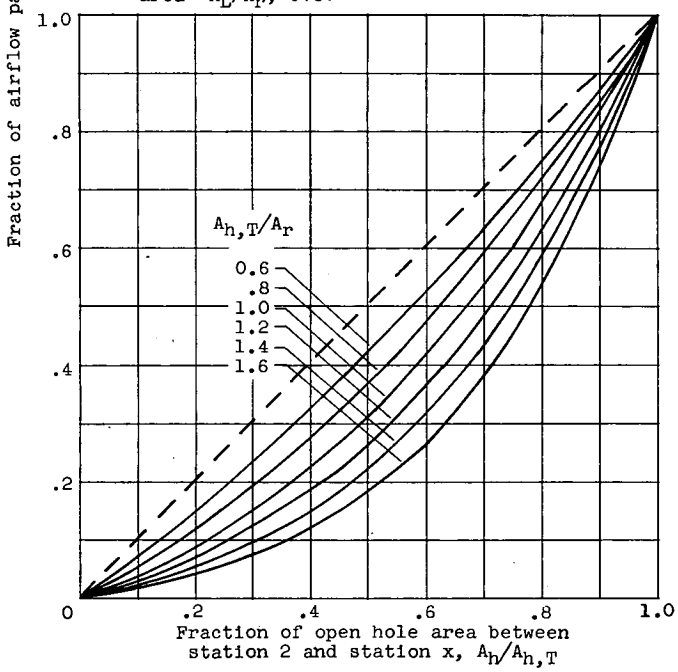

(h) Reference Mach number M_r, 0.15; ratio of liner cross-sectional area to reference area, A_L/A_r, 0.6.

Figure 16. - Continued. Effect of ratio of liner total open hole area to combustor reference area $A_{h,T}/A_r$ on airflow distribution. Incompressible- and compressible-cold-flow relations without annulus wall friction and with zero liner dome flow.

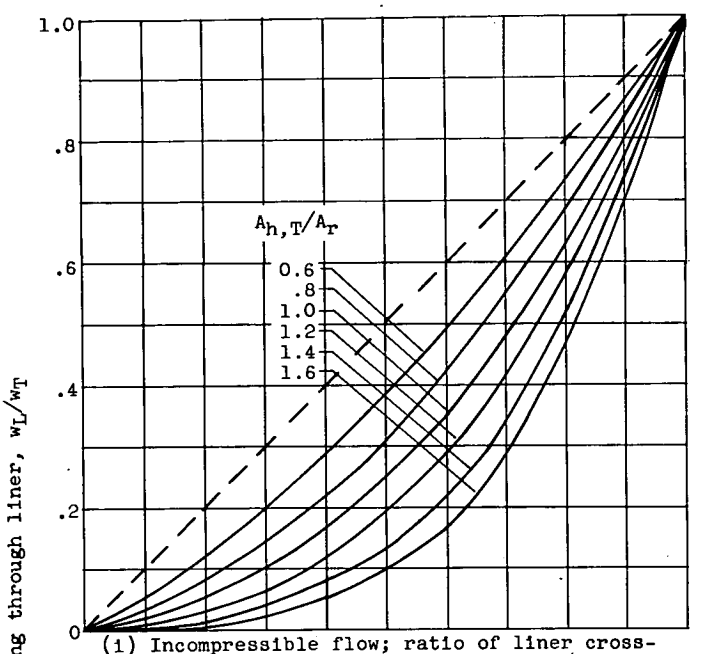

(i) Incompressible flow; ratio of liner cross-sectional area to reference area A_L/A_r, 0.7.

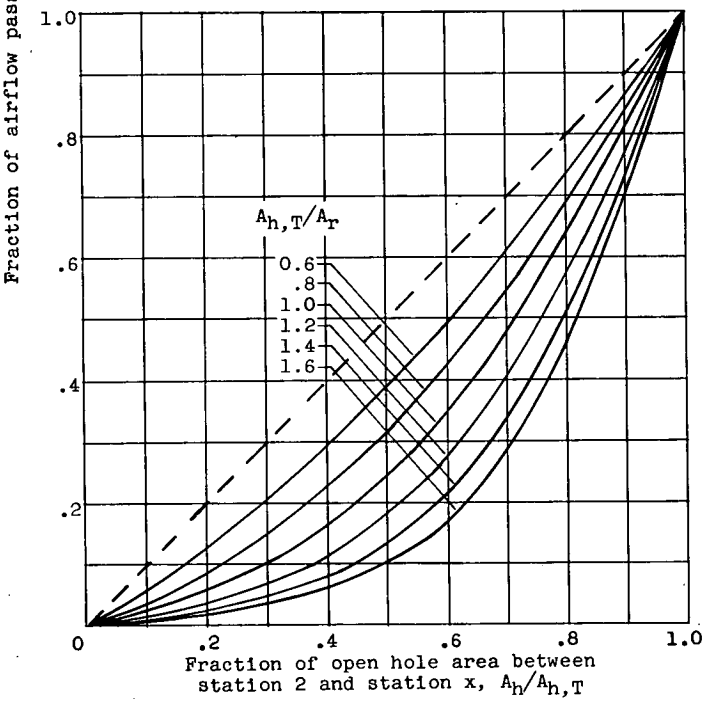

(j) Reference Mach number M_r, 0.05; ratio of liner cross-sectional area to reference area A_L/A_r, 0.7.

Figure 16. - Continued. Effect of ratio of liner total open hole area to combustor reference area $A_{h,T}/A_r$ on airflow distribution. Incompressible- and compressible-cold-flow relations without annulus wall friction and with zero liner dome flow.

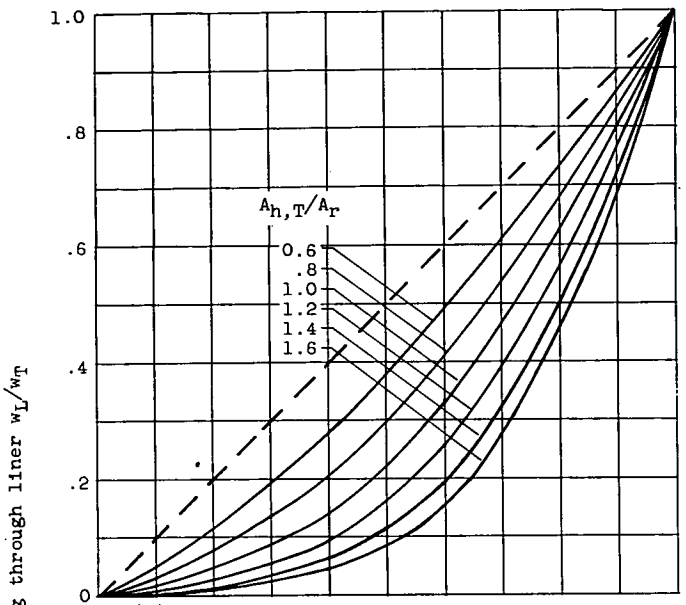

(k) Reference Mach number M_r, 0.10; ratio of liner cross-sectional area to reference area A_L/A_r, 0.7.

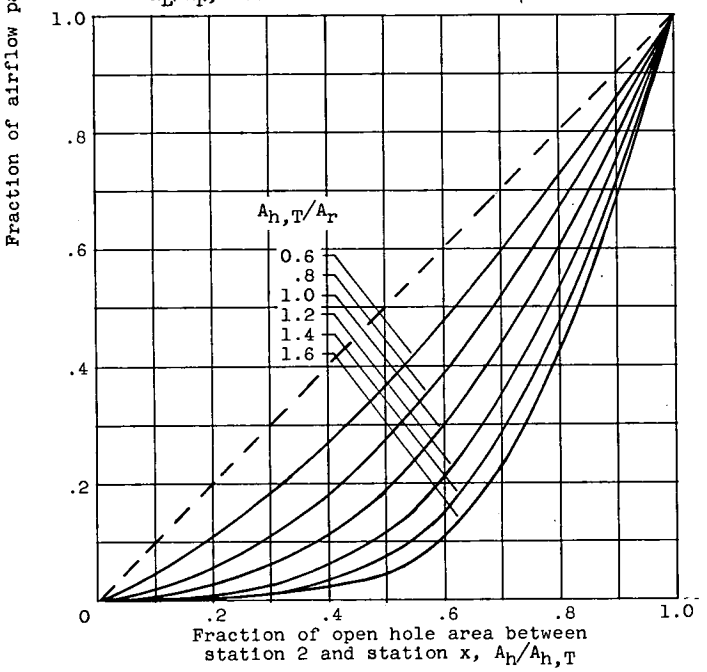

(l) Reference Mach number M_r, 0.15; ratio of liner cross-sectional area to reference area, A_L/A_r, 0.7.

Figure 16. - Concluded. Effect of ratio of liner total open hole area to combustor reference area $A_{h,T}/A_r$ on airflow distribution. Incompressible- and compressible-cold-flow relations without annulus wall friction and with zero liner dome flow.

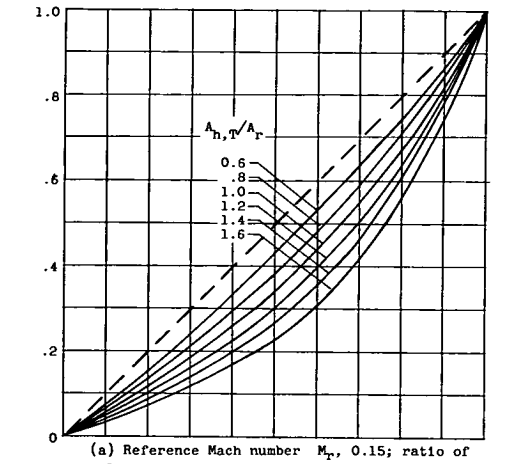

(a) Reference Mach number M_r, 0.15; ratio of liner cross-sectional area to reference area A_L/A_r, 0.5

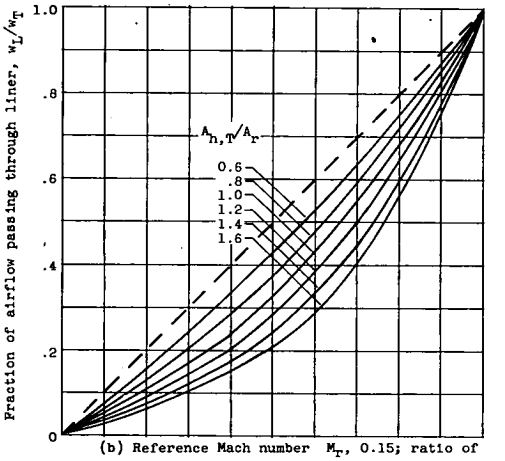

(b) Reference Mach number M_r, 0.15; ratio of liner cross-sectional area to reference area A_L/A_r, 0.6.

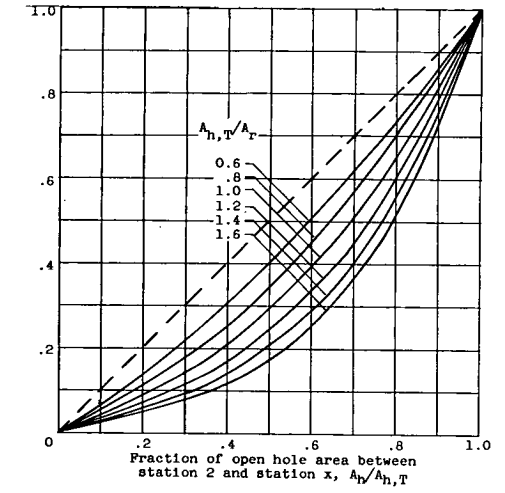

(c) Reference Mach number M_r, 0.05; ratio of liner cross-sectional area to reference area A_L/A_r, 0.7.

Figure 17. - Effect of ratio of liner total open hole area to combustor reference area $A_{h,T}/A_r$ on airflow distribution. Compressible-cold-flow relations including annulus wall friction with zero liner dome flow.

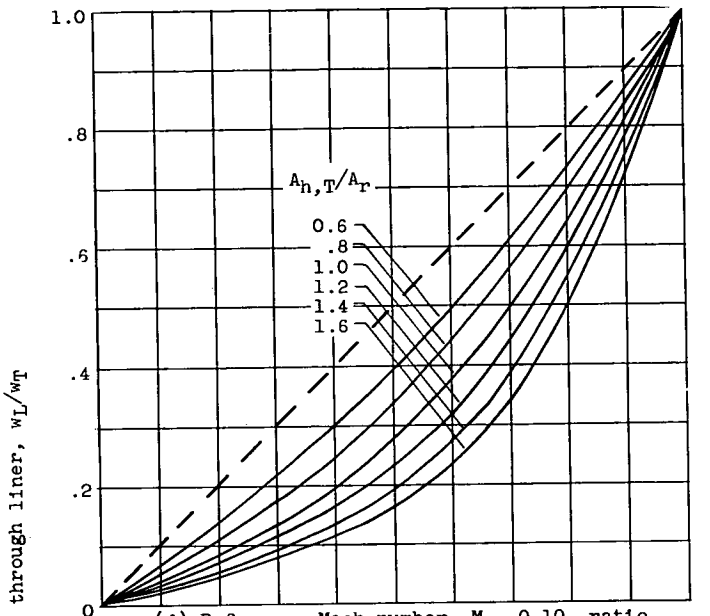

(d) Reference Mach number M_r, 0.10, ratio of liner cross-sectional area to reference area A_L/A_r, 0.7.

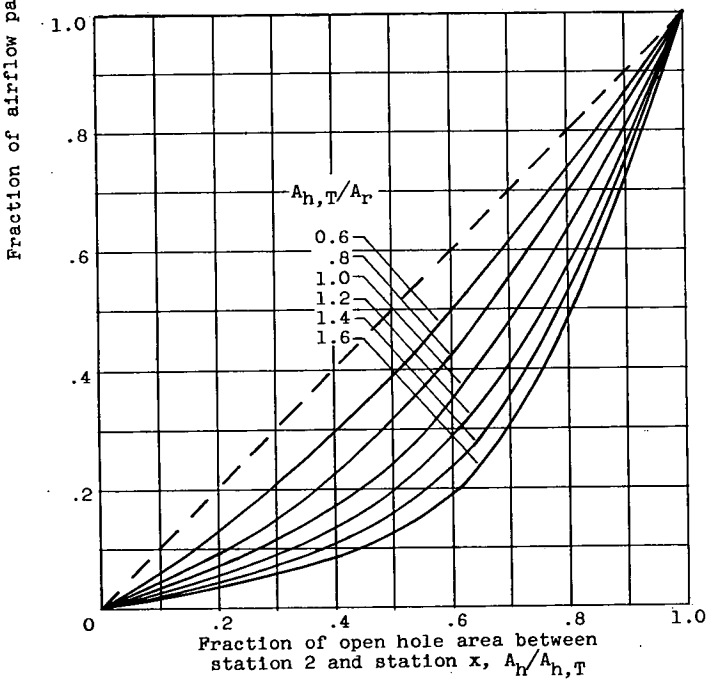

(e) Reference Mach number M_r, 0.15; ratio of liner cross-sectional area to reference area A_L/A_r, 0.7.

Figure 17. - Concluded. Effect of ratio of liner total open hole area to combustor reference area $A_{h,T}/A_r$ on airflow distribution. Compressible-cold-flow relations including annulus wall friction with zero liner dome flow.

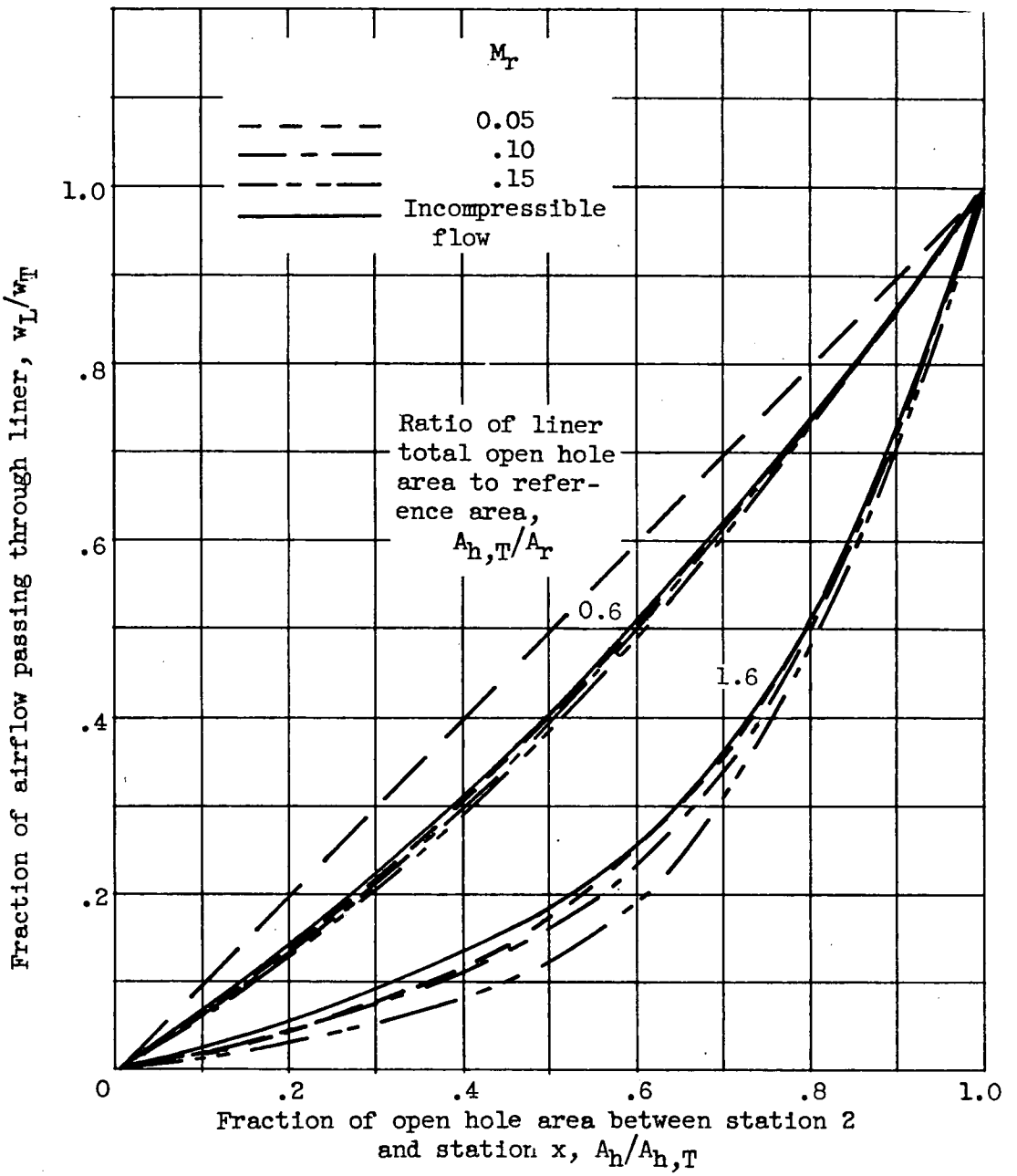

Figure 18. - Effect of reference Mach number M_r on airflow distribution. Compressible-cold-flow relations including annulus wall friction with zero liner dome flow; ratio of liner cross-sectional area to reference area A_L/A_r, 0.7.

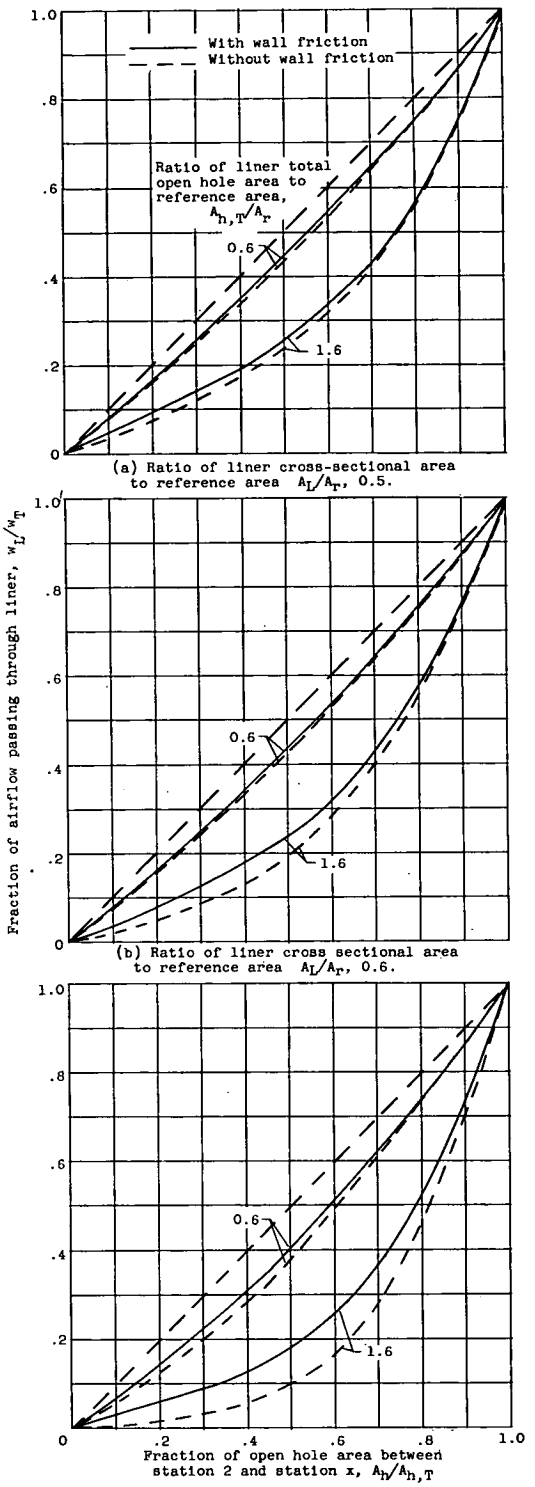

(a) Ratio of liner cross-sectional area to reference area A_L/A_r, 0.5.

(b) Ratio of liner cross sectional area to reference area A_L/A_r, 0.6.

(c) Ratio of liner cross-sectional area to reference area A_L/A_r, 0.7.

Figure 19. - Comparison of airflow distributions obtained from incompressible-cold-flow relations with and without annulus wall friction. Zero liner dome airflow.

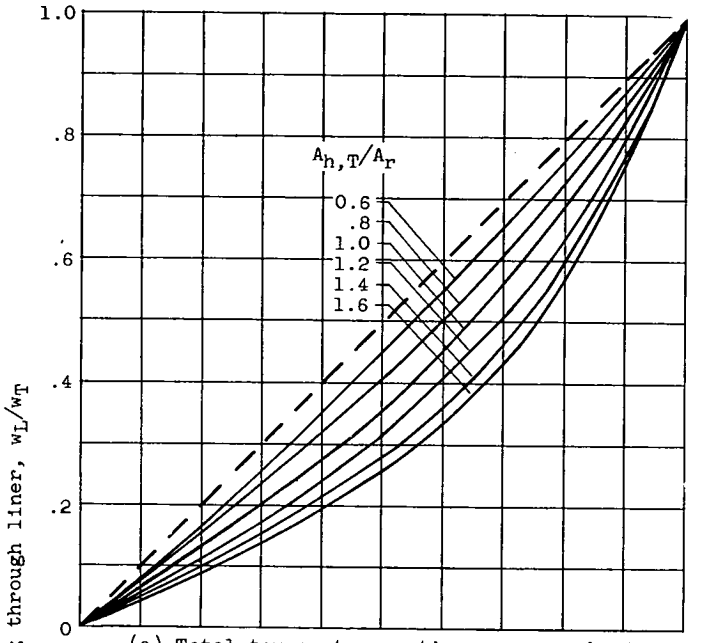

(a) Total-temperature ratio across combustor $T_{L,3}/T_1$, 1; ratio of liner cross-sectional area to reference area A_L/A_r, 0.5.

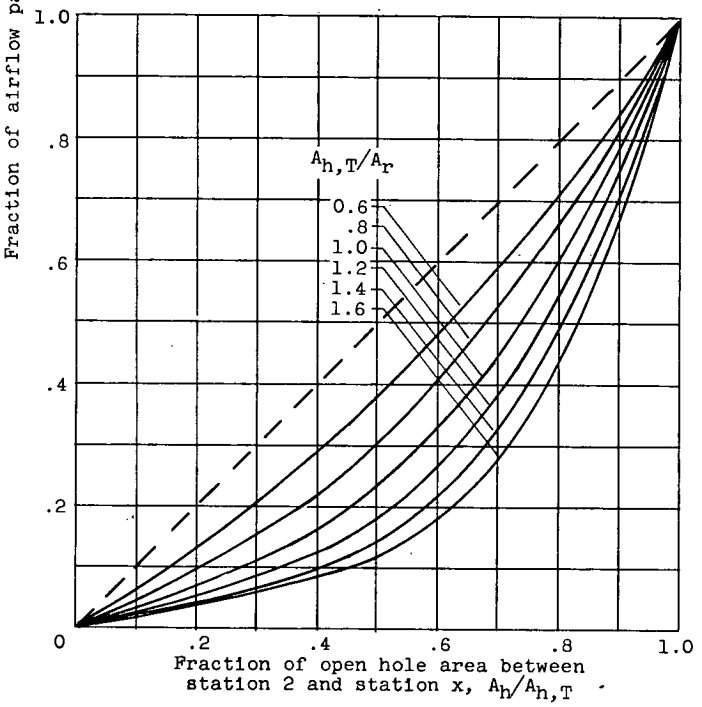

(b) Total-temperature ratio across combustor $T_{L,3}/T_1$, 2; ratio of liner cross-sectional area to reference area A_L/A_r, 0.5.

Figure 20. - Effect of ratio of liner total open hole area to reference area $A_{h,T}/A_r$ on airflow distribution. Incompressible-flow relations including annulus wall friction with zero liner dome flow.

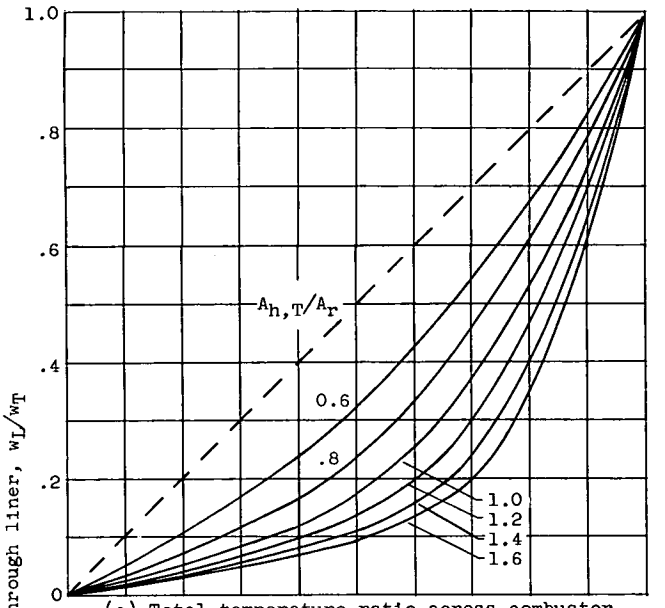

(c) Total-temperature ratio across combustor $T_{L,3}/T_1$, 3; ratio of liner cross-sectional area to reference area A_L/A_r, 0.5.

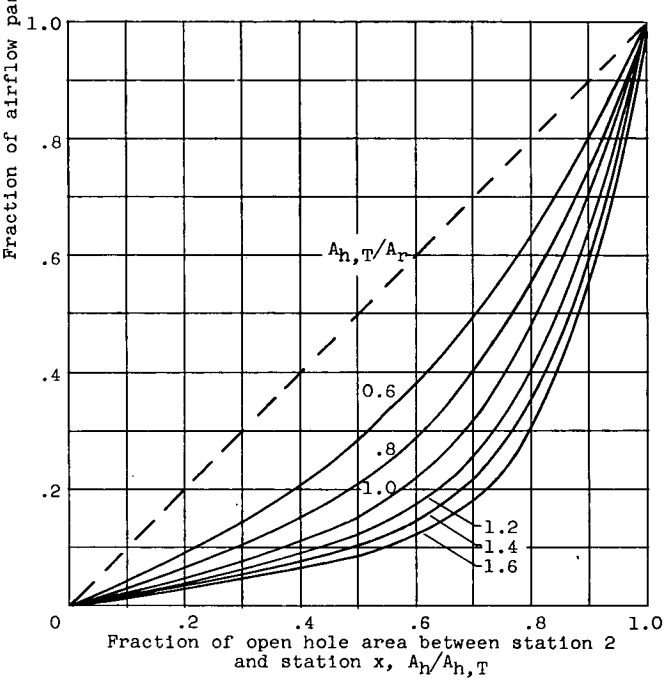

(d) Total-temperature ratio across combustor $T_{L,3}/T_1$, 4; ratio of liner cross-sectional area to reference area A_L/A_r, 0.5.

Figure 20. - Continued. Effect of ratio of liner total open hole area to reference area $A_{h,T}/A_r$ on airflow distribution. Incompressible-flow relations including annulus wall friction with zero liner dome flow.

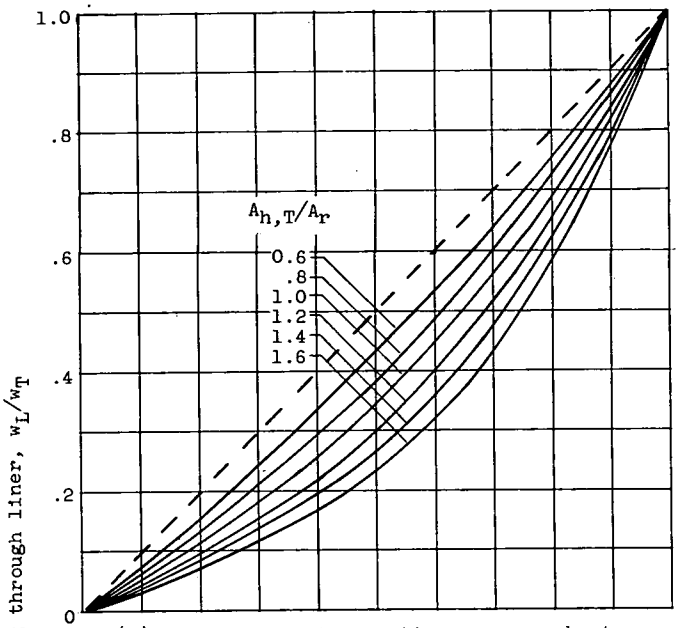

(e) Total-temperature ratio across combustor $T_{L,3}/T_1$, 1; ratio of liner cross-sectional area to reference area A_L/A_r, 0.6.

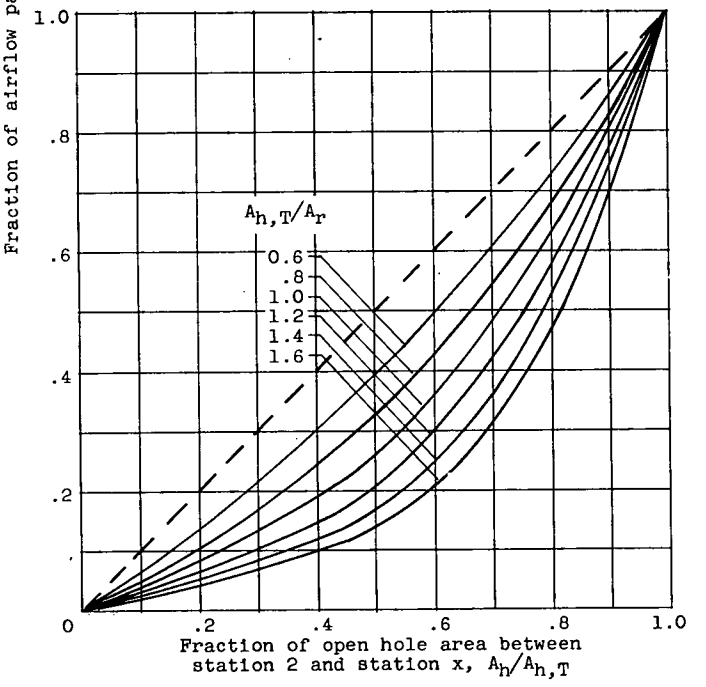

(f) Total-temperature ratio across combustor $T_{L,3}/T_1$, 2; ratio of liner cross-sectional area to reference area A_L/A_r, 0.6.

Figure 20. - Continued. Effect of ratio of liner total open hole area to reference area $A_{h,T}/A_r$ on airflow distribution. Incompressible-flow relations including annulus wall friction with zero liner dome flow.

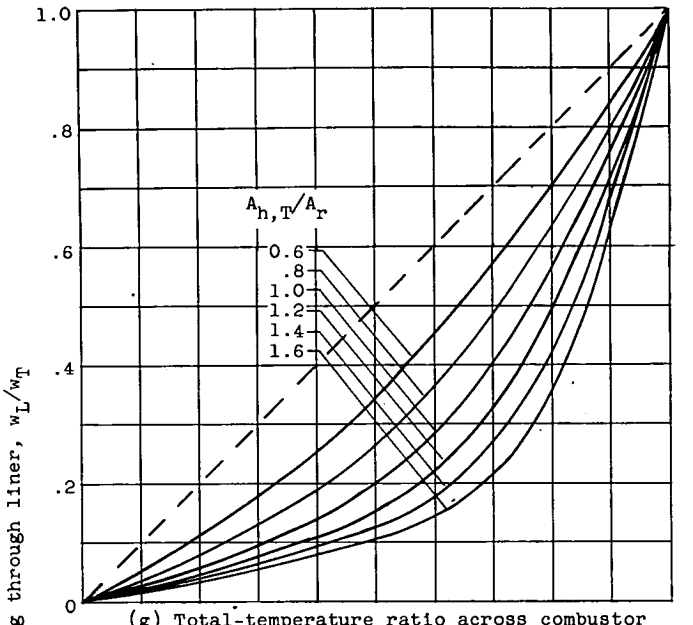

(g) Total-temperature ratio across combustor $T_{L,3}/T_1$, 3; ratio of liner cross-sectional area to reference area A_L/A_r, 0.6.

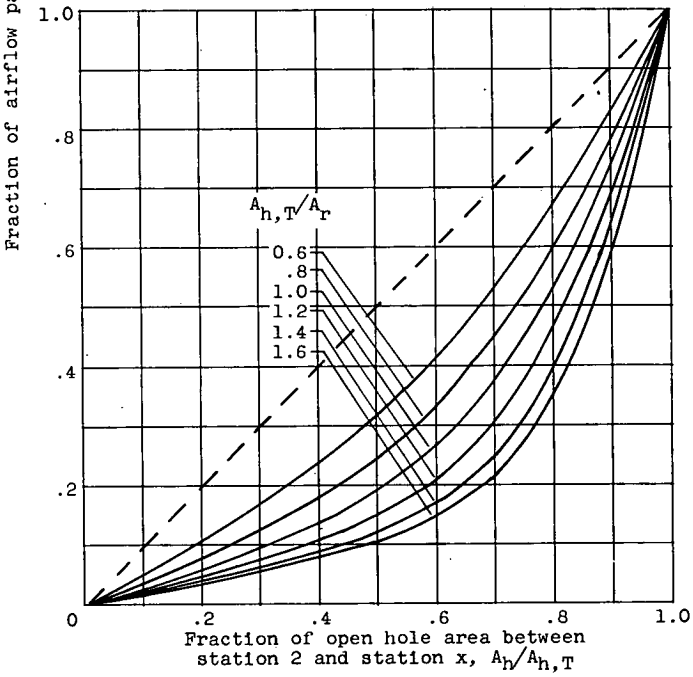

(h) Total-temperature ratio across combustor $T_{L,3}/T_1$, 4; ratio of liner cross-sectional area to reference area A_L/A_r, 0.6.

Figure 20. - Continued. Effect of ratio of liner total open hole area to reference area $A_{h,T}/A_r$ on airflow distribution. Incompressible-flow relations including annulus wall friction with zero liner dome flow.

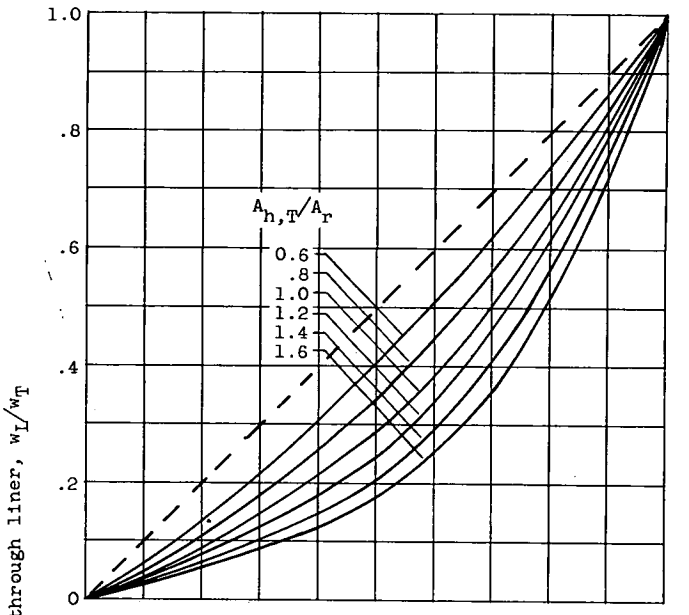

(i) Total-temperature ratio across combustor $T_{L,3}/T_1$, 1; ratio of liner cross-sectional area to reference area A_L/A_r, 0.7.

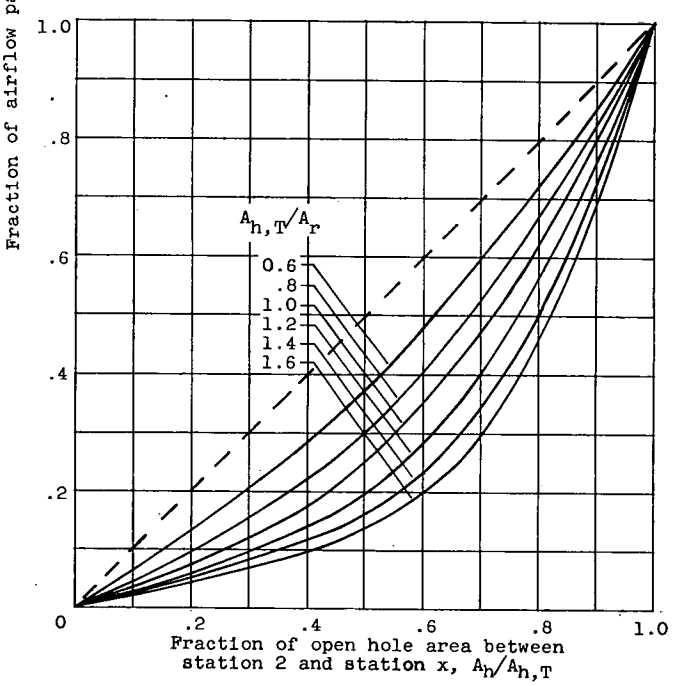

(j) Total-temperature ratio across combustor $T_{L,3}/T_1$, 2; ratio of liner cross-sectional area to reference area A_L/A_r, 0.7.

Figure 20. - Continued. Effect of ratio of liner total open hole area to reference area $A_{h,T}/A_r$ on airflow distribution. Incompressible-flow relations including annulus wall friction with zero liner dome flow.

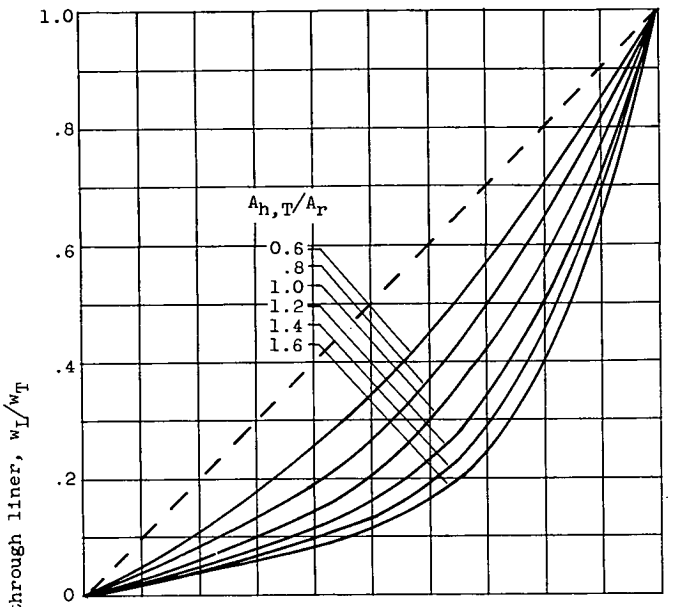

(k) Total-temperature ratio across combustor $T_{L,3}/T_1$, 3; ratio of liner cross-sectional area to reference area A_L/A_r, 0.7.

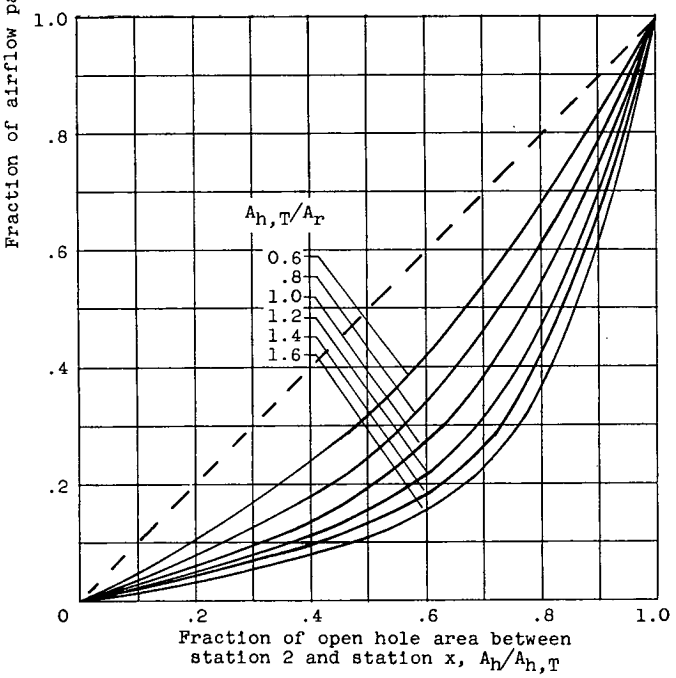

(l) Total-temperature ratio across combustor $T_{L,3}/T_1$, 4; ratio of liner cross-sectional area to reference area A_L/A_r, 0.7.

Figure 20. - Concluded. Effect of ratio of liner total open hole area to reference area $A_{h,T}/A_r$ on airflow distribution. Incompressible-flow relations including annulus wall friction with zero liner dome flow.

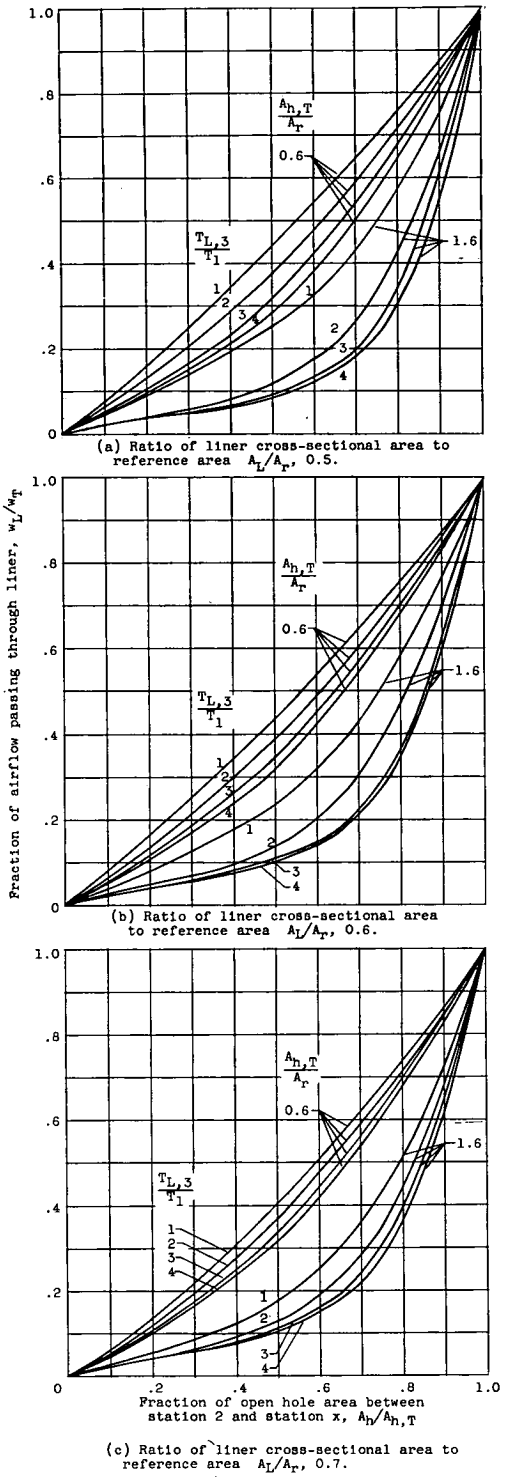

(a) Ratio of liner cross-sectional area to reference area A_L/A_r, 0.5.

(b) Ratio of liner cross-sectional area to reference area A_L/A_r, 0.6.

(c) Ratio of liner cross-sectional area to reference area A_L/A_r, 0.7.

Figure 21 - Effect of temperature ratio across combustor $T_{L,3}/T_1$ on airflow distribution for values of ratio of liner total open hole area to reference area $A_{h,T}/A_r$ of 0.6 and 1.6. Incompressible-flow relations with annulus wall friction and zero liner dome flow.

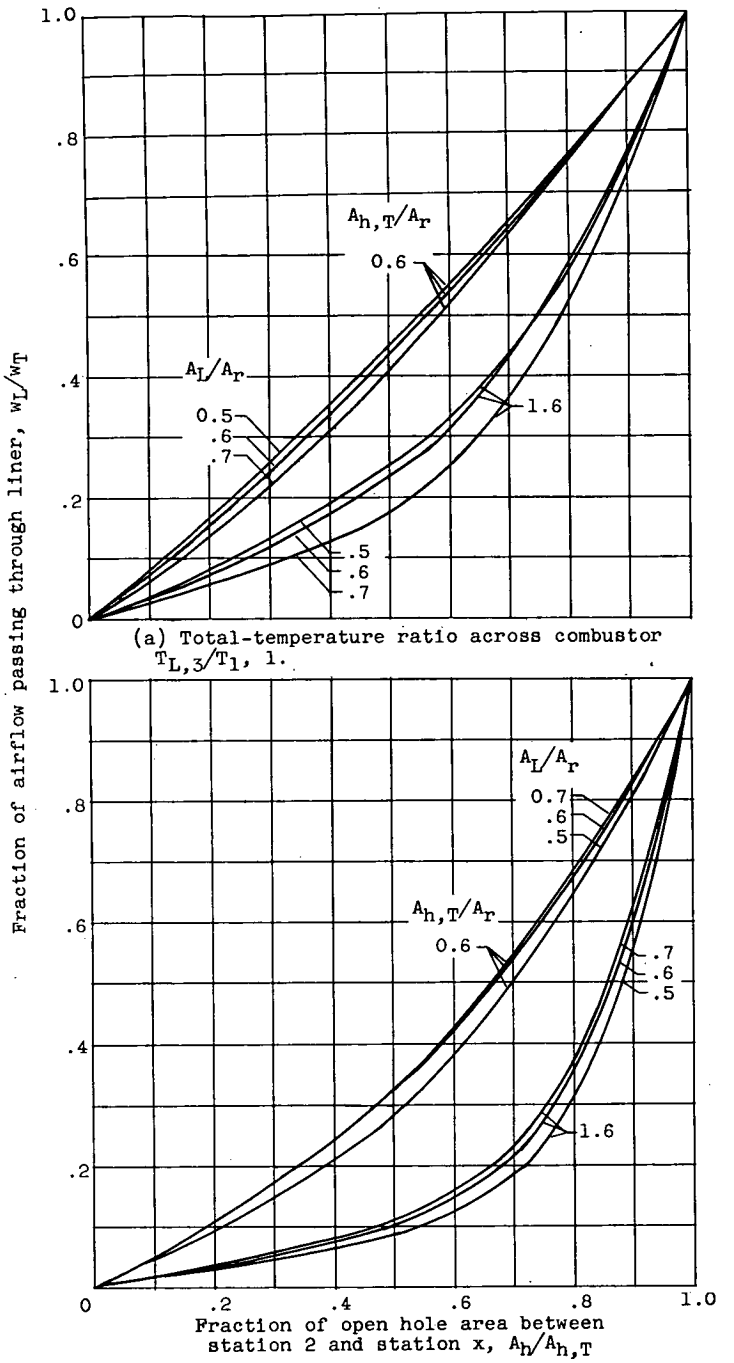

(a) Total-temperature ratio across combustor $T_{L,3}/T_1$, 1.

(b) Total-temperature ratio across combustor $T_{L,3}/T_1$, 4.

Figure 22. - Effect of ratio of liner cross-sectional area to reference area on airflow distribution for values of ratio of liner total open hole area to reference area $A_{h,T}/A_r$ of 0.6 and 1.6. Incompressible-flow relations with annulus wall friction and zero liner dome flow.

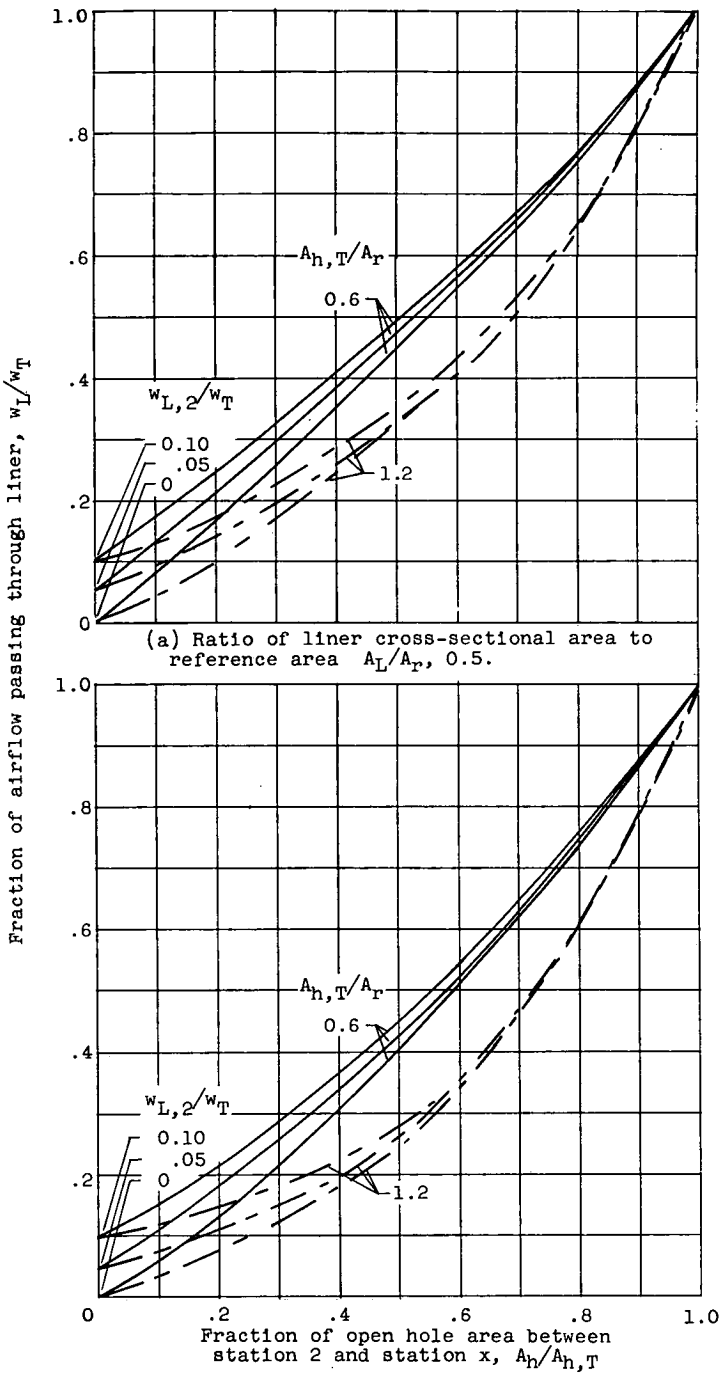

Figure 23. - Effect of airflow into liner dome $w_{L,2}/w_T$ on airflow distribution for values of ratio of liner total open hole area to reference area $A_{h,T}/A_r$ of 0.6 and 1.2. Incompressible-cold-flow relations with annulus wall friction.

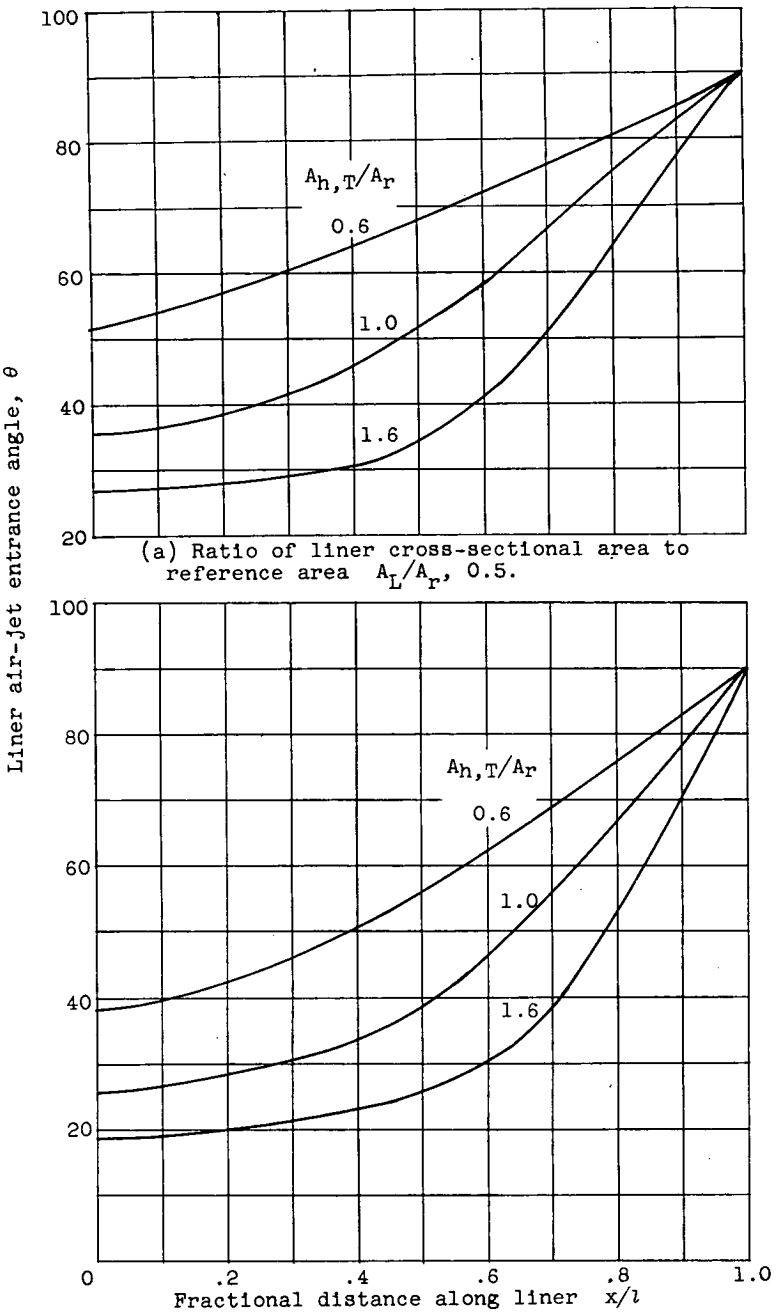

(a) Ratio of liner cross-sectional area to reference area A_L/A_r, 0.5.

(b) Ratio of liner cross-sectional area to reference area A_L/A_r, 0.7.

Figure 24. - Variation of liner air-jet entrance angle along liner for various values of ratio of liner total open hole area to reference area $A_{h,T}/A_r$. Incompressible-cold-flow relations including annulus wall friction with zero liner dome flow.

NACA - Langley Field, Va.